ΠΑΝΕΠΙΣΤΗΜΙΟ ΙΩΑΝΝΙΝΩΝ
ΤΜΗΜΑ ΜΑΘΗΜΑΤΙΚΩΝ

Σπυρίδων Κατσούδας

Αριθμητικες λυσεις της τυρβωδους ροης σε εσωτερικες και εξωτερικες ροες

ΜΕΤΑΠΤΥΧΙΑΚΗ ΔΙΑΤΡΙΒΗ

Ιωάννινα, 2024

UNIVERSITY OF IOANNINA
Department of Mathematics

Spyridon Katsoudas

Numerical solutions of turbulent flow in internal and external flows

Master's Thesis

Ioannina, 2024

Στην οικογένεια μου.

Η παρούσα Μεταπτυχιακή Διατριβή εκπονήθηκε στο πλαίσιο των σπουδών για την απόκτηση του Μεταπτυχιακού Διπλώματος Ειδίκευσης στα Εφαρμοσμένα Μαθηματικά και Πληροφορική που απονέμει το Τμήμα Μαθηματικών του Πανεπιστημίου Ιωαννίνων.

Εγκρίθηκε την 27/06/2024 από την εξεταστική επιτροπή:

Ονοματεπώνυμο	**Βαθμίδα**
Μιχαήλ Ξένος	Καθηγητής
Θεόδωρος Χωρίκης	Καθηγητής
Ευστράτιος Τζιρτζιλάκης	Καθηγητής

ΥΠΕΥΘΥΝΗ ΔΗΛΩΣΗ

"Δηλώνω υπεύθυνα ότι η παρούσα διατριβή εκπονήθηκε κάτω από τους διεθνείς ηθικούς και ακαδημαϊκούς κανόνες δεοντολογίας και προστασίας της πνευματικής ιδιοκτησίας. Σύμφωνα με τους κανόνες αυτούς, δεν έχω προβεί σε ιδιοποίηση ξένου επιστημονικού έργου και έχω πλήρως αναφέρει τις πηγές που χρησιμοποίησα στην εργασία αυτή."

Σπυρίδων Κατσούδας

Ευχαριστιες

Η παρούσα διατριβή εκπονήθηκε στα πλαίσια του Μεταπτυχιακού Διπλώματος Ειδίκευσης "Εφαρμοσμένα Μαθηματικά και Πληροφορική" του τμήματος Μαθηματικών, Πανεπιστημίου Ιωαννίνων, με επιβλέποντα τον Καθηγητή κ. Μιχαήλ Ξένο και μέλη της Τριμελούς Εξεταστικής Επιτροπής, κ. Θεόδωρο Χωρίκη και κ. Ευστράτιο Τζιρτζιλάκη.

Ευχαριστώ θερμά, τον κ. Μιχαήλ Ξένο, Καθηγητή του τμήματος Μαθηματικών του Πανεπιστημίου Ιωαννίνων, για την επίβλεψη της παρούσας μεταπτυχιακής διατριβής. Τον ευχαριστώ για την αδιάκοπη υποστήριξη, την καθοδήγηση, τον χρόνο καθώς και τις πολύτιμες συμβουλές που μου προσέφερε καθόλη τη διάρκεια της εκπόνησης της διατριβής.

Επίσης, ευχαριστώ τους, κ. Θεόδωρο Χωρίκη, Καθηγητή του τμήματος Μαθηματικών του Πανεπιστημίου Ιωαννίνων και κ. Ευστράτιο Τζιρτζιλάκη, Καθηγητή του Τμήματος Μηχανολόγων Μηχανικών του Πανεπιστημίου Πελοποννήσου, για την προθυμία τους να συμμετάσχουν στην Τριμελή Εξεταστική Επιτροπή και για τις πολύτιμες και εύστοχες παρατηρήσεις τους στην παρούσα εργασία.

Τέλος, θέλω να εκφράσω την ευγνωμοσύνη μου προς την οικογένειά μου. Ευχαριστώ θερμά τους γονείς μου, Ευθυμία Κουτσούκη και Χαρίλαο Κατσούδα, για την αμέριστη αγάπη και αδιάλειπτη στήριξή τους σε κάθε στιγμή και απόφαση της ζωής μου.

Ιωάννινα 2024,
Σπυρίδων Κατσούδας

Περιληψη

Η τυρβώδης ροή είναι ένα φαινόμενο που χαρακτηρίζεται από χαοτικές και απρόβλεπτες μεταβολές στο πεδίο ταχύτητας και πίεσης του ρευστού και απασχολεί τους επιστήμονες από τα αρχαία χρόνια καθώς η παρουσία της είναι καθολική στην φύση. Η κατανόηση των θεμελιωδών αρχών της διαδραματίζει καθοριστικό ρόλο σε πολλούς επιστημονικούς κλάδους όπως την αεροναυπηγική, την μηχανική, την μετεωρολογία και πολλούς άλλους. Η ραγδαία εξέλιξη της τεχνολογίας και των Η/Υ τις τελευταίες δεκαετίες, καθιστά δυνατό να υπολογίζονται πολλοί παράμετροι στην εμφάνιση της τύρβης και ως συνέπεια έχει την έντονη ενασχόληση των επιστημόνων με αυτό το φαινόμενο. Η παρούσα εργασία έχει ως στόχο να αναλύσει τις αρχές που διέπουν την τυρβώδη ροή, ερμηνεύοντας την εμφάνισή της σε "ταχείες ροές" (μεγάλα Reynolds), να την μοντελοποιήσει μαθηματικά αλλά και να αναλύσει τα μοντέλα μέσω των οποίων την προσομοιώνουμε, με την βοήθεια υπολογιστικών προγραμμάτων. Στην παρούσα εργασία θα γίνει χρήση των υπολογιστικών προγραμμάτων Matlab και Ansys Fluent, σε συνδυασμό με προηγμένες μαθηματικές τεχνικές και την βοήθεια της υπολόγιστικής ρευστοδυναμικής αυτή η μελέτη επιδιώκει να εμβαθύνει την κατανόησή μας για την χαοτική συμπεριφορά της τύρβης και να συμβάλει στο ευρύτερο σύνολο γνώσεων στο πεδίο.

Συγκεκριμένα στην εργασία εισάγονται οι έννοιες της στρωτής και τυρβώδους ροής και εισάγεται η συσχέτιση τους με τον αδιάστατο αριθμό Reynolds. Επίσης εισάγονται οι περίφημες εξισώσεις Navier-Stokes οι οποίες με την συνεισφορά τους έχουν θεμελιώσει τον κλάδο της ρευστοδυναμικής. Ύστερα αναλυεται ενδελεχώς το μοντέλο μέσων τιμών που πρότεινε ο Osborne Reynolds και παρουσιάζονται οι φαινόμενες τάσεις ή τάσεις Reynolds που προκύπτουν, οι οποίες έχουν κυρίαρχο λόγο στην μελέτη των τυρβώδων ροών. Οι τάσεις αυτές όντας δύσκολες στον υπολογισμό τους καθώς είναι μη γραμμικοί όροι αντιμετωπίζονται με την αρωγή των μοντέλων τύρβης στα οποία γίνεται αναφορά στο 3ο κεφάλαιο της εργασίας. Παρουσιάζεται η υπόθεση του Boussinesq το, μήκος ανάμιξη του Prandtl και η συνεισφορά του στον υπολογισμό της τυρβώδους ροής. Εν συνεχεία, στο τέλος τους δεύτερου κεφαλαίου αναλύονται ο "νόμος του τοίχου", η συχέτιση της ταχύτητας τριβής με την κανονικοποιημένη απόσ-

ταση από το σύνορο και τελικά η κλίμακα Kolmogorov αλλά και οι κλίμακες ενέργειας και αλληλουχίας.

Στο τρίτο κεφάλαιο γίνεται κατηγοριοποίηση των μοντέλων τύρβης σε αλγεβρικά, μίας εξίσωσης, δύο εξισώσεων, εξισώσεων διάτμησης και προσομοίωση των μεγάλων δινών (LES). Αναπτύσσονται λεπτομερώς τα αλγεβρικά μοντέλα των Cebeci και Smith και των Baldwin και Lomax, το μοντέλο μίας εξίσωσης των Spalart-Allmaras όπως επίσης και τα μοντέλα δύο εξισώσεων $k-\varepsilon$ και $k-\omega$ τα οποία αποτελούν σύγχρονα μοντέλα τύρβης με εξαιρετική ακρίβεια.

Εν συνεχεία με την ανάπτυξη σειριακού κώδικα στο πρόγραμμα Matlab, παρουσιάζονται οι αριθμητικές λύσεις ορισμένων εσωτερικών αλλά και εξωτερικών ροών καθώς και υλοποιούνται μαθηματικές προσομοιώσεις σε πολύ εξελιγμένους κώδικες πεπερασμένων όγκων και πιο συγκεκριμένα στο Ansys Fluent.

Abstract

Turbulent flow is a phenomenon characterized by chaotic and unpredictable changes in the velocity and pressure field of fluid and has been of concern to scientists as its presence is universal in nature. The understanding of its fundamental principles plays a decisive role in many scientific disciplines such as aeronautics, engineering, meteorology, and many others. The rapid development of technology and computers in recent decades has made it possible to calculate many parameters in the appearance of turbulence and as a consequence has the intense preoccupation of scientists with this phenomenon. This thesis aims to analyze the fundamental principles governing turbulent flow explaining why appears in "fast flows" (large Reynolds number), to model it but also analyze the models through which we simulate it with the help of computer programs. This work will be done using the computer programs Matlab and Ansys Fluent, in combination with advanced mathematical techniques and the help of computational mathematics this study seeks to deepen our understanding of the chaotic behavior of turbulence and contribute to the wider knowledge in the field.

Specifically, the concepts of laminar and turbulent flow are introduced and their correlation with the dimensionless Reynolds number is introduced, also the famous Navier-Stokes equations are introduced, which by their contribution they have established the field of fluid dynamics. Then is analyzed in the averaging method proposed by Osborne Reynolds, else called Reynolds decomposition, and presented the apparent stresses or Reynolds stresses that arise, which have a dominant place in the study of turbulent flow. These stresses are difficult to approximate as they are nonlinear terms and they are treated with the help of the turbulence models referred to in Chapter 3. The hypothesis of Boussinesq is presented, the mixing length of Prandtl, and his contribution to the calculation of turbulent flow. Finally, at the end of the second chapter, the "law of the wall" is analyzed, the correlation of friction velocity with the normalized distance from the boundary, and finally the Kolmogorov scale as well as the energy scale and cascade.

The third chapter categorizes the models of turbulence into algebraic, one equation, two equations, shear equations, large eddy simulation (LES), and direct numerical simulation (DNS). The algebraic models of Cebeci and Smith and Baldwin and Lomax are present in detail, the model of one equation of Spalart-Allmaras as well as the models of two equations $k-\varepsilon$ and $k-\omega$ which are modern models of turbulence with very good accuracy in comparison with experimental data.

Finally, with the development of specific codes in Matlab, the numerical solutions of some internal and external flows are presented as well and mathematical simulations are implemented in very sophisticated finite volume codes and more specifically in Ansys Fluent.

Contents

List of Figures

List of Symbols

A	Van Driest damping coefficient
C	Additive constant in the law of the wall
C_k	Kolmogorov constant
$\overline{c}$	Mean molecular speed
E	Total energy
$E(\kappa)$	Energy spectral density
F_k	Klebanoff intermittency function
k	Turbulent kinetic energy per unit mass or TKE;Von Karman's constant
l	Turbulence length scale; characteristic eddy size
l_{mfp}	Mean free path
L	Characteristic length scale
m	Molecular mass
p	Pressure
Re	Reynolds number
Re_T	Turbulence Reynolds number
U_∞	Freestream velocity
u_τ	Friction velocity
v	Kolmogorov velocity scale
y^+	Dimensionless, sublayer-scaled, distance
$y_{crossover}$	Inner/outer layer matching point
δ	Boundary-layer thickness
δ^*	Displacement thickness
ε	Turbulent viscous dissipation per unit mass
ε_t	Turbulent kinematic viscosity-Eddy Viscosity
η	Kolmogorov length scale
κ	Wave number
λ	Wavelength
μ	Dynamic Viscosity
ν	Kinematic Viscosity
σ_i	Perpendicular stresses
τ	Kolmogorov time scale
τ_{ij}	Shearing stresses
ω	Specific dissipation rate,Vorticity

CHAPTER 1

Introduction

Turbulence is a complex phenomenon that occurs universally in nature. Scientists have been studying turbulence for centuries, and many theories have been supported about its fundamental principles. The modern study of turbulence started about 150 years ago and continues to evolve rapidly as it is one of the unsolved problems of the classical sciences. Some of the greatest mathematicians and physicists have dealt with the enigmatic nature of turbulence such as Kolmogorov, Boussinesq, Prandtl, Reynolds and many more. On the journey to understanding turbulence, scientists introduced turbulence models which are crucial tools in addressing this problem, including advanced mathematics tools. These models incorporate advanced mathematical tools that are closely related to the physical interpretation of turbulence. Numerous classical models were introduced in the 20th century, and to this day, a multitude of models is created by experienced scientists, and some of them are remarkably embraced by the academic community.

1.1 Historical Review

The observation of fluid behavior near solid boundaries dates back to ancient times with the Heron of Alexandria and continues with scholars such as Leonardo Da Vinci with his famous paintings of fluid flow in a pool. Ancient and medieval scientists observed this chaotic motion of flow but lacked mathematical modeling to analyze it. Da Vinci was a pioneer and with his observations in the 15th century laid the foundation for future studies. In the last decades of the 19th century Osborne Reynolds in 1883 introduced the concept of dimensionless Reynolds number [44] which is very useful until today for understanding the circumstances where turbulence occurs and the characterization of flow. Continuing, Albert Einstein in 1905 [9] with his pa-

per on Brownian motion laid the groundwork for understanding the stochastic nature of turbulent fluctuations, and in the 30s and 40s, the statistical properties of turbulence started to be studied with the help of Ludwig Prandtl's turbulent boundary layer and its behavior near a solid wall as well Andrey Kolmogorov with his work in 1941 [15], the birth of energy cascade concept and the scaling laws for turbulent fluctuations. The need for more advanced mathematical modeling of turbulence has led John Lumley and George Batchelor [38] to introduce the eddy viscosity concept, a tool that proved vital for the development of RANS equations which was first given birth by Osborne Reynolds. With this contribution, the field experienced tremendous growth with the turbulence modeling theory, with Launder and Spalding introducing the $k - \varepsilon$ model, Wilcox, introduced his famous $k - \omega$ model [43], the first widely used RANS model, its frequent use is due to its practical ease of simulation of turbulence. With the development of computers, science evolved with more advanced models such as LES and DNS and in the last decade of the 20th century and the first two of the 21st, the attention is focused on the hybrid models between one or two equations models and DNS or LES, to lower the computational cost and increase the precision comparatively with experimental data. Finally with the development of artificial intelligence, turbulent flows can be predicted through big databases of previously calculated flows, this field of turbulence modeling is rapidly expanding and more scientists are starting to interact with neural networks and machine learning since its possibilities are unlimited.

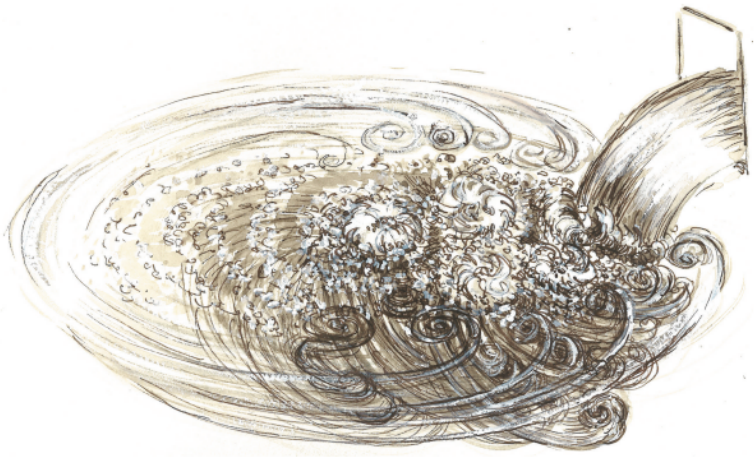

Figure 1.1: Leonardo's drawing of turbulent flow as water flows with the effects of turbulence into a pool.

1.2 Laminar and Turbulent Flow

The boundary layer (B.L.) is crucial in fluid mechanics with countless applications, the transition from the laminar B.L. to the turbulent one that occurs is an essential aspect of fluid mechanics and plays a crucial role in a wide range of applications such as aircraft design, power generation, and hydrodynamics. A boundary layer is a layer of fluid that develops near the surface of a solid object when it is exposed to a fluid flow. It can be classified into two types laminar and turbulent. The laminar B.L. is described by smooth flow, whereas the turbulent B.L. is described by chaotic, irregular flow.

The transition from laminar to turbulent B.L. is a significant occurrence in many engineering and scientific applications. It is an area of ongoing research, as understanding the transition mechanism is crucial for predicting the performance of fluid systems [8]. The transition from laminar to turbulent boundary layer can occur in a variety of ways, including through natural fluctuations in the flow, the introduction of disturbances from the surface, or the presence of roughness on the surface. The onset of turbulence can be predicted using various criteria, including the Reynolds number, which is the ratio of inertial forces to viscous forces in the flow and is dimensionless.

The first scientist to notice this strange state of fluid motion was Leonardo Da Vinci who named it "Turbulence". In modern times turbulence is examined by Osborne Reynolds in 1883

Leonardo Da Vinci was probably the first to distinguish this special state of the fluid motion and use the term "turbulence". Modern turbulence started with the experiments of Osborne Reynolds in 1883, who examined the conditions leading to the transition of smooth fluid flows in pipes to turbulent ones. In this process, he concluded with the creation of a dimensionless quantity, called "Reynolds number" which represents quantitative measurement so that we can decide on the fluid state as they flow.

$$Re = \frac{\text{inertial forces}}{\text{viscous forces}} = \frac{uL}{\nu},$$

where u is the free stream velocity and L is a characteristic length scale of the flow. Reynolds number determines fluid flow behavior by comparing inertial forces to viscous forces in a given system, crucial for predicting turbulence. In fluid dynamics, Reynolds number serves as a dimensionless quantity, indicating the transition between laminar and turbulent flow in various applications.

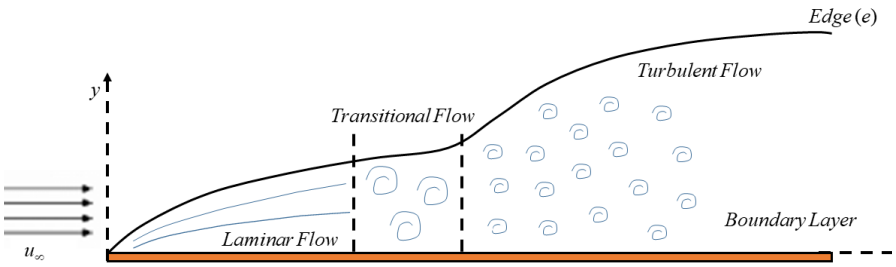

Figure 1.2: Visualization of the transition from laminar to transitional and to turbulent flow on B.L.

In the laminar B.L., the flow is defined as smooth and ordered, the velocity profile is parabolic in shape. However, as the fluid moves downstream, the mean velocity profile becomes flat, and the flow becomes unstable. Small disturbances in the flow can be amplified, leading to the formation of vortices, which cause the flow to become increasingly chaotic.

As the B.L. transitions from laminar to turbulent, the velocity fluctuations increase, resulting in greater mixing of the fluid. This mixing leads to an increase in the rate of mass and heat transfer, which can have significant effects on the performance of fluid systems. For example, in aircraft design, the transition from laminar to turbulent B.L. has significant impact on drag and consequently fuel efficiency.

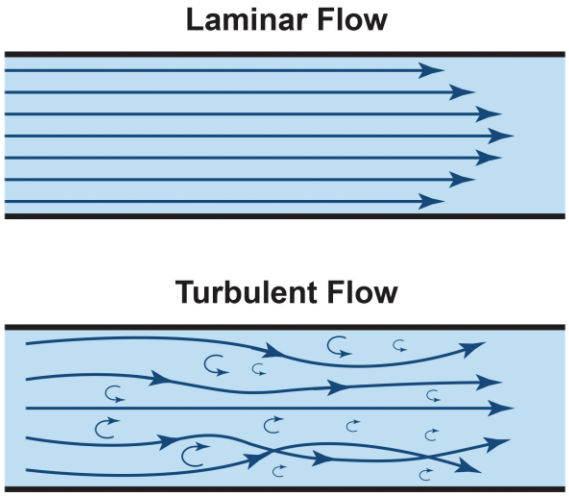

Figure 1.3: Laminar and turbulent flow in a channel [19].

Several factors can influence this transition, a determining factor is the Reynolds number. When the Reynolds number overcomes a critical value, the laminar B.L. becomes unstable and the flow transitions [11] to a turbulent regime. The critical Reynolds number is influenced by the shape of the object that interacts with the flow, the viscosity of the fluid, and the flow velocity. Another factor that can influence the transition is the surface roughness of the object. Roughness can cause disturbances in the flow, leading to the amplification of vortices and the onset of turbulence.

1.3 Navier Stokes Equations

The need to describe and predict fluid flows led to describe the equations of motion of ideal fluids, Euler used Newton's second axiom and derived a relative equation. Analogously, Navier and Stokes arrived at equations of motion of real fluids ($\mu \neq 0$) which connected the kinematic characteristics of the flow with the equivalent dynamic characteristics of the flow. In vector form, the system of equations that describe the laminar flow of homogeneous, incompressible and real fluids are :

$$\frac{D\overline{q}}{Dt} = \overline{F} - \frac{1}{\rho}\overline{\nabla}p + \nu\overline{\nabla}^2\overline{q}, \qquad \frac{D\overline{q}}{Dt} = \frac{\partial\overline{q}}{\partial t} + (\overline{q}\cdot\overline{\nabla})\cdot\overline{q} \tag{1.1}$$

where $q = (u, v, w)$ is the velocity vector, p : pressure, ρ : density, ν: kinematic viscosity.

On the left side there is the Stokes operator $\frac{D}{Dt}$ which is applied to velocity $\overline{q}$, the first term $\frac{\partial\overline{q}}{\partial t}$ is called local derivative and it represents the change of velocity in terms of time for the same point of space. The term $(\overline{q}\cdot\overline{\nabla})\cdot\overline{q}$ represents the change of velocity due to the motion of the fluid and it is called convective derivative [44].

In cartesian coordinates,

$$\begin{aligned}
&u\frac{\partial u}{\partial x} + v\frac{\partial u}{\partial y} = F_x - \frac{1}{\rho}\frac{\partial p}{\partial x} + \nu\left(\frac{\partial^2 u}{\partial x^2} + \frac{\partial^2 u}{\partial y^2}\right), && \text{x-momentum}\\
&u\frac{\partial v}{\partial x} + v\frac{\partial v}{\partial y} = F_y - \frac{1}{\rho}\frac{\partial p}{\partial y} + \nu\left(\frac{\partial^2 v}{\partial x^2} + \frac{\partial^2 v}{\partial y^2}\right), && \text{y-momentum}\\
&\frac{\partial u}{\partial x} + \frac{\partial v}{\partial y} = 0, && \text{continuity eq.}
\end{aligned} \tag{1.2}$$

the above system of PDE's describe the homogeneous, incompressible, real fluids for the two-dimensional flow, in steady state, in orthogonal coordinates (x,y).

On the left side of Navier-Stokes equations, there are the inertial terms, which they are in equilibrium with the right side terms of pressure, friction outer forces. Under the influence of the no-slip condition the fluid particles that adhere to the solid boundary stick to it. The boundary surface is static which means that the velocity of fluid particles is zero.

The Navier-Stokes equations are the cornerstone for the modeling of turbulence, as they lack the ability to turbulent flows, a new method will introduced in the next chapter to achieve the modeling of the deterministic part of the phenomenon.

CHAPTER 2

Mathematical Modeling of Turbulent Flow

2.1 Mean values Mathematical model-RANS

In this chapter is introduced and analyzed the mathematical modeling of turbulent flows. Turbulent flow is defined as a flow, in which macroscopic mixing is observed between the fluid layers, as it flows. Turbulence is characterized by chaotic changes in velocity and pressure gradient and appears in a multitude of natural phenomena, this is the reason why scientists are so interested in its study. To this day it is one of the open problems of classical studies since it has no mathematical analytical solutions.

Reynolds introduced the averaging concept in his paper in 1894 [29] with his consideration, he analyzed every function in the flow (velocity, pressure, temperature) to mean value plus its fluctuating part, so in every point of space, every function can be described as the mean value of the function and the fluctuating part. Turbulence can be characterized by its velocity mean value, if the average velocity does not vary with time, this is called stationary turbulence (statistically steady), on the contrary, we call it non-stationary turbulence, as can be seen in the Figure 2.1. The heart of turbulence is in the motion of a single fluid "point" in non-stationary, non-homogeneous turbulence, as this non-idealized fluid may be relevant to transport to decaying real phenomena flows.

In this work, it will be studied the case of isotropic and homogeneous turbulence, although it is an idealization case of turbulence that is not found in nature, it is widely used by scientists because it is applied as a step for understanding more complex turbulence phenomena and it provides us with useful information about the nature of turbulence. Additionally, more properties of

turbulence must be defined, especially flows are defined as isotropic if rotation and buoyancy effects can be neglected since they are considered insignificant. Turbulence is also defined as homogeneous if the spatial gradients are absent in any averaged quantity, so it can be assumed that rotation and buoyancy forces don't suppress vertical motions and create anisotropy between vertical and horizontal directions [27].

2.1.1 Mean Values and Fluctuations

There are 3 basic forms of averaging that are utilized in turbulence modeling, these are time average, spatial average, and ensemble average. Spatial averaging is being used for homogeneous turbulence on turbulent flows that, on average, are uniform in all directions. To achieve the result we average over all spatial coordinates by doing a volume integral. In the ensemble average, it must be done N conducted identical experiments, with initial and boundary conditions whose differences are only small random infinitesimal perturbations, from their results we take the average of these experiments. Due to the nature of turbulence, the principle of time averaging was introduced as a tool, aiming to describe the turbulent fluctuations via statistical measures. This principle is not only of theoretical value but is mandatory for the development of turbulence models, in every applicable way. Time average is appropriate for stationary turbulence flows that on average do not vary with time [43]. Via time averaging, the flow variables are separated into mean flow and fluctuating components.

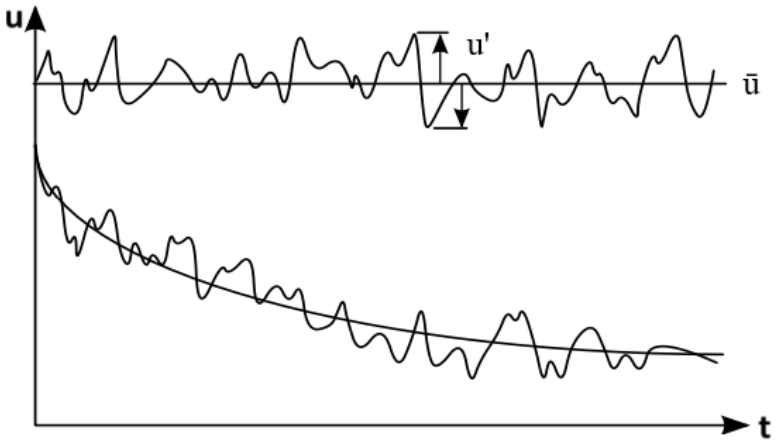

Figure 2.1: Stationary and non-stationary turbulence.

Thus, any flow point in a turbulent flow can be defined as the combination of the average and fluctuating part (time-varying). This process is called Reynolds decomposition. For example, in a two-dimensional flow, the variables that are of interest are the two components of velocity and pressure, so:

$$u = \overline{u} + u', \quad v = \overline{v} + v', \quad p = \overline{p} + p'. \tag{2.1}$$

Through statistical knowledge, the mean value is given by the integral:

$$\overline{u} = \frac{1}{T}\int_0^T u(t)dt \quad \text{or} \quad \frac{1}{T}\int_{t_0}^{T+t_0} u(t)dt, \tag{2.2}$$

with all the instantaneous values (f') over a large enough period T to be zero, this occurs due to the definition of the mean value. Thus, for a random function f :

$$f' = f - \overline{f} \Rightarrow \overline{f'} = \overline{f} - \overline{\overline{f}} \xrightarrow{\overline{\overline{f}}=\overline{f}} \overline{f'} = 0. \tag{2.3}$$

So, in three-dimensional flow the mean values of the fluctuating part of the 3 components of velocity u, v, w, and pressure p are zero.

$$\overline{u'} = 0, \quad \overline{v'} = 0, \quad \overline{w'} = 0, \quad \overline{p'} = 0.$$

The mean square value of a fluctuation is not zero and indeed physically it describes the intensity of the turbulence:

$$\overline{u'}^2 = \frac{1}{T}\int_0^T u'^2 dt \neq 0.$$

Below are listed properties of the average value [32]. If f and g are two functions:

$$\overline{\overline{f}} = \overline{f}, \quad \overline{f+g} = \overline{f} + \overline{g}, \quad \overline{f \cdot g'} = 0, \quad \overline{\overline{f} \cdot g} = \overline{f} \cdot \overline{g}, \quad \overline{f \cdot g} = \overline{f}\,\overline{g} + \overline{f' \cdot g'},$$

and some properties of the derivative:

$$\overline{\frac{\partial f}{\partial x}} = \frac{\partial \overline{f}}{\partial x}, \quad \overline{\frac{\partial^2 f}{\partial x^2}} = \frac{\partial^2 \overline{f}}{\partial x^2}.$$

By substituting the variables, with the Reynolds decomposition approach, in the Navier-Stokes equations some extra terms occur which are called apparent or Reynold stresses, these terms cannot be explained physically so they are considered to behave as stresses, contribute to the flow as additional viscosity and are termed universally in the literature [41]. They can characterized as convective acceleration terms because the density appears in them.

Proposition 2.1.1. *The equation of continuity, in a turbulent flow, is satisfied by mean and fluctuating velocity components in incompressible fluids.*

Proof. Getting started by substituting, with the Reynolds decomposition, in the continuity equation:

$$\vec{\nabla} \cdot \vec{q} = 0 \Rightarrow \frac{\partial \overline{u}}{\partial x} + \frac{\partial \overline{v}}{\partial y} + \frac{\partial \overline{w}}{\partial z} + \frac{\partial u'}{\partial x} + \frac{\partial v'}{\partial y} + \frac{\partial w'}{\partial z} = 0. \tag{2.4}$$

This equation is very useful because if we apply the averaging approach, with the help of the time average properties above, the result will be:

$$\frac{\partial \overline{u}}{\partial x} + \frac{\partial \overline{v}}{\partial y} + \frac{\partial \overline{w}}{\partial z} + \frac{\partial \overline{u'}}{\partial x} + \frac{\partial \overline{v'}}{\partial y} + \frac{\partial \overline{w'}}{\partial z} = 0. \tag{2.5}$$

But it is proven that the following terms are zero:

$$\overline{u'} = 0 \quad , \overline{v'} = 0, \quad \overline{w'} = 0. \tag{2.6}$$

In conclusion:

$$\frac{\partial u'}{\partial x} + \frac{\partial v'}{\partial y} + \frac{\partial w'}{\partial z} = 0. \tag{2.7}$$

Which has a direct consequence:

$$\frac{\partial \overline{u}}{\partial x} + \frac{\partial \overline{v}}{\partial y} + \frac{\partial \overline{w}}{\partial z} = 0. \tag{2.8}$$

Eventually, the divergence of the mean velocity component is zero as well the divergence of the fluctuating component is zero. So they both satisfy the equation of continuity for incompressible fluids:

$$\vec{\nabla} \cdot \vec{\overline{q}} = 0 \quad \& \quad \vec{\nabla} \cdot \vec{q'} = 0, \quad \vec{q} = (u, v, w). \tag{2.9}$$

□

2.1.2 Apparent-Reynolds Stresses

By applying the Reynold decomposition in momentum equations of steady Navier-Stokes we can observe:

- Quadratic terms in time average remain unchanged because they are stable over time.
- Linear terms $(\frac{\partial u'}{\partial t}, \frac{\partial^2 u'}{\partial x^2}, ...)$ become zero due to $\overline{u'} = 0$.
- Mixed terms $(\overline{u}u')$ become zero for the same reason as linear terms.

And the momentum equations for a three-dimensional steady-state flow are transformed as follows:

$$\rho\left(\overline{u}\frac{\partial \overline{u}}{\partial x} + \overline{v}\frac{\partial \overline{u}}{\partial y} + \overline{w}\frac{\partial \overline{u}}{\partial z}\right) = -\frac{\partial \overline{p}}{\partial x} + \mu\nabla^2\overline{u} - \rho\left[\frac{\partial \overline{u'}^2}{\partial x} + \frac{\partial \overline{u'v'}}{\partial y} + \frac{\partial \overline{u'w'}}{\partial z}\right]$$

$$\rho\left(\overline{u}\frac{\partial \overline{v}}{\partial x} + \overline{v}\frac{\partial \overline{v}}{\partial y} + \overline{w}\frac{\partial \overline{v}}{\partial z}\right) = -\frac{\partial \overline{p}}{\partial y} + \mu\nabla^2\overline{v} - \rho\left[\frac{\partial \overline{u'v'}}{\partial x} + \frac{\partial \overline{v'}^2}{\partial y} + \frac{\partial \overline{v'w'}}{\partial z}\right]$$

$$\rho\left(\overline{u}\frac{\partial \overline{w}}{\partial x} + \overline{v}\frac{\partial \overline{w}}{\partial y} + \overline{w}\frac{\partial \overline{w}}{\partial z}\right) = -\frac{\partial \overline{p}}{\partial z} + \mu\nabla^2\overline{w} - \rho\left[\frac{\partial \overline{u'w'}}{\partial x} + \frac{\partial \overline{v'w'}}{\partial y} + \frac{\partial \overline{w'}^2}{\partial z}\right]$$

These equations are the same as steady Navier-Stokes for the mean values, but they have some additional terms, due to turbulent fluctuations of the flow. These terms are called turbulent stresses or else known as Reynolds stresses because they have a dimension of stress. They are summed with the viscous terms of Navier-Stokes. So they have a similar influence in the flow, for which they are caused by eddy viscosity [32] and their tensor matrix form is :

$$-\rho\begin{bmatrix} \overline{u'^2} & \overline{u'v'} & \overline{u'w'} \\ \overline{v'u'} & \overline{v'^2} & \overline{v'w'} \\ \overline{w'u'} & \overline{w'v'} & \overline{w'^2} \end{bmatrix}.$$

2.1.3 Stresses Tensor

The relation that is formed between turbulent stress tensors and the turbulent rate of deformations can be expressed as

$$\begin{pmatrix} \sigma'_x & \tau'_{xy} & \tau'_{xz} \\ \tau'_{xy} & \sigma'_y & \tau'_{yz} \\ \tau'_{xz} & \tau'_{yz} & \sigma'_z \end{pmatrix} = -\rho\begin{bmatrix} \overline{u'^2} & \overline{u'v'} & \overline{u'w'} \\ \overline{v'u'} & \overline{v'^2} & \overline{v'w'} \\ \overline{w'u'} & \overline{w'v'} & \overline{w'^2} \end{bmatrix}$$

The tensor is symmetric, because is assumed homogeneous isotropic turbulence. So there are six additional unknowns added in the equations of motion, as a result, the problem becomes under-defined because the number of unknowns is greater than the number of equations. This means that we either need to :

- Generate six additional equations for the apparent stresses, or
- Express stress tensor components in terms of flow variables to make the problem solvable (well-posed) without having to add extra equations.

This challenge is referred to as the Turbulence Closure Problem and it is what motivated researchers over many decades to develop general ways to address closure, which "gave birth" to the turbulence mathematical modeling field. Finally the relation of stresses-rate of deformation [32] are given by:

Perpendicular stresses:

$$\begin{aligned} \sigma_x &= -p + 2\mu\frac{\partial \overline{u}}{\partial x} - \rho\overline{u'}^2, \\ \sigma_y &= -p + 2\mu\frac{\partial \overline{v}}{\partial x} - \rho\overline{v'}^2, \\ \sigma_z &= -p + 2\mu\frac{\partial \overline{w}}{\partial x} - \rho\overline{w'}^2. \end{aligned} \tag{2.10}$$

Shearing stresses:

$$\begin{aligned} \tau_{xy} &= \mu\left(\frac{\partial \overline{u}}{\partial y} + \frac{\partial \overline{v}}{\partial x}\right) - \rho\overline{u'v'}, \\ \tau_{xz} &= \mu\left(\frac{\partial \overline{u}}{\partial z} + \frac{\partial \overline{w}}{\partial x}\right) - \rho\overline{u'w'}, \\ \tau_{yz} &= \mu\left(\frac{\partial \overline{v}}{\partial z} + \frac{\partial \overline{w}}{\partial y}\right) - \rho\overline{v'w'}. \end{aligned} \tag{2.11}$$

Apparent (eddy) stresses are greater than laminar (viscous) stresses, as is verified experimentally. As a result, the latter may be omitted in many cases with a good degree of approximation [32].

2.2 Turbulence Kinetic Energy (TKE)

A useful tool for measuring the intensity of turbulence in a flow is turbulence kinetic energy or TKE, which is widely used in turbulence modeling.

Turbulence kinetic energy (TKE) is a universal quantity used to describe the magnitude of turbulence in fluid flows. It takes place in various sectors, including engineering and atmospheric science [8].

Turbulence kinetic energy is connected with the energy that is related to the random motion of fluid particles within a turbulent flow field. Essentially is a measure of the fluctuations in velocity, and its magnitude directly corresponds to the level of turbulence present in the system. Turbulence kinetic energy is very important in many phenomena such as mixing processes, heat transfer, and pollutant dispersion and is defined as the sum of the three normal Reynolds stresses and multiplied by $\frac{1}{2}$, we denote by symbol k.

$$k = \frac{1}{2}\overline{u_i' u_i'} = \frac{1}{2}(\overline{u'}^2 + \overline{v'}^2 + \overline{w'}^2). \tag{2.12}$$

Many turbulence models seek to predict k but don't predict individual components, assuming that the fluctuations are isotropic: $\overline{u'}^2 \approx \overline{v'}^2 \approx \overline{w'}^2$ [43]. By definion kinetic energy is given by the expression $\frac{1}{2}mv^2$ so:

$$k = \frac{\text{Kinetic Energy}}{\text{unit mass}},$$

in terms of dimensions k is defined as the mean kinetic energy per unit mass for a turbulent flow.

The significance of TKE lies in its ability to approximate the energy cascade from large-scale motions to smaller eddies within a turbulent flow. Accurate measurement of TKE is critical for ratifying and optimizing turbulence models.

Continuing is introduced the TKE Budget equation below [8]. The partial differential equation helps in the understanding of vital parts of the Navier-Stokes and RANS equations such as the turbulent production and advection behavior of the pressure and diffusion terms. To conclude for the stability and the capabilities of flow in production and diffusion the turbulence terms are utilized by analyzing the contribution of each of the above budget terms in equation (2.13). With this analysis, a detailed picture of the turbulent flow behavior can be derived and utilized for complex models such as LES or DNS.

To summarize, the TKE budget refers to the analysis of the different processes that contribute to the generation, transport, and dissipation of the kinetic energy of a flow. The TKE budget equation is derived from the Navier-Stokes equations and it is provided by the following partial differential equation:

$$\frac{\partial k}{\partial t} + \overline{u}_j \frac{\partial k}{\partial x_j} = -\overline{u_i' u_j'} \frac{\partial \overline{u_i}}{\partial x_j} - \nu \overline{\frac{\partial u_i'}{\partial x_j} \frac{\partial u_i'}{\partial x_j}} + \frac{\partial}{\partial x_j} \left[\nu \frac{\partial k}{\partial x_j} - \frac{1}{2} \overline{u_i' u_i' u_j'} - \overline{\frac{p' u_j'}{\rho}} \right], \quad (2.13)$$

where:

- $\frac{\partial k}{\partial t}$ is the local derivative
- $\overline{u}_j \frac{\partial k}{\partial x_j}$ is the advection term.
- $-\overline{u_i' u_j'} \frac{\partial \overline{u_i}}{\partial x_j}$ is a production term.
- $-\nu \overline{\frac{\partial u_i'}{\partial x_j} \frac{\partial u_i'}{\partial x_j}}$ is the turbulent viscous dissipation term (per unit mass), which is usually denoted as ε.
- $\nu \frac{\partial k}{\partial x_j}$ is a molecular diffusion term.
- $-\frac{1}{2} \overline{u_i' u_i' u_j'}$ is the turbulent transport term.
- $-\overline{\frac{p' u_j'}{\rho}}$ is the pressure diffusion term or Buoyancy flux.

2.3 Turbulent Boundary Layer

The turbulent Boundary Layer is a fundamental problem that exists in every flow in nature that includes solid boundaries, it is widely examined by many researchers and it is used in modern Fluid Mechanics, as it is a crucial factor for energy saving and good overall performance of an airfoil.

The system of equations that describe the turbulent B.L., for the two-dimensional, steady-state case is [32]:

$$\begin{gathered} \frac{\partial \overline{u}}{\partial x} + \frac{\partial \overline{v}}{\partial y} = 0, \\ \overline{u} \frac{\partial \overline{u}}{\partial x} + \overline{v} \frac{\partial \overline{u}}{\partial y} = -\frac{1}{\rho} \frac{\partial \overline{p}}{\partial x} + \frac{\partial}{\partial y} \left(\nu \frac{\partial \overline{u}}{\partial y} - \overline{u'v'} \right), \\ \frac{\partial \overline{p}}{\partial y} = 0, \end{gathered} \quad (2.14)$$

with boundary conditions, $y = 0 : \overline{u} = \overline{v} = 0, y \to \infty : \overline{u} = U_\infty$

Remarks:

- Compared to the typical Navier-Stokes equations, the velocity, and pressure terms are replaced by their time averages.
- The term $\frac{\partial}{\partial x}\overline{(v'^2 - u'^2)}$ which is generated by the normal stresses (after replacing the time-averaged terms), due to the boundary layer simplifications, can be ignored.
- Originally, the term $\frac{\partial \overline{p}}{\partial y}$ is equal to $-\frac{\partial \overline{v'^2}}{\partial y}$ but is typically presumed that this term is negligible within the boundary layer(it is roughly 0.4% of free stream dynamic pressure) and as a result, $\frac{\partial \overline{p}}{\partial y} = 0$.
- The inertia terms and the pressure term remain unchanged while the friction term $\nu\frac{\partial^2 u}{\partial y^2}$ is replaced by $\frac{\partial}{\partial y}\left(\nu\frac{\partial \overline{u}}{\partial y} - \overline{u'v'}\right)$. Thus, the laminar viscous force per unite volume $\frac{\partial \tau_l}{\partial y}$ shall be replaced by $\frac{\partial}{\partial y}(\tau_l - \tau_t)$.
- The aforementioned quantity $\tau_t = \varepsilon_t = -\rho\overline{u'v'}$ is the Reynolds stress term (apparent turbulent stress term) [32].

2.4 Eddy Viscosity

Eddy viscosity is crucial and plays a vital role in turbulence mathematical modeling. The first turbulence models were eddy viscosity models and they continue to be used today because of their simplicity, small computational cost, and easy implementation. The first scientist who tried to solve the closure problem was Joseph Valentin Boussinesq to achieve his goal he introduced the concept of eddy viscosity. In 1877 Boussinesq proposed relating the turbulence stresses to the mean flow [43], through an eddy (or turbulent) viscosity, denoted as μ_t. The Reynolds stresses are treated as laminar stress terms, where instead of using fluid viscosity it is replaced with eddy viscosity. Boussinesq's hypothesis is at the heart of eddy viscosity models, which are widely used in the examination and numerical solving of turbulent flows. In practice, Reynolds stress models reduce to eddy viscosity models. Their biggest disadvantage is that they are based on local equilibrium concepts because they consider the transport terms in the governing equations to be negligible so they lack generality [36].

For the simplicity of eddy viscosity in the use of turbulence models, some approaches compute the mixing length, a variable that is related to the mean free path in a gas, via the kinetic theory of gases. In this hypothesis, there is a crucial difference that must be emphasized, molecular viscosity is a property of the fluid, contrariwise to the eddy viscosity, consequential to mixing length, which is a property of the flow. Due to this fact, the eddy viscosity must be determined in advance, in algebraic turbulence models through an algebraic relation between eddy viscosity and length scales of the mean flow. Consequently, algebraic models are incomplete turbulence models since some information for the flow is needed before the simulation. In differential turbulence models, the solution is obtained through some differential equations, for the desired quantities, different for each model, and then obtain the eddy viscosity values. This is not restrictive, for incomplete models, as they have been proven to be very efficient and to be in very good agreement with experimental results in many fluid mechanics fields [43].

2.4.1 Molecular Transport of Momentum

The movement of molecules is responsible for the creation of stresses that needed to be studied to advance in the analysis of turbulent flows. In this section, the momentum transport at the molecular level will be analyzed. An important remark is that molecules and eddies are fundamentally different. The molecular transport is vital for the understanding of the Boussinesq approximation, crucial in turbulence modeling, as it is a cornerstone of a group of models known as eddy viscosity models.

Theorem 2.4.1. *The shear stress resulting from the molecular transport of momentum in a perfect gas is provided by:*

$$\tau_{xy} = \mu \frac{d\overline{u}}{dy}, \tag{2.15}$$

where μ:molecular viscosity, defined as $\mu = \frac{1}{2}\rho v_{th} l_{mfp}$

Proof. In order to prove the following theorem we must examine the microscopic level of fluid mechanics and more specific the molecules movement. In the figure below we consider the flux of momentum across the plane y=0, a molecule is moving with random magnitude and direction. Molecules migrating across y=0 to the upward or downward direction. This motion of a lump

of molecules moving up brings a momentum deficit and vice versa, this process is creating a shear stress τ_{xy} [43].

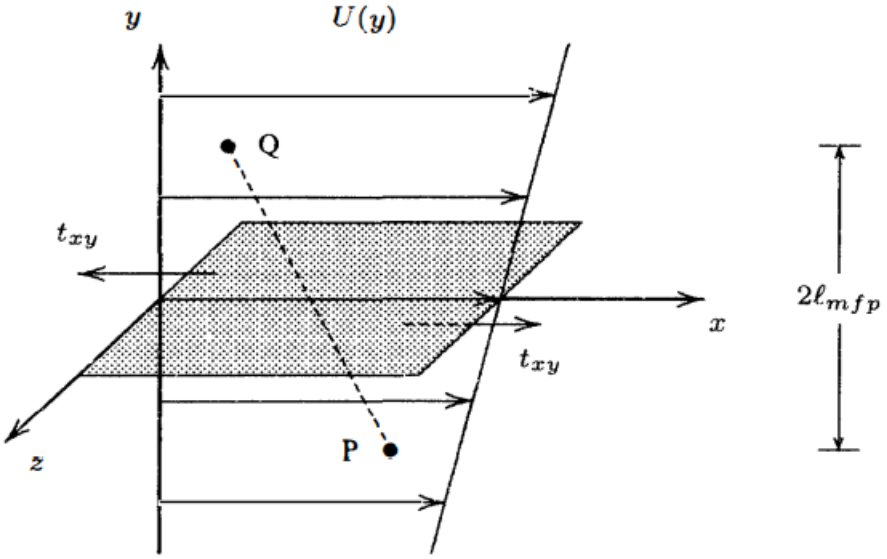

Figure 2.2: Shear flow with two fluid particles (lump of fluid) Q and P [43].

At the molecular level, the decomposition of velocity can be provided by the following expression:

$$u = \overline{u} + u'', \tag{2.16}$$

where $\overline{u}$ is the average velocity and u'' the random molecular motion. The instantaneous flux of a molecular cross $y = 0$ is proportional to the velocity normal to the plane which, for this flow, is v''. So instantaneous flux in x-momentum dp_{xy} across dS normal to the y direction is:

$$dp_{xy} = \rho(\overline{u} + u'')v''dS, \tag{2.17}$$

and by performing an ensemble average over all molecules the result is the following:

$$d\overline{p_{xy}} = \rho\overline{u''v''}dS. \tag{2.18}$$

The stress in $y = 0$ is:

$$\sigma_{xy} = \frac{d\overline{p_{xy}}}{dS}. \tag{2.19}$$

Finally by using $\sigma_{ij} = p\delta_{ij} - \tau_{ij}$, where τ_{ij}: viscous stress tensor the result is the same to the Reynolds-stress tensor.Thus:

$$\tau_{xy} = -\rho\overline{u''v''}. \tag{2.20}$$

Tennekes and Lumley (1972) [38] made a hypothesis, a stress that is generated as a momentum flux can always be written in this form. The only real difference is that, at the macroscopic level, the turbulent fluctuations, u' and v', replace the random molecular fluctuations, u'' and v''. This resemblance is at the heart of the eddy-viscosity approximation by Boussinesq.

Additionally, considering the average number of all lump of molecules moving across the unit area in the positive y direction. By the kinetic theory of gases, it is known that molecular velocities follow the Maxwelian distribution, so all directions are probable, so half of the number of molecules move downward and the other half upwards. For the motion of a lump of molecules, start from a point P crosses the $y = 0$ plane and they cover the distance of one mean free path, the mean free path being the average distance a molecule travels between collisions with other molecules [43]. Each molecule starting from a point P below $y = 0$ brings a momentum deficit of $m[\overline{u(0)} - \overline{u(-l_{mfp})}]$, where m is the molecular mass and l_{mfp} is the mean free path [43]. Hence, the momentum flux from below is:

$$\Delta \mathrm{P}_{-} = \frac{1}{4}\rho u_{th}[\overline{u(0)} - \overline{u(-l_{mfp})}] \approx \frac{1}{4}\rho u_{th} l_{mfp}\frac{d\overline{u}}{dy}, \tag{2.21}$$

where u_{th} is the thermal velocity.
For the final equation (2.21), is used the Taylor expansion of term $\overline{u(-l_{mfp})}$, by taking the two first terms and using the definition of density $\rho = mn$. Similarly, the momentum flux from above is:

$$\Delta \mathrm{P}_{+} = \frac{1}{4}\rho u_{th}[\overline{u(l_{mfp})} - \overline{u(0)}] \approx \frac{1}{4}\rho u_{th} l_{mfp}\frac{d\overline{u}}{dy}. \tag{2.22}$$

So, the final shearing stress is:

$$\tau_{xy} = \Delta \mathrm{P}_{+} + \Delta \mathrm{P}_{-} = \frac{1}{2}\rho u_{th} l_{mfp}\frac{d\overline{u}}{dy}. \tag{2.23}$$

We conclude that the shear stress from the molecular transport of momentum is:

$$\tau_{xy} = \mu\frac{d\overline{u}}{dy}, \tag{2.24}$$

where μ is the molecular viscosity, $\mu = \frac{1}{2}\rho v_{th} l_{mfp}$ □

This last equation (2.24) is the same as the experimental law of Newton in a laminar flow which case is analogous to a perfect gas. The arguments that lead to the last two equations are approximate, but they are very accurate as it is verified experimentally. From the kinetic theory of gases, it is known that an analytical solution yields $\mu = 0.499\rho v_{th} l_{mfp}$. In conclusion, the fact that the Taylor series was used and that the assumption holds that u'' remained Maxwellian does not affect the validity of the equations [43].

2.4.2 Boussinesq's hypothesis

Boussinesq took advantage of this theorem by assuming that turbulent stresses behave like viscosity stresses, which entails that the turbulent stresses are proportional to the velocity gradient.

Definition 1. *The coefficient of proportionality is called the "eddy viscosity" and is defined by:*

$$\tau_{tur} = -\rho\overline{u'v'} = \rho\varepsilon_t \frac{d\overline{u}}{dy}, \tag{2.25}$$

where ε_t is the kinematic eddy viscosity or turbulent kinematic viscosity so that $\varepsilon_t = \dfrac{\mu_t}{\rho}$.

This relation can also be written as:

$$\tau_{tur} = -\rho\overline{u'v'} = \mu_t \frac{d\overline{u}}{dy}, \tag{2.26}$$

where μ_t is a mixing factor for the Reynolds stresses. So, Boussinesq proposed shear stress with strain rate relationship for time-averaged flows of a one-dimensional nature of the form:

$$\tau_{lam} + \tau_{tur} = \rho(\nu + \varepsilon_t)\frac{d\overline{u}}{dy}. \tag{2.27}$$

By Newton's experimental law τ_{lam} can calculated as:

$$\tau_{lam} = \mu \frac{\partial u}{\partial y}. \tag{2.28}$$

The general idea behind (2.27) is that the effect of the turbulent mixing of momentum (τ_{tur}) is analogous to the molecular transport of momentum, which leads to the laminar stress τ_{xy}. Thus we might imagine that the role of turbulence is to increase the effective viscosity from ν to $\nu + \varepsilon_t$, where ε_t is much

greater than ν [8]. The concept of an eddy viscosity is now commonly used for flows of arbitrary complexity, and the three-dimensional generalization of the above equation is:

$$t_{turb} = t_{ij} = -\rho\overline{u_i' u_j'} = \mu_t \left(\frac{\partial \overline{u}_i}{\partial x_j} + \frac{\partial \overline{u}_j}{\partial x_i} \right) - \frac{2}{3}\delta_{ij} k, \tag{2.29}$$

where $k = \frac{1}{2}\overline{u_j' u_i'}$ depicts the turbulent kinetic energy.

2.4.3 Prandtl's mixing length

Definition 2. *The term μ_t is called dynamical eddy viscosity by Prandtl and is calculated by the relation that is given below:*

$$\mu_t = \rho l^2 \left| \frac{\partial \overline{u}}{\partial y} \right|, \tag{2.30}$$

where l is called the mixing length of the turbulent eddies.

Prandtl's mixing length can be modeled in various ways, this is the cornerstone problem of turbulence models, the calculation of this quantity, Prandtl modeled it with the help of mixing length l, a property of the flow. Prandtl's consideration of the mixing length is analogous to the "mean free path" of molecules in the kinetic theory of gases. More specifically, microscopic movement is studied in the kinetic theory of gases of molecules. The use of mixing length by Prandtl leads to the mesoscopic motion of large aggregates of liquid particles study. Near a solid wall, l is approximately proportional to the distance from the wall and Von Karman suggested:

$$l \approx k \cdot y, \tag{2.31}$$

where k is called Von Karman constant ≈ 0.41 after experiments [43].

The choice of length and velocity scale is a big issue in modern times and it is very challenging for scientists. By equation (2.25) it can be derived that the dimensions of $\varepsilon_t \sim$ length$\times$velocity.

By substituting (2.30) in (2.26) :

$$\tau_{tur} = -\rho\overline{u'v'} = \rho l^2 \left| \frac{\partial u}{\partial y} \right| \frac{\partial u}{\partial y}. \tag{2.32}$$

So, it can be observed, from equations (2.23) and (2.32) that there is an analogy, of the mean free path l_{mfp} with the mixing length l and this of the mean molecular speed with the gradient of velocity, this Boussinesq's motivation.

All seems perfect, but the kinetic theory of gases deals with molecules that collide and by definition are discrete, in contrast with turbulence which is a continuous phenomenon. Prandtl in essence proposed that with eddy viscosity certain eddies of macroscopic size are moving as a whole and thus their motion approximate the motion of free molecules of a gas. But these two considerations are different. Since the motion of the molecules of a gas is determined by the temperature of the gas and is not affected by the fluid motion, molecular viscosity is a property of a fluid in contrast with eddy viscosity which isn't. Prandtl with his empirical mixing length l replaced Boussinesq's ε_t and concluded that for flows near solid boundaries, the mixing length is proportional to the distance from the surface. Finally, for free shear flows the mixing length is proportional to the width of the layer δ and it is observed that the mixing length is different for every flow thus someone must know it in advance to obtain a solution, and that is the reason why all models who use eddy viscosity are incomplete.

Another interesting observation is that by substituting (2.25) to (2.14), the two-dimensional, steady-state turbulent boundary layer can also be written in a very useful form that is usually used in computational fluid dynamics:

$$\begin{gathered} \frac{\partial \overline{u}}{\partial x}+\frac{\partial \overline{v}}{\partial y}=0, \\ \overline{u}\frac{\partial \overline{u}}{\partial x}+\overline{v}\frac{\partial \overline{u}}{\partial y}=-\frac{1}{\rho}\frac{\partial \overline{p}}{\partial x}+\frac{\partial}{\partial y}\left[(\nu+\varepsilon_t)\frac{\partial \overline{u}}{\partial y}\right], \\ \frac{\partial \overline{p}}{\partial y}=0. \end{gathered} \tag{2.33}$$

2.5 Turbulence Scales and the Cascade

For turbulence modeling, turbulence scale and cascade is an important topic that is very useful for understanding turbulence. The turbulence scale represents the range of sizes or lengths over which turbulent structures exist within a flow, and these scales can range from large-scale (Integral scales) to small-scale (Kolmogorov scales) eddies. The identification and characterization of

these scales are essential for the development of effective turbulence models.

A fundamental concept associated with turbulence scales is the cascade process. The cascade describes the transfer of energy from larger scales of motion to smaller scales in a turbulent flow as a spectrum because turbulence is a continuum phenomenon and not discrete. These eddies interact and as a result, larger vortices transform into smaller eddies, releasing energy that drives the turbulence at smaller scales. This cascade phenomenon is fundamental for understanding the phenomenon of energy dissipation within turbulent flows, and turbulence models such as the family of Large Eddy Simulation utilize the energy cascade.

Turbulence is made of a continuous spectrum of scales, which varies from large to small eddies. To visualize turbulent flow with a spectrum of scales, it can be translated into a problem of eddies. Turbulent eddy can be defined as a local swirling motion whose scale is quantified by the local turbulent scale or in a more mathematical definition the k-wavelength definition will be introduced. Wavelength resulting from the Fourier transform in the spatial direction [43]. Eddies have a unique feature, larger eddies carry smaller ones so a large eddy can contain multiple, smaller scale, eddies and all of them are moving as one, structure.

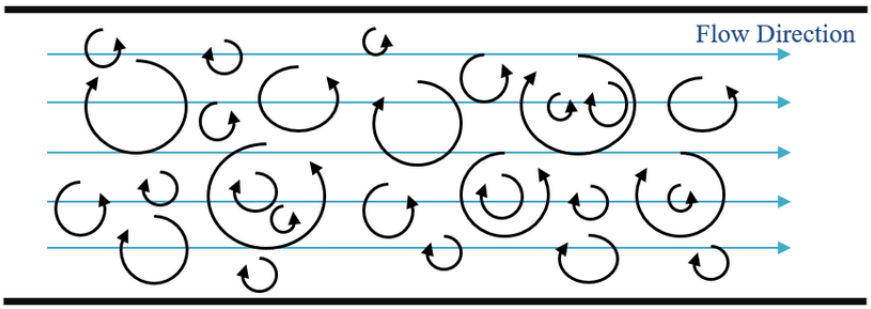

Figure 2.3: Representation of larger eddies carry smaller ones [25].

The second fundamental feature is the cascade process which can be described as a procedure of eddies which, as the turbulence decays, become smaller and so its kinetic energy transfers from large to small eddies. At the final stage, the smallest eddies dissipate into heat or increase of entropy and acoustics through the action of molecular viscosity. So, it can be concluded that similarly to any viscous flow, any turbulent flow is always dissipative [43].

In Figure 2.4 this procedure is being visualized.

As David C Wilcox states "The state of a turbulent flow at a given position depends upon upstream history and cannot be uniquely specified in terms of the local strain-rate tensor as in laminar flow". In a typical boundary layer, the larger eddies are estimated thirty times the width of the flow (thickness of boundary layer) $l \sim 30\delta$ [43].

In conclusion, turbulence behavior is dominated by the large eddies, which are the main factor for the enhanced diffusivity and the stresses in the flow. For the smaller eddies it can be proposed that they dissipate turbulence energy through viscous actions [43] and the rate of dissipation is controlled by the rate at which they receive energy from the larger ones. This is a very important factor in the creation of turbulence models.

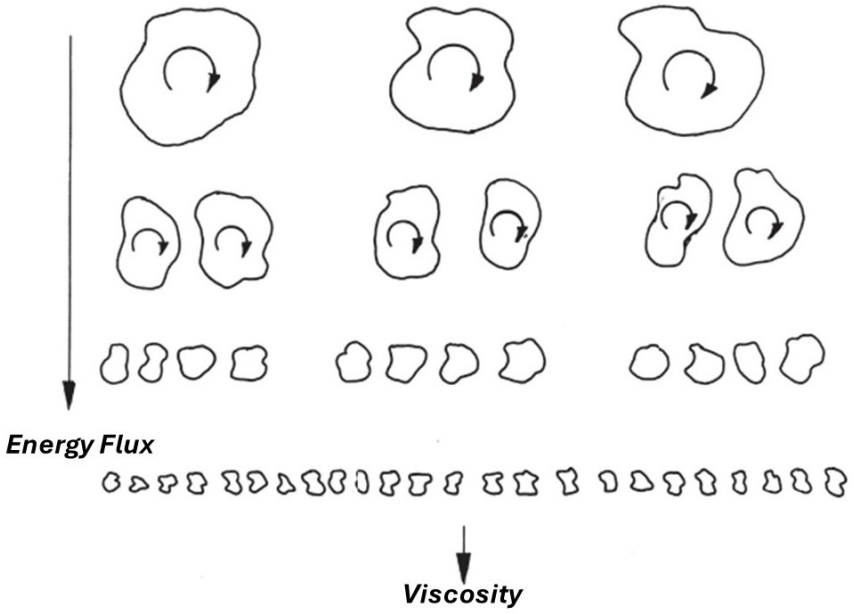

Figure 2.4: Representation of energy cascade with small-medium-big eddies [8].

2.5.1 Kolmogorov's scale

Turbulence is a continuum phenomenon as this follows from the fact that the smallest scales are much larger (orders of magnitude) than the molecular

length scale. In this subsection, it will be analyzed the magnitude of these molecular scales and the physics of turbulence at small scales.

Turbulence Kinetic Energy (TKE) plays a vital role in turbulence, the dissipation of TKE through molecular physics happens at a small time scale in contrast with large eddies where the time scale is large (slow), so the smallest scales are relatively unaffected by the larger ones. Hence the rate at which small eddies dissipate energy through molecular viscosity must be the same as the rate at which smaller eddies receive energy from the large ones, that was the thought of Andre Nikolaevich Kolmogorov through one of the premises that he made in the Universal Equilibrium theory. His results included that the motion of smaller eddies should depend on the rate at which the larger eddies supply energy ε and on the effect of kinematic viscosity.

Definition 3. *Turbulent viscous dissipation per unit mass measuring the energy loss due to the conversion of turbulent kinetic energy into thermal energy within a fluid, per unit mass of the fluid,* ε *is:*

$$\varepsilon = -\frac{dk}{dt} \quad where \quad k : TKE. \tag{2.34}$$

With the help of dimensional analysis, the dimensions of ε are $length^2/time^3$ and so Kolomogorov introduced the following length (η),time (τ) and velocity (v) scales with the help of ε and kinematic viscosity (ν).

$$\eta = (\nu^3/\varepsilon)^{1/4}, \qquad \tau = (\nu/\varepsilon)^{1/2}, \qquad v = (\nu\varepsilon)^{1/4}. \tag{2.35}$$

These small scales are known by the name of their creator, Kolmogorov scales and they are affected only by μ, ν and ε. To understand further the magnitude of how small these scales are, in a typical boundary layer under specific circumstances, the Kolmogorov length scale is $\eta \approx 4.5 \cdot 10^{-4}$ cm, and the mean free path of molecules is $l_{mfp} = 6.3 \cdot 10^{-6}$ cm [43]. So the difference in magnitude is approximately two scales of magnitude. It has been calculated experimentally that:

$$\frac{\eta}{l_{mfp}} \approx 72. \tag{2.36}$$

2.5.2 Kolmogorov's -5/3 Law

As mentioned above, turbulence consists of a spectrum (continuous) of scales, and for its study is convenient to discuss the spectral distribution of

energy. This spectral representation is made through Fourier decomposition into wave numbers κ or in another way into wavelengths $\lambda = 2\pi/\kappa$, where $E(\kappa)$ is the TKE contained between wave numbers κ and $\kappa + d\kappa$, it can be said:

$$k = \int_0^\infty E(\kappa) d\kappa, \tag{2.37}$$

where k is the turbulent kinetic energy per unit mass and $E(\kappa)$ is the energy spectral density (or energy spectrum function) which is connected with the Fourier transform of k. A useful observation that emerges is that:

- Low wave numbers represent the largest scales of energy.
- Large wave numbers represent the smallest scales of energy.

Because large eddies have a strong influence in the turbulence it is observed that $E(\kappa)$ is a function of length(l) and the mean strain rate S [43]. So Taylor in 1935 with the help of dimensional analysis concluded that [37]:

$$\varepsilon \sim \frac{k^{3/2}}{l} \quad \Rightarrow \quad k \sim (\varepsilon l)^{2/3}. \tag{2.38}$$

The characteristic length scale l is the main tool for the simulation of many turbulence models. So in this case it is assumed that there is a wide variance of scales and l is much larger than the Kolmogorov length scale.

$$l \gg \eta. \tag{2.39}$$

With the help of the equations above, it can be created a dimensionless quantity similar to Reynolds number :

$$\frac{\eta u}{\nu} = 1, \tag{2.40}$$

this is expected because the small-scale motion is viscous so the Reynolds number should be small. By substituting (2.35) and (2.38):

$$\frac{l}{\eta} = \frac{l}{(\nu^3/\varepsilon)^{1/4}} \sim \frac{l(k^{3/2}/l)^{1/4}}{\nu^{3/4}} \sim Re_T^{3/4}, \tag{2.41}$$

where $Re_T = \frac{k^{1/2} l}{\nu}$. This quantity is called turbulence Reynolds number. Thus with the assumption that $l \gg \eta$, it can be resulted that Re_T is large and this is expected as an inviolable condition for turbulence is a high Reynolds number,

$$Re_T \gg 1. \tag{2.42}$$

Finally, with Kolmogorov's assumption of a wide separation of scales through turbulence, he added that for large Reynolds there is a large number of scales between the largest and smallest eddies for which the cascade process is independent of the statistics of the energy-containing eddies and the direct effects of molecular viscosity, so l and ν can be ignored [43]. So, he concluded with the famous Kolmogorov's -5/3 Law :

Theorem 2.5.1. *The Kolmogorov's -5/3 Law is:*

$$E(\kappa) = C_K \varepsilon^{2/3} \kappa^{-5/3}, \quad \frac{1}{l} \ll \kappa \ll \frac{1}{\eta}, \tag{2.43}$$

where C_K is the Kolmogorov constant and κ is the wavenumber.

This law has been confirmed experimentally and can be visualized in Figure 2.5. It can be stated that spatial scales (eddies) are divided into three subranges, regarding their energy spectrum. In this figure, three regions can be pointed out:

1. The region of energy containing large eddies which are referred to as the integral scale.
2. The mid-range which is between large and small ones where the energy spectrum is calculated by the -5/3 Kolmogorov's Law.
3. The small eddies region where the eddies dissipate when they reach the Kolmogorov scale.

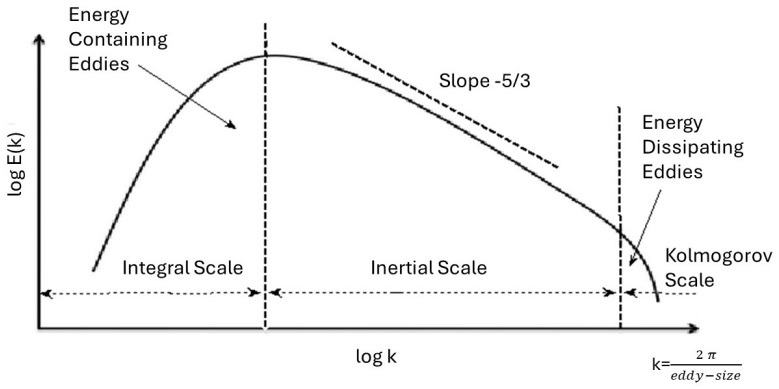

Figure 2.5: Energy spectrum for a turbulent flow [35].

In turbulence simulations, a widely used concept is this of fully turbulent flow. As flow transitions, from laminar to turbulent with the help of a grid into the path of a laminar flow, as it can be seen in the figure 2.6(a), a field of turbulence is generated. Initially, vortices are starting to create, as it is observed in 2.6(b)-stage(i) and after this, stage(ii) follows where we find a field of fully developed turbulence. This region contains the full range of scales from the bigger eddies (integral scale) to the smaller ones, the most dissipative eddies (Kolmogorov's scale). This state of turbulence is also referred to as the asymptotic state of turbulence. Additionally, we have the freely evolving or freely decaying turbulence 2.6(b)-stage(iii) which is a continuation of stage(ii), in this region the larger eddies dominate the turbulence as the smaller ones decay faster. Finally, there is a stage(iv) where the turbulent flow is going to a complicated laminar flow which is not of importance to discuss and is not shown in the Figure 2.6 [8]. In 2.6(c) it can be seen the flow visualization of grid turbulence using smoke from Davidson [8] which experimentally confirms the stages(i-iii).

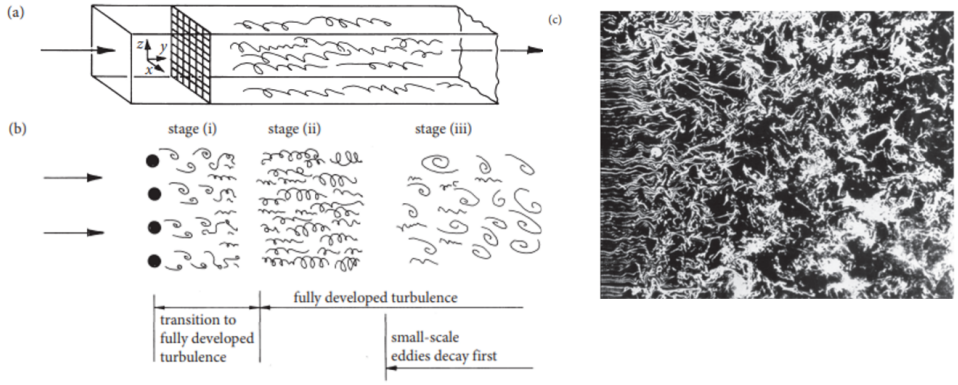

Figure 2.6: (a) Generation of grid turbulence. (b) Visualization of the various stages of development of grid turbulence. (c) Flow visualization of grid turbulence using smoke [8].

2.6 Law of the Wall

The law of the wall is an empirically determined relationship in turbulent flows near walls or more general bounded flows. It is very useful for turbulence mathematical modeling, it is discovered experimentally and it is valid for all

types of flows (internal or external). Is interpreted as the streamwise velocity in the flow near the wall changes logarithmically with distance from the surface $u \sim log(y)$. This result is known as the law of the wall or universal law. It can be also observed, in high Reynolds numbers, that the pressure gradient very close to the wall is very small [43].

The behavior of the flow close to the surface in a turbulent flow is affected by several factors. The first is the rate at which momentum is transferred to the surface, per unit area per unit of time, which is equal to the local shear stress, τ, also by molecular diffusion of momentum, which plays a crucial role close to the boundary. In the far region from the boundary, the details of the eddies are of little importance to the near-wall flow statistics [43]. The shear stress in turbulent flow is known and it is provided by the relation:

$$\tau_w = \mu \frac{\partial \overline{u}}{\partial y} - \rho \overline{u'v'}, \tag{2.44}$$

the turbulent fluctuation can be erased because near the wall the eddies are very small (and increase with the distance from the wall) so by mixing length of Prandtl $l \ll 1$ we consider the term $\rho \overline{u'v'} = 0$.

It is verified experimentally that eddies close to the wall are small and grow with the distance from the wall. This arises from the fact that δ increases with Reynolds number and this creates a wide variety of scales in high Reynolds. Although τ varies near the surface, the variation with distance from the surface, y, is fairly slow. Hence, for the dimensional-analysis arguments to follow, the surface shear stress, τ_w, can be used in place of the local shear stress. Since turbulence behaves the same in gases as in liquids, it is reasonable, to begin with, $\frac{\tau_w}{\rho}$ and kinematic viscosity, $\nu = \frac{\mu}{\rho}$, as primary dimensional quantities, effectively eliminating fluid density, ρ, as a primary dimensional quantity.

The next step is to examine the dimensions of $\frac{\tau_w}{\rho}$, it is observed that they are $(length\ /\ time)^2$. So by using the square root, it is derived a new velocity known as friction velocity:

$$u_\tau = \sqrt{\frac{\tau_w}{\rho}}, \tag{2.45}$$

with dimension $length\ /\ time$. This quantity is important because it defines a velocity scale that represents velocities close to the wall. It also derived the quantity ν/u_τ which is a length scale because the dimensions of kinematic viscosity(ν) are $length^2\ /\ time$ and it follows that ν/u_τ has a dimension of $length$. The next step is to introduce a correlation between $\dfrac{\partial \overline{u}}{\partial y}$ and u_τ, $\dfrac{\nu}{u_\tau}$.The

result with the help of dimensional analysis is:

$$\frac{\partial \overline{u}}{\partial y} = \frac{u_\tau}{y} F\left(\frac{u_\tau y}{\nu}\right), \tag{2.46}$$

where $F(u_\tau y/\nu)$ is presumed to be a universal function. Many scientists engaged with the introduction of this function by gathering data about various boundary layers and more especially Coles and Hirst indicate that as a good leading order approximation:

$$F(u_\tau y/\nu) \to \frac{1}{k} \quad \text{as} \quad \frac{u_\tau y}{\nu} \to \infty, \tag{2.47}$$

where k: Von Karman's constant. This constant is dimensionless and in recent years is calculated experimentally between 0.35-0.42 in most cases it is universally accepted as $k \approx 0.41$. The fact that function $F(u_\tau y/\nu)$ has a constant value is valid with the consideration that viscous effects decreases as it moves away from the boundary wall moving towards the potential flow [43].

Another very important result follows from integrating 2.46 over y:

$$\frac{\overline{u}}{u_\tau} = \frac{1}{k} ln\left(\frac{u_\tau y}{\nu}\right) + c, \tag{2.48}$$

where c is a dimensionless constant with value $c \approx 0.5$ but it depends in some cases on the wall roughness. This last equation (2.48) is the famous "Law of the Wall" or else "Logarithmic Law" and it is vital in simulations near solid boundaries [43]. Dimensionless quantities are additionally defined :

$$u^+ = \frac{\overline{u}}{u_\tau} \quad \text{and} \quad y^+ = \frac{u_\tau y}{\nu}. \tag{2.49}$$

Theorem 2.6.1. *In viscous sublayer, for $y^+ < 5$ the following hold, $u^+ = y^+$.*

Proof. For the region close to the surface of the viscous sublayer it is proven that:

$$\tau_w = \mu \frac{\partial \overline{u}}{\partial y} - \cancel{\rho \overline{u'v'}} \Rightarrow \overline{u} = \frac{\tau_w y}{\mu}. \tag{2.50}$$

From (2.49)

$$\overline{u} = \frac{u^+}{u_\tau} \quad \text{and} \quad y = \frac{y^+ v}{u_\tau}. \tag{2.51}$$

By substituting (2.51) to (2.50):

$$\overline{u}u_\tau = \frac{t_w y^+ v}{\mu u_\tau} \Rightarrow u^+ = \frac{\tau_w \mu \rho y^+}{\mu \rho t_w} \Rightarrow u^+ = y^+. \tag{2.52}$$

□

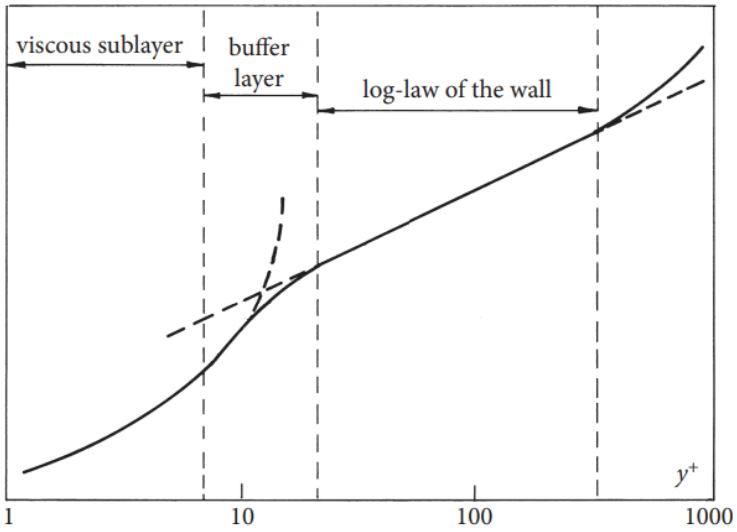

Figure 2.7: Visualization of the Log Law [8].

Remark:

The graph can be divided into 3 regions:

- Very close to the wall viscous forces dominate, this region is called the viscous sublayer, we proved that in this region $u^+ = y^+$ and additionally it is validated experimentally is discovered that this region is for $y^+ < 5$. In this region the Reynolds shear stress is insignificant compared with the viscous stress. For $5 < y^+ < 30$ exists the buffer layer which is a transitional region.
- The next area for $y^+ > 30$ is called the Log Layer and in this region exists the law of the wall and the equation (2.48) hold.
- Eventually, the "defect layer" or outer layer is the region where u^+ reaches the free stream velocity (u_∞) where the effect of viscosity is negligible.

- In summary, the Law of the Wall is a specific empirical relationship used to describe the velocity profile in the turbulent boundary layer near a solid wall.

2.7 Velocity Distribution in Turbulent B.L.

To obtain the behavior of velocity distribution in the turbulent boundary layer, Prandtl's mixing length hypothesis is used to divide the profile into three major zones:

- The region that is close to the boundary and is influenced by the presence of the wall is called the Inner Region or Near-wall Region. It is important to note that only 15% of the turbulent boundary thickness is found at the top of the Near-wall zone.
- As a result, the Near-wall region can be divided into two sub-zones:
  - A thin zone, near the wall where the boundary layer is practically laminar, is called Laminar Sublayer. The reasoning behind this phenomenon is mostly because, within the region, turbulence is suppressed by viscosity.
  - The zone at the end of the laminar sublayer, where the turbulent effect starts to increase but the shear stresses effects still exist and though the laminar influence is still present, is called Buffer Zone.
  - The free stream turbulent effects slowly increase in strength through the inner layer, and the laminar behavior is lost, although the presence of the wall still influences the flow
- The zone where the Near-Wall region transitions to the Outer Layer is called the Overlap layer
- Beyond the Near-wall region is the edge of the boundary layer, a zone where free stream turbulence effects dominate the flow and is called the Outer Layer or Defect Layer.

This distribution can be visualized in Figure 2.8, in which the distinction of the layers is highlighted. This visualization is important in applications and in the understanding of turbulence modeling.

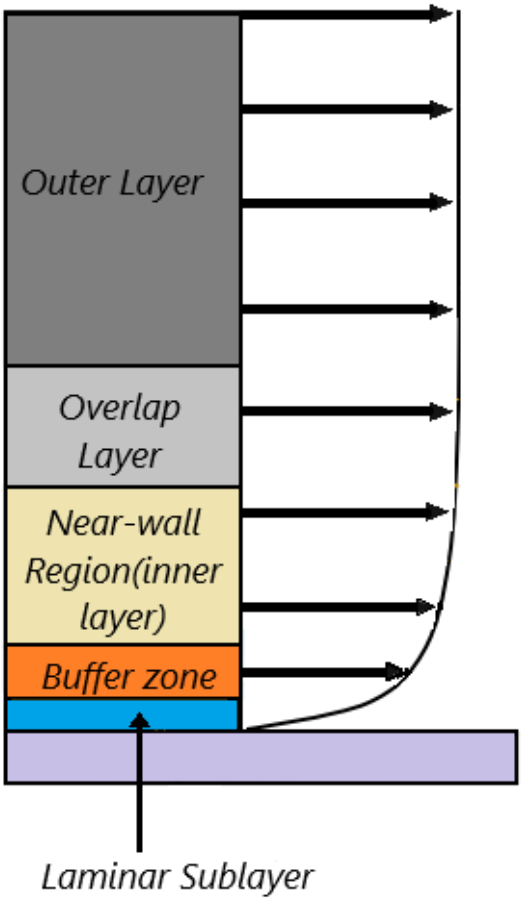

Figure 2.8: Turbulent Boundary Layer Velocity Distribution.

CHAPTER 3

Turbulence Models

In this chapter, it will be presented the most prevalent turbulence models, which are utilized to solve the RANS closure problem. The closure problem refers to the procedure, in solving the RANS equations, or the process of solving any variation of Navier Stokes equations with the utilization of Reynolds decomposition. As presented in the previous chapter RANS equations for the three-dimensional case consist of three momentum and the conservation of mass equations, but the number of unknown variables is ten. Therefore, to solve these equations there are two options, the first one is to articulate the stress tensor components regarding flow variables, which is what algebraic or else zero equation models do, the second option is to add more PDEs in the RANS system, to calculate some selected variables, that describe properties of the flow, such as turbulent kinetic energy or energy dissipation, and finally with the use of these additional variables the stress tensor can be calculated as a function of the latter.

Turbulence models are at the heart of turbulence modeling in pursuit of getting the numerical solution, and they occupy scientists until today with great discoveries of new elegant mathematical models. Many of them evolve existing models or modify them to increase accuracy, some even discover new interesting ways to solve RANS by creating original modern ones. A thorough understanding of the basic principles governing turbulent flow, as described in the previous chapter, is pivotal for comprehending the function of these models and for this reason, the great scientific discoveries in the field are made by very experienced and renowned scientists.

The absence of advanced computers, in the past, forced researchers to limit the study of turbulent flow problems to simple geometries. At first, the initial tries to predict the B.L. were empirical and were based on algebraic equations, by the middle of this century, a leap forward in computers took place. This development had a tremendous result, since the mid-60s the development of

models based on some partial differential equations. The development of computers but also the need to study turbulent flow in complex geometries and large problems in terms of space, have forced scientists, over the decades, to develop enough turbulence models approximating this complex phenomenon. Some of these family of models are:

1. **Algebraic or zero-equation models.** These models use algebraic equations-relations between the eddy viscosity and some properties of the flow to calculate the Reynolds stress tensor (mixing length theory).

2. **One equation models.** These models use a partial differential equation for the turbulent viscosity along with the mean flow equations.

3. **Two-equation models.** They are models that use an additional partial differential equation from the previous ones. That is, except for the partial differential equation for turbulent velocity(fluctuating parts) also use one more equation for an additional parameter e.g. ω, ε.

4. **Models of shear equations.** These models use some differential equations for all terms of the Reynolds stress tensor.

5. **Large Eddy Simulation - LES.** In that method, calculations are made for the three-dimensional, time-dependent structure of large eddies, as well as the use of RANS equations for the small energy scales of turbulence.

6. **Direct Numerical Simulation - DNS.** In that method no turbulence model is used, the complete spectrum of turbulence scales is resolved from the smallest eddies (Kolmogorov's scale) to large energy-bearing eddies (Integral scale) via stress tensor, it is extremely computationally expensive.

The most simple of all turbulence models are characterized as algebraic, they are the oldest and simplest in understanding and implementation, their great advantage is their correctness which is confirmed by experiments combined with their easy application in scientific computer programs. Nowadays these models stop to evolve as the scientific community exhausts their potential by hitting the peak of their amplifiers. The most popular models, which are still used by scientists, are the Cebeci-Smith and the Baldwin-Lomax which is an improved version of the previous one. One or two-equation models use partial differential equations as an advanced evolution of algebraic ones to achieve

better accuracy in numerical solutions of turbulence. The models most commonly employed by scientists are the two-equations models and hybrid models that include two-equation models, which are the most precise out of the three above categories and they are evolving with the help of the academic community, in their journey for optimal solutions in many real-world applications like flows near airfoils, airplanes in fields such as hydrodynamics, hemodynamics, aerodynamics and many others. These methods are still in progress and have a great perspective on the effort being made for better and more precise results. Finally, there is the LES, it seems that this is the technique that will be able to accurately handle the complex and difficult flows in geometry with the exchange of the large computational cost and DNS which resolves all scales of energy but has a huge cost that only a lucky few can use due to the titanic computing power they require.

3.1 Algebraic Models

Algebraic models like all turbulence models are divided into two categories the differential and the integral ones. The differential models have a direct hypothesis for the turbulent shear stresses in every point and they are seeking the solution of the equations, algebraic or differential, that describe the problem. On the other side, integral models contain integral parameters of the boundary layer such as momentum thickness or coefficient of skin friction drag. The advantage of integral models is that direct resolution of partial differential equations is avoided, something that is very useful because in most cases this solution is very difficult or even impossible to acquire [45].

3.1.1 Cebeci-Smith Model

Cebeci-Smith model calculates the turbulent kinematic viscosity ε_t, so it is an eddy viscosity model [4]. This model produces quite accurate results as its correctness has been confirmed by experimental data in many different types of flows. It has also been confirmed to achieve accurate results for a lot of physical applications that concern engineers. It is widely used for boundary layer simulation and in a wide variety of fluid flows such as simulations near a solid boundary. The heart of this model is that ε_t is a bifurcated function, particularly the flow field in the boundary layer consisting of internal and external regions, with each region having its viscosity formula. This model is described in detail in [3]. More specifically, the turbulent kinematic viscosity

is given by the relation:

$$\varepsilon_t = \begin{cases} (\varepsilon_t)_i & ,\text{if} \quad y \leq y_{crossover}, \\ (\varepsilon_t)_o & ,\text{if} \quad y > y_{crossover}, \end{cases}$$

where $(\varepsilon_t)_i$ is the inner eddy viscosity, $(\varepsilon_t)_o$ is the outer and $y_{crossover}$ is the smallest distance from the surface where $(\varepsilon_t)_i = (\varepsilon_t)_o$. Eddy viscosity in inner regions, for the two dimensions case, is given by:

$$(\varepsilon_t)_i = l^2 \left| \frac{\partial u}{\partial y} \right| \gamma_{tr} \gamma. \tag{3.1}$$

For completeness, the model must additionally relate the length l to the geometry flow characteristics, as it is said the algebraic models are incomplete. The main parameter is the distance from the wall, so Prandtl's and Karman's hypothesis (2.30) and (2.31) was later modified by Van Driest (1956) with the purpose of all these expressions to described by a single function, so by including a damping function to improve precision:

$$l = ky \left[1 - exp\left(-\frac{y^+}{A^+} \right) \right], \tag{3.2}$$

where k is the Von Karman constant, and constant A^+ depends on the conditions of the flow such as the pressure gradient, wall roughness, etc. Its value for a smooth impervious plate is equal to 26. Likewise, the Van Driest damping coefficient can be different than 26 for special conditions and approached as:

$$A^+ = 26 \frac{\nu}{N} u_\tau^{-1}, \qquad N = \left[\frac{p^+}{u_w^+} [1 - \exp(11.8u^+)] + \exp(11.8u^+) \right]^{1/2}, \tag{3.3}$$

to improve the estimation accuracy for pressure gradient boundary layers, for incompressible flows. In compressible flows, damping coefficient A^+ will be multiplied by $\left(\frac{\rho}{\rho_w}\right)^{1/2}$.
Quantities γ_{tr} and γ are given by:

$$\gamma_{tr} = 1 - exp\left[-G_{tr}(x - x_{tr}) \int_{x_{tr}}^{x} \frac{dx}{u_e} \right] \quad ,\gamma = F_K, \tag{3.4}$$

$$\text{with} \quad G_{tr} = 8.33 \cdot 10^{-4} \frac{u_e^3}{\nu_e^2} (R_x)^{-1.34} \quad , R_x = \frac{u_e x}{\nu_e}. \tag{3.5}$$

The term γ_{tr} is an intermittency factor that is being used for the transition region from laminar to turbulent flow. The other term γ, in literature, is being named as F_K, is a second intermittency factor that is used for the reason that in the region of free stream, turbulence becomes discontinuous. Additionally, the term G_{tr} has dimensions of $velocity \times (length)^2$ and is calculated at the point of transition of the flow from laminar to turbulent.

Finally, the eddy viscosity in outer regions is given by:

$$(\varepsilon_t)_o = K \left| \int_0^\infty (u_e - u) dy \right| \gamma_{tr} \gamma, \tag{3.6}$$

where $K = 0.0168$ is the Clauser's constant and the Klebanoff intermittency function $F_K = \gamma$:

$$F_K = \left[1 + 5.5 \left(\frac{y}{\delta} \right)^6 \right]^{-1}. \tag{3.7}$$

F_K is utilized to deal with the discontinuities created due to the iterative transition from laminar to turbulent flow in a B.L.

3.1.2 Baldwin-Lomax Model

The Baldwin-Lomax model was created for advanced flows where the boundary layer thickness, δ, and displacement thickness, δ_v^*, are difficult to determine. The great advantage of this model is that it is created to avoid determining the edge of the boundary layer of the Cebeci-Smith model. This model shares the same principle as that of C-S, because it consists of an internal and an external area for the modeling of turbulent kinematic viscosity, with each region having its unique type for it. More specifically, the turbulent kinematic viscosity is defined as:

$$\varepsilon_t = \begin{cases} (\varepsilon_t)_i & \text{, if} \quad y \leq y_{crossover} \\ (\varepsilon_t)_o & \text{, if} \quad y > y_{crossover}. \end{cases}$$

For two-dimensional flows and for the internal region, Baldwin-Lomax considers, essentially, Prandtl-Van Driest modeling, given by the relation:

$$(\varepsilon_t)_i = l^2 |\overline{\omega}|, \qquad y \leq y_{crossover}, \tag{3.8}$$

where l is the mixing length which is provided by the expression:

$$l = ky \left[1 - exp \left(-\frac{y^+}{A^+} \right) \right], \tag{3.9}$$

and $|\overline{\omega}|$ is the vorticity vector for dimensional flows (two and three dimensional). For three dimensional flows $|\overline{\omega}|$ is given by:

$$|\overline{\omega}| = \sqrt{\left(\frac{\partial u}{\partial y} - \frac{\partial v}{\partial x}\right)^2 + \left(\frac{\partial v}{\partial z} - \frac{\partial w}{\partial y}\right)^2 + \left(\frac{\partial w}{\partial x} - \frac{\partial u}{\partial z}\right)^2}, \tag{3.10}$$

where u, v, w are the velocity components. For the two dimension case, the vorticity is given by:

$$|\overline{\omega}| = \left|\frac{\partial u}{\partial y} - \frac{\partial v}{\partial x}\right|, \tag{3.11}$$

where u, v are the components of the velocity in x and y direction. By using the boundary layer assumptions for two dimensional flows $\left(\frac{\partial v}{\partial x} \ll \frac{\partial u}{\partial y}\right)$ vorticity yields as:

$$|\overline{\omega}| = \left|\frac{\partial u}{\partial y}\right|. \tag{3.12}$$

For $(\varepsilon_t)_o$ is being used the Clauser constant $K = 0.0168$ and considered as:

$$(\varepsilon_t)_o = KC_{\mathrm{CP}}F_{\mathrm{WAKE}}F_{\mathrm{K}}, \qquad y > y_{crossover}, \tag{3.13}$$

where F_K is the Klebanoff intermittency function, $C_{CP} = 1.6$ is a constant and F_{WAKE} is defined as:

$$F_{\mathrm{WAKE}} = \begin{cases} y_{\mathrm{MAX}}F_{\mathrm{MAX}} \\ \text{or} \\ C_{\mathrm{WK}}y_{\mathrm{MAX}}U^2_{\mathrm{DIF}}/F_{\mathrm{MAX}}, \end{cases} \tag{3.14}$$

where $C_{\mathrm{WK}} = 0.25$, for the selection of F_{WAKE} every time it is used the smaller quantity of equation (3.14). Quantities y_{MAX} and F_{MAX} are determined by:

$$F(y) = y|\overline{\omega}|\left[1 - exp\left(-\frac{y^+}{A^+}\right)\right], \tag{3.15}$$

In case of a wake (the region of recirculating flow immediately behind a moving or stationary blunt body, caused by viscosity) quantity $exp\left(-\frac{y^+}{A^+}\right)$ is zero, F_{MAX} is the maximum of $F(y)$ and y_{MAX} is the point of y which $F(y)$ is maximum. The discontinuous Klebanoff intermittency function F_{KLEB} is defined as:

$$F_{\mathrm{KLEB}}(y) = \left[1 + 5.5\left(\frac{C_{\mathrm{KLEB}.}y}{y_{\mathrm{MAX}}}\right)^6\right]^{-1}, \tag{3.16}$$

where $C_{\mathrm{KLEB}} = 0.3$. Finally U_{DIF} is the difference between maximum and minimum speed. So, for two-dimensional flows it is provided by the expression:

$$U_{\mathrm{DIF}} = (\sqrt{u^2 + v^2})_{\mathrm{MAX}} - (\sqrt{u^2 + v^2})_{\mathrm{MIN}}. \tag{3.17}$$

The term $(\sqrt{u^2 + v^2})_{\mathrm{MIN}}$ is always zero except in the case of a wake, for boundary layers it is always zero. The equations ((3.12)-(3.14)) that calculate eddy viscosity in the outer region can be used in a wake or a boundary layer with or without separation. The terms $y_{\mathrm{MAX}} \times F_{\mathrm{MAX}}$ is replacing $\delta_v^* U_e$ and $y_{\mathrm{MAX}} U_{\mathrm{DIF}}^2 / F_{\mathrm{MAX}}$ is replacing δU_{DIF} in C-S modeling.

The main difference between B-L and C-S is that in B-L the calculation of the edge of the boundary layer is omitted due to the use of vorticity, to determine the scale of various lengths characteristic of the boundary layer.

These two models are the most popular algebraic models, their results have been verified and they yield quite accurate results for applications such as fully developed channel flow and flow over a solid boundary and these models stem from Prandtl's mixing length theory. A notable remark is that in channel flows even the smallest difference in a model's prediction for Reynolds stress can direct to a different velocity profile and this is a common dilemma that is treated differently in each turbulent case. The results from these models are also reasonably well for mild adverse pressure gradients and not very intense pressure gradients [43].

Their disadvantage is located in the accuracy of separated flows, because of their incapacity to consider flow history effects since the turbulent eddies near separation occur in a time scale independent of the mean strain rate. Tries to avoid this problem have been made by some modified models such as Johnson and King [13] which solve an extra differential equation and it is defined as a half-equation model.

3.2 One equation Models

The development of one-equation models came after the creation of algebraic models, since the mixing length is based on correlations of simple shear flows, its physical application is limited and it is not accurate enough for very complex flows, therefore, the use of more advanced turbulence models is required. The first who tried this were Prandtl and Kolmogorov, they proposed that the turbulent viscosity has to be described by a differential equation

rather than an algebraic model. More especially they proposed a correlation between eddy viscosity and turbulent kinetic energy and not the gradient of velocity or vorticity as C-S and B-L models perform. One equation models are more accurate and more complex than algebraic as they solve an extra partial differential equation. Nowadays these models have been abandoned as they are less accurate than two-equation turbulence models.

Many models have been proposed through time with the most popular being the Spalart-Allmaras model which was developed in the early 90s and is known for its cheap computational cost with good accuracy in comparison with experimental data. Baldwin-Barth is a modern model that simulates flows which is widely being used for large Reynolds numbers.

3.3 Two equations Models

Two equations models are the most popular and widely used family of turbulence models. The researchers need to eliminate the calculation of mixing length, related to its position within the flow, which led to the creation of two-equation turbulence models. These models consist of two transport equations to describe flow properties due to turbulence. This allows a two-equation model to account for effects like convection and diffusion of turbulent energy. These turbulence models continue to make an impact in research and modern two-equation models are in the process of continued development. At most times the first variable is, calculated by the first partial differential equation, k TKE, this is not pejorative a lot of models don't use TKE. The choice of the second variable varies across turbulence models. The most common is ω which is the specific dissipation rate or ε, turbulent dissipation [43]. A lot of models with modified variables have been proposed as these of Robinson-Harris-Hassan [30] for axisymmetric and planar free shear flows k-ζ model where ζ is enstrophy, or Coakley [6] who developed $k^{1/2} - \omega$ model for the compressible Navier-Stokes equations.

This family of turbulence models has been the main tool in turbulence CFD development through the past four decades. The vital difference between one and two-equation models is the incompleteness that characterized the one-equation models in contrast with two-equation models which are complete since they calculate for both k and length scale. In this thesis, it will be presented analytically both the $k - \varepsilon$ model and $k - \omega$, as two cornerstone models of the family of two-equation models.

3.3.1 The $k-\varepsilon$ Model

In this section will introduce the three most popular $k-\varepsilon$ versions, Standard, RNG, and Realizable, these three models have a similar structure since they use two transport equations for the determination of k and ε. Their greatest differences are about the turbulent viscosity (μ_t) calculation, the importance of the Prandtl number in the equations (for flows with heat exchange), and the generation and destruction terms in the ε equations. In general, these three versions of this model are very similar and each is an improved version of the previous one, either for better accuracy or for the expansion in a wider range of flows.

The first version, which will be analytically described, is the Standard $k-\varepsilon$ model, its robustness, low computational cost, and quite a good accuracy for a broad spectrum of turbulent flow justify the significant utilization by the scientific community. It is a semi-empirical model since the transport equation for ε is obtained using physical reasoning. In the derivation of the $k-\varepsilon$ model, the assumption is that the flow is fully turbulent and the effect of molecular viscosity is negligible, so it is valid only for full turbulent flows [17]. It does not perform well for complex flows, like flows that involve great pressure gradient, separation, and strong streamline curvature. The weakness of this model is the insensitivity to flows with adverse pressure gradients and the numerical stiffness when equations are integrated through the viscous sublayer which is treated with damping functions that have stability issues [20].

The transport equations of the Standard $k-\varepsilon$ model for the turbulence kinetic energy k and its rate of dissipation ε yields by the following PDE's:

$$\frac{\partial}{\partial t}(\rho k)+\frac{\partial}{\partial x_i}(\rho k u_i)=\frac{\partial}{\partial x_j}\left[\left(\mu+\frac{\mu_t}{\sigma_k}\right)\frac{\partial k}{\partial x_j}\right]+P_k+P_b-\rho\varepsilon-Y_M+S_k \quad (3.18)$$

$$\frac{\partial}{\partial t}(\rho\epsilon)+\frac{\partial}{\partial x_i}(\rho\varepsilon u_i)=\frac{\partial}{\partial x_j}\left[\left(\mu+\frac{\mu_t}{\sigma_\varepsilon}\right)\frac{\partial \varepsilon}{\partial x_j}\right]+C_{1\varepsilon}\frac{\varepsilon}{k}\left(P_k+C_{3\varepsilon}P_b\right) \quad (3.19)$$
$$-C_{2\varepsilon}\rho\frac{\varepsilon^2}{k}+S_\varepsilon.$$

The calculation of turbulent viscosity is given by:

$$\mu_t=\rho C_\mu\frac{k^2}{\varepsilon}, \quad (3.20)$$

where ρ: density, k: TKE, ε: rate of dissipation and C_μ: constant. The term P_k stands for the production:

$$P_k = -\rho\overline{u_i' u_j'}\frac{\partial u_j}{\partial x_i}. \tag{3.21}$$

The effect of buoyancy:

$$P_b = \beta g_i \frac{\mu_t}{\mathrm{Pr}_t}\frac{\partial T}{\partial x_i}, \tag{3.22}$$

where Pr_t is the turbulent Prandtl number for energy and g_i is the component of the gravitational vector in the ith direction. For the standard and realizable - models, the default value of Pr_t is 0.85. The coefficient of thermal expansion, β , is defined as:

$$\beta = -\frac{1}{\rho}\left(\frac{\partial \rho}{\partial T}\right)_p. \tag{3.23}$$

Finally, the Standard model constants are:

$$C_{1\varepsilon} = 1.44, \quad C_{2\varepsilon} = 1.92, \quad C_\mu = 0.09, \quad \sigma_k = 1.0, \quad \sigma_\varepsilon = 1.3 \quad C_{1\varepsilon} = -0.33,$$

these values have been determined from experimental data with fluids like air or water for a wide range of turbulent shear flows.

In the equations above the term P_k describes the generation of TKE due to the mean velocity gradients, the term P_b describes the generation of TKE due to buoyancy and Y_M represents the contribution of the fluctuating dilatation in compressible turbulence to the overall dissipation rate [17].

The next version of $k-\varepsilon$ model is the RNG which uses renormalization group theory, a statistical technique. The difference with the Standard version is that it solves an extra differential equation for turbulent viscosity (μ_t) but for high Reynolds number the turbulent viscosity is calculated as the Standard $k-\varepsilon$ method. The main advantage of this model in comparison with the Standard version is that the RNG has an extra term in the ε transport equation which increase significantly the accuracy for rapidly strained flows. The effects of swirl are also included in RNG which means greater accuracy for swirling flows. Finally, the Standard version is a high-Reynolds model in contrast with RNG which has a special formula for the calculation of viscosity for low-Reynolds which makes it more popular and widely used for this case. However, the accuracy of this depends on the appropriate treatment of the near-wall region.

Last but not least is the Realizable $k-\varepsilon$ method which is the latest of the three versions and has been verified for a wide range of flows [34]. It differs

from the Standard and RNG $k-\varepsilon$ in the formulation of the turbulent viscosity because C_μ is not a constant but it is computed separately for every flow and it is a function of the mean strain and rotation rate, the angular velocity and k and ε, to increase accuracy in complex geometries where the other two versions perform poorly. The second vital difference is the transport equation for ε which is now derived from an exact equation for the transport of the mean-square vorticity fluctuation [34].

The term realizable comes from the fact that this model satisfies certain mathematical constraints on the Reynolds stresses consistent with the physics of turbulent flows, the latter two versions are not realizable. Its greater advantage is its superior performance for flows involving rotation and boundary layers under strong adverse pressure gradients. As Launder and Spalding mention, after experiments, in their original paper, "The results show that the present model performs better than the standard $k-\varepsilon$ model in almost all the cases tested." in which case they include rotating homogeneous shear flows, boundary-free shear flows, channel flow, boundary layer flows and backward-facing step flows [34]. Due to the RNG and Realizable being modern models, there is not yet a sufficient amount of work to have a clear conclusion as to which is more accurate.

Many studies have been published that compare the latter three $k-\varepsilon$ versions, like the paper of Qinfu Hou and Zongshu Zou [12] in which they compare Standard and Renormalization k–ε models in simulation of swirling flow tundish. Another study [33] compares the Standard and RNG $k-\varepsilon$, in this work it is discussed the latter comparison in curved and confluent channels.

3.3.2 The $k-\omega$ Model

This family of models also uses two transport equations one for the turbulent kinetic energy k and one for the specific dissipation rate ω, or else the rate of dissipation of TKE into thermal energy. The first effort for a $k-\omega$ model was made by Andrey Kolmogorov in 1942, many more followed his idea with models like Wilcox's $k-\omega$ model (1988), Menter's SST variation and more modern $k-\omega$ models like Wilcox's modified model (2006). In this subsection, it will be discussed Wilcox's $k-\omega$ model of 1988 [42]. The Figure 3.1 presents a short history timeline of the most important versions of this family of models in the last eighty years, starting from Kolmogorov in 1942 and ending with the last modified version of Wilcox $k-\omega$ turbulence model which is also called as the standard $k-\omega$ model.

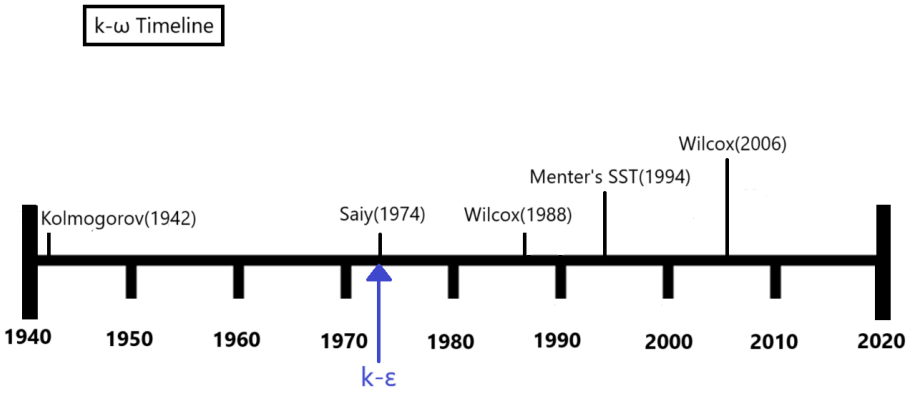

Figure 3.1: The development, timeline, of $k-\omega$ models over the years.

The following equations describe Wilcox's $k-\omega$ model from his paper in 1988 [42]. Eddy viscosity is given by:

$$\varepsilon_t = \frac{k}{\omega}. \tag{3.24}$$

Turbulence kinetic energy yields from the following PDE's:

$$\frac{\partial k}{\partial t} + u_j \frac{\partial k}{\partial x_j} = \tau_{ij} \frac{\partial u_i}{\partial x_j} - \beta^* k\omega + \frac{\partial}{\partial x_j}\left[(\nu + \sigma^* \varepsilon_t)\frac{\partial k}{\partial x_j}\right]. \tag{3.25}$$

The specific dissipation rate by:

$$\frac{\partial \omega}{\partial t} + u_j \frac{\partial \omega}{\partial x_j} = \alpha \frac{\omega}{k} \tau_{ij} \frac{\partial u_i}{\partial x_j} - \beta \omega^2 + \frac{\partial}{\partial x_j}\left[(\nu + \sigma \varepsilon_t)\frac{\partial \omega}{\partial x_j}\right]. \tag{3.26}$$

And finally the closure coefficients and auxiliary relations:

$$\alpha = \frac{5}{9} \quad , \beta = \frac{3}{40} \quad , \beta^* = \frac{9}{100} \quad , \sigma = \frac{1}{2} \quad , \sigma^* = \frac{1}{2} \quad , \varepsilon = \beta^* \omega k. \tag{3.27}$$

The most used variation of $k-\omega$ models is Menter's SST $k-\omega$ model [21] which has a unique feature, combining the advantages of $k-\varepsilon$ and $k-\omega$ models. The Shear Stress Transport model mixes the robust and accurate formulation of the $k-\omega$ model in the near-wall region with the free-stream independence of the $k-\varepsilon$ model in the outer region. The blending function that is used has

the role of making the solution smooth and both the standard $k-\omega$ and the transformed $k-\varepsilon$ model are multiplied by this function. It is created in a way to be one in the near-wall region, which activates the standard $k-\omega$ model, and zero away from the surface, which activates the transformed $k-\varepsilon$ model. It is the most efficient as it provides excellent results for flows with separation than most RANS models and also it is known for its good accuracy in adverse pressure gradients.

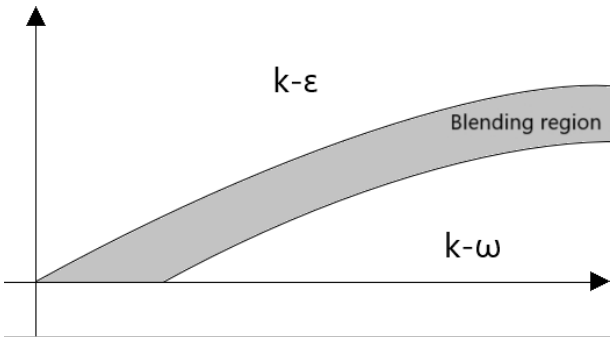

Figure 3.2: SST $k-\omega$ model visualization combining two important turbulence mathematical models.

Some adjustments in the standard $k-\omega$ model of Wilcox(1998) make the SST more accurate and it is widely used by scientists for a wide variety of flows with great and well compared results.

Every new model of Wilcox's $k-\omega$ is more accurate in some cases than the previous one or it covers a wider variety of flows, the most important difference in Wilcox's model (2006) is that he added a "cross-diffusion" term and a built-in "stress limiter", modification that express eddy viscosity as a function of k and ω and effectively the ratio of turbulence-energy production of turbulence-energy dissipation [43]. Additionally, these improvements in previous models expand the range of its applicability, retains the advantages of previous ones and increases significantly the accuracy in free shear flows or separated flows, where previous $k-\omega$ models face accuracy problems. Finally, as Wilcox mentions the version of 2006 is as good as that of 1988 for attached boundary layer, mildly separated flows and backward-facing steps, Wilcox's (1988) is of great agreement with measurements for these flows. This model also applies to both wall-bounded and free-shear flows, as this is a great advantage, of any turbulence model, because complex flows include both types [43].

3.4 Models of shear equations

Models of shear equations are also called models of many equations. These models use differential equations to express each term of the stress tensor or Reynolds tensor. So, as it is understood for these models, the number of equations to be solved is very large, since in the RANS equations that describe the flow are added, at best, another three differential equations to describe turbulence. However, the calculations become very extensive and cumbersome. The result of this is that the evolution of these models is relatively small due to the high computational cost that is required.

3.5 Large Eddy Simulation - LES

This method is a combined approach between RANS and DNS due to the computation of both the mean flow by RANS and the large energy-containing eddies exactly like DNS does. The small-scale structures, in this method, are parameterized by some simple mathematical model or RANS approach [8].

The main idea of this model is that the energy travels down the energy cascade, also called as forward cascade, and not in a reverse way, by larger eddies to smaller ones, for this reason, the main information is at the integral scale, the large eddies and smaller eddies are somewhat passive with main action to dissipate the energy that is coming from the larger ones.

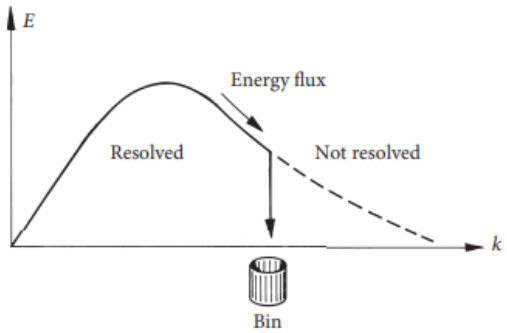

Figure 3.3: A schematic of LES, the energy flux in vertical axis and the wavenumber κ in horizontal one [8].

The attraction of LES lies in the fact that it is the large scales that are

the most important. For example, they dominate the transfer of momentum, heat, and chemical pollutants or reactants. So, if the spectrum is being cut at some point, and provides a dustbin for the energy flux, then the large scales will not notice the lack of smaller scales as it can be seen in Figure 3.3 [8].

The main concern of scientists in these models is the computational cost, more expensive methods provide better accuracy, so scientists try to balance out the accuracy and cost with the intention of achieving the best possible result. The comparison between the computational cost of the latter methods and some hybrid models between them can be summarized in Figure 3.4.

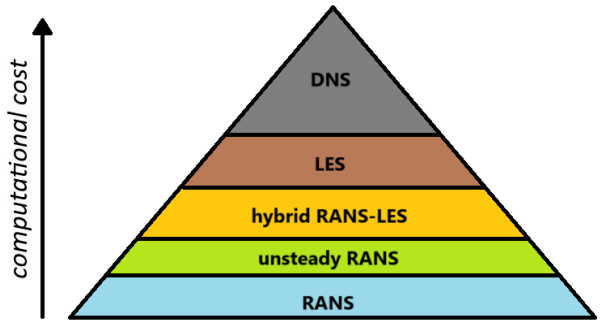

Figure 3.4: Computational cost of the introduced mathematical turbulence models RANS, LES, DNS and hybrid methods.

3.6 Direct Numerical Simulation-DNS

In 1972 Orszag and Patterson demonstrated that a direct way of simulation of a fully developed turbulent flow is possible [24]. This was groundbreaking because DNS does not need a turbulence model to parameterize the influence of turbulent eddies. It uses the progress of Navier-Stokes equations in time in a certain domain and it can be seen as an experiment, but better because in this experiment the initial conditions can be changed with ease, so they are called numerical experiments [8]. This method does not need to make any simplifications to the Navier-Stokes equations, but they are solved directly to give a solution for quantities like velocity, pressure, density, and temperature. This method reveals the chaotic nature of RANS equations.

The great benefit is that the initial conditions can be controlled very easily with the touch of a button, unlike the physical experiment which is difficult to achieve an initial condition. However, the amount of data is very large due

to the history of $u(x,t)$ which is available for inspection.

As stated in the previous chapter, the Kolmogorov microscale, or the approximate size of the smallest eddies is given by:

$$\eta = Re^{-3/4} l, \tag{3.28}$$

where l is the size of eddies in integral scale, the large energy-containing eddies, and as mentioned the bigger the Re the smallest the η. It is easy to estimate how the number of grid points at which u must be calculated to analyze every eddy in the turbulence spectrum. The spatial separation of the sampling points, Δx, cannot be very large compared to η, so the simulation is accurate enough. A minimum, we require $\Delta x \sim \eta \sim Re^{-3/4} l$. So the number of points which is needed at any instant for a three-dimensional simulation is:

$$N_x^3 \sim \left(\frac{L_{BOX}}{\Delta x}\right)^3 \sim \left(\frac{L_{BOX}}{l}\right)^3 Re^{9/4}, \tag{3.29}$$

where N_x is the grid points in any direction and L_{BOX} is a linear dimension of the computational domain. A useful observation can be derived if we transform the equation into the following form:

$$Re \sim \left(\frac{l}{L_{BOX}}\right)^{4/3} N_x^{4/3}. \tag{3.30}$$

The relation between the Reynolds number and the number of grid points is nonlinear consequently, for large Reynolds numbers a very large number of grid points is required [8], in real life application Reynolds number is high therefore this increases significantly the computational cost and makes this method a very computational expensive tool.

CHAPTER 4

Numerical Solutions of Turbulent Flow

In fluid mechanics, the process of acquiring a numerical solution, through computational mathematics, is at the heart of turbulence nature as exact solutions are absent. The comparison of turbulent numerical solutions with experimental data is vital, due to the chaotic nature of various real-world phenomena and practical applications in mechanical problems. This chapter will introduce the processes through numerical results with the succor of turbulence models, as described in the third chapter. Advanced computational methods with the purpose of achieving the best results possible for the desired flows will be introduced. Additionally, will be utilized the fundamental principles, presented in the second chapter, of turbulence nature and useful semi-empirical laws, for example, the logarithmic law of the wall and numerical techniques that offer a comprehensive description of this turbulent aspect of fluid dynamics.

4.1 Numerical Schemes Overview

4.1.1 Finite Volume Method (FVM)

The Finite Volume Method, used in this thesis, is a second-order accuracy method, due to the difference scheme used to discretize the governing equations representing conservation laws over differential volumes. This method transforms partial differential equations, linear or non-linear, into discrete algebraic ones over finite volumes. Initially, F.V.M. discretizes the geometric domain into control volumes (finite volumes) as presented in Figure 4.1. Then, the system of partial differential equations is discretized into a system of algebraic

equations by integrating over each discrete control volume. Finally, the system of algebraic equations is solved with any desired solver to obtain the values of the dependent variable on each of the cells (every discrete volume) [22].

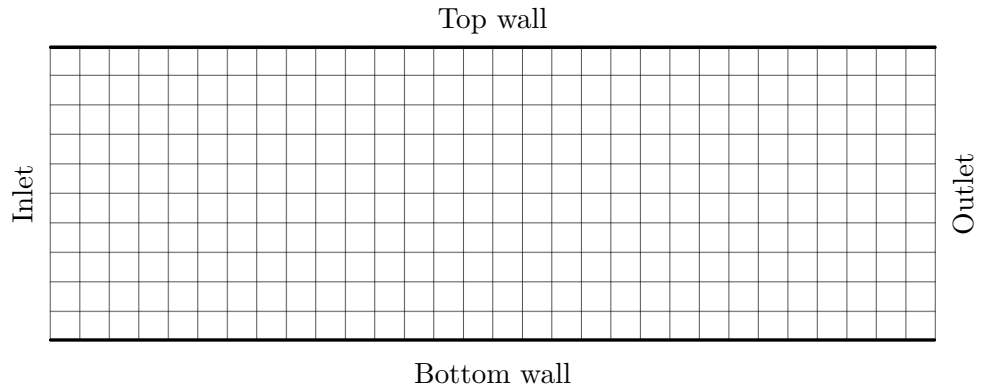

Figure 4.1: A discretized domain with F.V.M. of a rectangle (channel) with square control volumes with $\Delta x = \Delta y$.

In the F.V.M. the terms in the conservation of mass equation are transformed into face fluxes and evaluated at the finite volume faces. Because the flux entering a given volume is identical to that leaving the adjacent volume, the F.V.M. is strictly conservative and divergence-free, $\overline{\nabla} \cdot \overline{q} = 0$ condition is required, so in every control volume an integral conservation law statement is imposed.

Definition 4. *An integral conservation law asserts that the rate of change of the total amount of a flux with density u in a fixed control volume T is equal to the total flux of the substance through the boundary ∂T.*

$$\frac{d}{dt}\int_T u dx + \int_{\partial T} f(u) \cdot d\overline{\eta} = 0, \quad \overline{\eta} : \textit{normal unit vector.} \tag{4.1}$$

Another advantage of the F.V.M. is that it can be formulated in the physical space on unstructured polygonal meshes, thus it is easy to implement a variety of boundary conditions in a noninvasive manner since the unknown variables are evaluated at the centroids of the volume elements, not at their boundary faces [22].

All these advantages have made the F.V.M. method a great tool for solving difficult CFD, and related transport phenomena problems which include

heat or mass transfer [26]. With the progression of numerical analysis and computational mathematics, this method has proven effective for all kinds of complex geometries.

As mentioned, the first step of the method is the discretization of the domain Ω into subdomain $CV_i \subseteq \Omega, \quad i = 1, 2, ..., N$, the second step is to integrate the governing differential equations over each control volume CV_i, as can be seen in Figure 4.2, with the resulting discrete algebraic equations contain the unknown parameters, such as the velocity components or the pressure, on the grid points with one equation of difference for each CV. At the end of this process, a solver is used to calculate the values of the unknown parameters, on the grid points. Finally, present the corresponding plot to visualize the desired flow or pressure field. In the Finite Volume Method, these resolved values form the numerical solution, resulting in a more practical and easy-to-implement method [26].

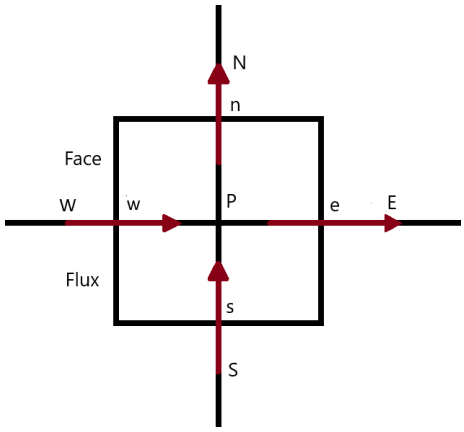

Figure 4.2: Control Volume (CV_i) of Finite Volume Method.

The Finite Volume Method has consolidated as a fundamental discretization scheme, in a wide variety of flows from simple to complex geometry ones, the great advantage that placed this method in a top position in the scientific community is the Integral Conservation Law, which ensures that each volume respects the conservation physical laws that represent CFD problems. It makes it possible to represent natural phenomena such as transport phenomena, mass, momentum and energy conservation. The applications of this method are countless in various sectors of fluid mechanics such as Magnetohydrodynamic and Ferrohydrodynamic effects in a channel flow [5], in biomedical applications and hemodynamics which study the cardiovascular system and especially the Magnetohydrodynamic effects on a pathological vessel [16] or aerodynamic applications such as of wind-turbine-blade profile study [31].

The Finite Volume Method is being used in this thesis for the discretization of RANS and RABL equations for the numerical solution of turbulent channel flow and turbulent B.L. flow respectively, as well as for the preliminary

results of the backward step flow. The discretization plays a crucial role in the stability and quality of the obtained results and has to be chosen properly, considering the particular needs of the flow.

4.1.2 Upwind Scheme

The Upwind Scheme is a discretization method that transforms a system of partial differential equations in discrete-algebraic form similarly to the Finite Volume Method, it is also referred to as the donor-cell method or the upstream difference scheme. The first work that laid the groundwork for this method was by Courant, Isaacson and Rees and after many modifications resulted in the modern model that is widely used in the twenty-first century.

The Upwind Scheme tries to correct the central differencing scheme by erasing the admission that the convected property Φ_e is the average of Φ_E and Φ_P and exploits the direction of the flow by considering that, for the convection term, the value of Φ_e is calculated by the value of Φ at the grid point on the upwind side of the face [26]. This scheme is essential for turbulent flows and generally for flows with flow reversal. This method provides very good results compared to experimental data, since it is developed for strong convective flows with suppressed diffusion effects. The scheme is based on the backward differencing scheme, so it is proven that the accuracy of the method is first order, in contrast with the F.V.M. which is a second order method and it is preferred in cases where accuracy is vital, especially in complex flows.

Specifically:

$$\Phi_e = \Phi_P, \qquad \text{if} \quad F_e > 0, \tag{4.2}$$

$$\Phi_e = \Phi_E, \qquad \text{if} \quad F_e < 0, \tag{4.3}$$

where the variable Φ_e is the convection mass flux.

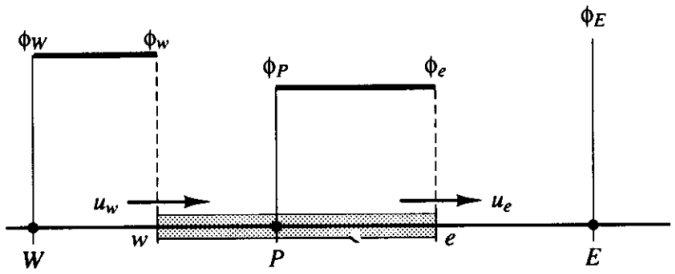

Figure 4.3: Visualization of the Upwind Scheme for positive F_e [40].

In Figure 4.3 the Upwind Scheme is visualized, for the calculation of cell face value, in the case where F_e is positive, and the direction of the flow is from west to east. In this thesis, it is utilized for the simulation of turbulent B.L. and turbulent channel flow in the advanced computational program Fluent (Ansys,Canonsburg, Pennsylvania).

4.1.3 Newton's Method

Most phenomena in nature are described by nonlinear differential equations systems, and through their transformation into nonlinear algebraic systems, arises the need to solve them. The most widely-known method for solving nonlinear algebraic systems is Newton's method, also known as the Newton–Raphson method, which is based on the relationship of a function to its tangent at a point (initial guess) close to where the roots of the equation exists. The initial guess is crucial for the convergence of the method, also defined as a local method [28].

A system of n equations and n unknown variables is assumed, this system will be solved after the process of discretization such as the Finite Volume Method or Upwind Scheme discretization. So the system is defined as:

$$\overline{f}(\overline{x}) = \overline{0}, \tag{4.4}$$

where $\overline{f} = (f_1, ..., f_n)^T$, $\overline{x} = (x_1, ..., x_n)^T$ and $\overline{0} = (0, ..., 0)^T$.
To start the method an initial guess is needed $\overline{x}^{(0)}$ that is not a root of $\overline{f}$ so $\overline{f}(\overline{x})^{(0)} \neq 0$. Taylor series expansion is required so that: $\overline{f}\left(\overline{x}^{(0)} + \Delta\overline{x}^{(0)}\right) = 0$. We seek the first-order Taylor series information around $\overline{x}^{(0)}$:

$$\overline{f}\left(\overline{x}^{(0)} + \Delta\overline{x}^{(0)}\right) = \overline{f}\left(\overline{x}^{(0)}\right) + \overline{\mathbf{Jac}}^{(0)}\Delta\overline{x}^{(0)}, \tag{4.5}$$

where $\mathbf{Jac}$ is the $n \times n$ Jacobian matrix:

$$\mathbf{Jac}^{(0)} = \left(\overline{\nabla} f_1\left(\overline{x}^{(0)}\right), ..., \overline{\nabla} f_n\left(\overline{x}^{(0)}\right)\right)^T. \tag{4.6}$$

It is demanded that $\overline{f}\left(\overline{x}^{(0)} + \Delta\overline{x}^{(0)}\right) = 0$ so arises the need to compute the term $\Delta\overline{x}^{(0)}$ and this can be computed approximately as:

$$\Delta\overline{x}^{(0)} \approx \left(\mathbf{Jac}^{(\nu)}\right)^{-1}\overline{f}\left(\overline{x}^{(\nu)}\right). \tag{4.7}$$

The vector $\overline{x}$ is updated as:

$$\overline{x}^{(\nu+1)} = \overline{x}^{(\nu)} + \Delta\overline{x}^{(\nu)} = \overline{x}^{(\nu)} + \left(\mathbf{Jac}^{(\nu)}\right)^{-1} \overline{f}\left(\overline{x}^{(\nu)}\right), \tag{4.8}$$

where ν, is the Newton iteration. This algorithm is iteratively performed until the error between two successive iterations is less than the specified tolerance that it is picked and the algorithm stops as it has obtained the solution and has updated the vector $\overline{x}^{(\nu+1)}$. If the error is higher than the specified Newton's iteration is increased by one and the process is repeated [7].

The convergence is guaranteed after certain conditions and the method is not globally convergent, and the initial guess must be close enough to the roots. The Newton's method is called a locally convergent method.

Trust Region Algorithm

The trust region method is a procedure that generates steps through a quadratic model of the desired function with the aim of minimizing it. More specifically, they create a region all around the current iteration which they trust, to be a valid approximation of the function and they choose a step to be the approximate local minimizer. The choice of the direction and length of the step is implemented at the same time. If this step is not achieving to reduce the function, these models reduce the size of the region and try to find a new minimizer. The size of the step is vital for the trust region as there are risks of error, in the case of a small step a chance of fast reduction of the function is lost, in the other case if the size of the step is very large the minimizer of the trust region model can be in long distance from the minimizer of the desired function locally. So, the size of the trust region is vital for the performance of the model, in most cases after previous work done with the model, the choice can be easily made to achieve an optimal performance. For a reliable and well-tested model, the size of the trust region can be increased and take a larger step, consequently have a faster convergence [23].

One of the most commonly used model functions is the quadratic so with the use of Taylor series expansion the objective function of f around the point x_k is:

$$m_k(p) = f(x_k) + \overline{\nabla}^T f(x_k)p + \frac{1}{2}p^T B_k p, \tag{4.9}$$

where $m_k = f(x_k + p)$ is the model function which is used iteratively for each k and B_k is a symmetric matrix which replacing the term $\overline{\nabla}^2 f(x_k + tp)$.

The error that we allow, with this substitution, is $O(||p^2||)$ which is small because also $||p||$ is small, due to the assumption that $B_k = \overline{\nabla}^2 f(x_k + tp)$, this assumption leads to the trust-region Newton method [23]. To obtain each step, we seek a solution to the sub problem:

$$\min_p m_k(p) = \min_p \left(f(x_k) + \overline{\nabla}^T f(x_k)p + \frac{1}{2}p^T B_k p \right), \quad ||p|| \leq \Delta_k, \qquad (4.10)$$

where Δ_k is the radius of the trust-region. The trust-region method solves a sequence of problems 4.10 in which the objective function and constrain are both quadratic. More details about this method can be found in [23].

4.1.4 SIMPLE Algorithm

The SIMPLE algorithm is an iterative numerical method developed to solve the Navier-Stokes equations and stands for Semi Implicit Method for Pressure Linked Equations. Proposed by Patankar and Spalding, it follows a path of initial guess and find procedure to obtain the corrected pressure and then the velocity field. It is widely used by the scientific community because of its convenient solving strategy, as well as all of its advanced variations like SIMPLEC or SIMPLER [26].

A direct way to deal with the Navier-Stokes equations in two or three dimensions is to solve the coupled system of partial differential equations, 2 or 3 momentum equations (2D or 3D case) coupled with conservation of mass equation. This algorithm proposes a slightly different approach than the direct method. The problem will be defined, along with the preferred equations and the boundary conditions for the desired problem will be applied as can be seen in Figure 4.4. Then an initial guess is required for the pressure values, in each flow they are proposed different strategies for applying the initial guesses by bibliography. In the first step of SIMPLE the discretized momentum equations are solved

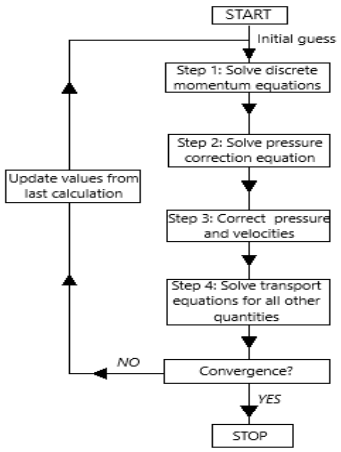

Figure 4.4: Stages of the SIMPLE algorithm.

with the pressure to be known and equal to the initial guess. The conservation of mass isn't included in the first step, so the solution for the components of velocity won't verify it. In the second step, a pressure corrector equation , is derived from the continuity and momentum equation, and is solved to approximate more accurate the pressure (pressure correction equation-Poison equation). In the third step, the updated pressure is used to correct the velocity components but this time coupled with the conservation of mass equation, in order to verify it. These last results for velocity in addition with the corrected pressure are the result of the algorithm. At the fourth step, any other transport equations are solved to acquire the quantities that are studied, for example in turbulent flows and especially in two differential equations turbulence models like $k-\omega$ or $k-\epsilon$ the desired quantities would be the T.K.E. k, specific dissipation rate ω and dissipation rate ε. The whole process is repeated iteratively until a convergence criterion that has been chosen is reached [40] as depicted in Figure 4.4.

4.2 Turbulent Boundary Layer

The turbulent B.L. occurs after the transition from laminar and transitional B.L. and is a phenomenon that concerns scientists, who try to deal with it efficiently, to achieve the best results possible, for example, to optimize the shape of an airplane or airfoil in order to reduce the drag and consequently save fuel and money. In fluid mechanics, fluid particles in a flow near a solid boundary, are slowed down by wall friction. If the flow is sufficiently decelerated due to the effect of an adverse pressure gradient, the momentum, and equivalent energy, of those particles will be interrupted by both wall shear stresses and pressure gradient. At the separation point, a location between forward and inverse flow where the wall shear stress is zero, the viscous layer leaves from the surface, the streamlines will leave the body. Thus it can be stated that the B.L. separation occurs.

The phenomenon of separation of the boundary layer is associated with large energy losses, something that mechanics and engineers try to avoid at any cost, and so most of the times the performance of many practical devices is directly associated with the separation point. For example, if separation is postponed, we have the following benefits, the pressure drag of a steep body, like a ball, is reduced, the circulation and hence the lift of an airfoil at a high angle of attack is increased and the pressure recovery of a diffuser is improved. When we refer to boundary layer control, we include any mechanism or process through which

the boundary layer is disturbed and behaves differently than it normally would. A wide range of examples can be mentioned such as the delay of transition or separation of the boundary layer, the reduction of skin friction or pressure drag, heat transfer, or lift. In aerodynamics it is desired to postpone the separation of the boundary layer so that form drag (pressure drag) is minimum, stall is delayed or avoided at all and lift is increased. Flow separation is currently employed, for example with the help of vortex generators, blown flaps or slats on older generation supersonic fighters, or leading edge extensions and strakes on newer generation, or cooling, heating of the wall by blowing air from slots [10]. The most acceptable technique for turbulent boundary-layer control is the suction/injection technique. Another technique is the localized suction which is to apply continuous suction in a region confined between $x = a$ and $x = b$, $0 < a < b < L$ where L is the whole length of the boundary surface.

Turbulent boundary layer due to its chaotic nature is at the center of interest for scientists, trying to study and control it. In many cases where there are no practical solutions, nature is observed and mechanics try to imitate it, such as the examples of winglets or shark skin. Winglet technology was implemented by Richard Whitcomb's research in the 1970s at NASA resulting in the reduction of drag in airplanes. German airline company Lufthansa installed artificial shark skin throughout her fleet, which led to drag reduction. This artificial shark skin consists of small geometries with the shape of triangles or rectangles called riblets, which allow the fluid to flow with small resistance and reduce the skin friction drag similarly to shark skin effect.

4.2.1 Numerical Solutions of Turbulent Boundary Layer

Many research works have been published, throughout the years, in numerical solutions of the turbulent boundary layer with the effect of pressure gradients, adverse or favorable, with separation control like suction/injection or riblets, additionally heat and mass transfer are studied or Magnetohydrodynamics and Ferrohydrodynamics [14].

An interesting work that combines some of the latter, is this of Kafoussias and Xenos (2000) [14] which presents a numerical investigation of 2D turbulent B.L. with an adverse pressure gradient, for compressible flow with suction and injection with heat transfer, over a finite smooth surface. In this thesis, we will analyze this work only for the case of the adiabatic wall ($S_W = 1$), which means we won't deal with heat transfer (heating/cooling of the wall).

Initially, this work formulates the problem and more specifically, the steady

two-dimensional compressible boundary layer flow over a smooth flat permeable surface. The surface is located at:

$$y = 0, \qquad 0 \leq x \leq L, \qquad -\infty < z < \infty, \tag{4.11}$$

it is parallel to the free stream of a perfect gas flowing with velocity u_∞. The equations that describe this kind of flow are the Reynolds averaged boundary layer equations which can be written in orthogonal coordinates (x,y) as follows:
continuity equation

$$\frac{\partial}{\partial x}(\overline{\rho}\ \overline{u} + \overline{\rho' u'}) + \frac{\partial}{\partial y}(\overline{\rho}\ \overline{v} + \overline{\rho' v'}) = 0. \tag{4.12}$$

x-momentum equation

$$(\overline{\rho}\ \overline{u} + \overline{\rho' u'})\frac{\partial \overline{u}}{\partial x} + (\overline{\rho}\ \overline{v} + \overline{\rho' v'})\frac{\partial \overline{u}}{\partial y} = -\frac{\partial \overline{p}}{\partial y} + \frac{\partial}{\partial y}\left[\mu \frac{\partial \overline{u}}{\partial y} - (\overline{\rho u' v'} - \overline{\rho' u' v'})\right]. \tag{4.13}$$

y-momentum equation

$$\frac{\partial \overline{p}}{\partial y} = 0. \tag{4.14}$$

By the Reynolds Averaged Navier Stokes it is known that for the instantaneous quantities (u,v,p) it is true that $f = f' + \overline{f}$, where $\overline{f}$ is the mean value and f' is the fluctuating part. With the use of Bernoulli's equation, the term $\partial \overline{p}/\partial x$ in the x-momentum can be substituted by:

$$-\frac{\partial \overline{p}}{\partial x} = -\frac{d\overline{p}}{dx} = \rho_e u_e \frac{du_e}{dx}. \tag{4.15}$$

Also by using the abbreviation $\overline{\rho v}$ for $\overline{\rho}\ \overline{v} + \overline{\rho' v'}$, and omitting, for simplicity the overbars on the basic time average variables u, v, p and ρ. Also the eddy kinematic viscosity ε_t is defined by the expression:

$$\varepsilon_t = \frac{-\overline{u' v'}}{\frac{\partial u}{\partial y}}. \tag{4.16}$$

By applying the latter to the equations(4.2-4.4) the new system of equations can be written as:

$$\frac{\partial}{\partial x}(\rho u) + \frac{\partial}{\partial y}(\overline{\rho v}) \tag{4.17}$$

$$\rho u \frac{\partial u}{\partial x} + \overline{\rho u}\frac{\partial u}{\partial y} = \rho_e u_e \frac{du_e}{dx} + \frac{\partial}{\partial y}\left[(\mu + \rho \varepsilon_t)\frac{\partial u}{\partial y}\right] \tag{4.18}$$

$$y = 0: \quad u = 0, \quad v = v_w(x), \tag{4.19}$$

$$y = \delta: \quad u = u_e(x), \tag{4.20}$$

where $u_e(x)$ is the external velocity which is given by Howarth's flow formula:

$$u_e(\overline{x}) = u_\infty(1 - \overline{x}), \tag{4.21}$$

where u_∞ is the free stream velocity, $\overline{x} = x/L$ and L is the boundary permeable surface (porous wall). Additionally, v_w is the suction/injection velocity at the wall which is given by:

$$v_w = \frac{1}{2}v_0[1 + tanh\beta(x - a)], \qquad 0 < x \leq \frac{a+b}{2}, \tag{4.22}$$

and

$$v_w = \frac{1}{2}v_0[1 - tanh\beta(x - a)], \qquad x > \frac{a+b}{2}, \tag{4.23}$$

where for this work $a = 0$, $b = 1.2$m, $\beta = 10$ and v_0 is a constant as described above. Furthermore, the authors introduce the compressible version of the Falkner-Skan transformation which is defined as:

$$\eta(x, y) = \int_0^y \sqrt{\frac{u_e(x)}{v_e(x)x}} \frac{\rho(x, y)}{\rho_e(x)} dy, \tag{4.24}$$

$$\psi(x, y) = \sqrt{\rho_e \mu_e u_e x} f(x, y), \tag{4.25}$$

and the definition of stream function ψ for compressible flow, that satisfied the continuity equation, by the relations:

$$\rho u = \frac{\partial \psi}{\partial y}, \qquad \overline{\rho v} = -\frac{\partial \psi}{\partial x}. \tag{4.26}$$

Finally with the help of transformation and the definition of stream function Kafoussias and Xenos [14] conclude in the final system of equations. The turbulence model that is used is the simplest algebraic model, of Cebeci and Smith and for the numerical scheme, they use a backward difference modification of the Keller's-box method and the resulting non-linear algebraic system is solved using a multidimensional Newton-Raphson iteration scheme.

To show the effects of mass transfer in the compressible boundary layer, authors conducted numerical calculations with different values of free stream Mach numbers. In this study, will discuss the case of adiabatic flow ($S_w = 1$),

flow with no heat transfer, in such a case it is worth examining only the velocity field and the skin friction coefficient.

Drag consists of two main components pressure and friction drag. The skin friction coefficient is a parameter, dimensionless, which is defined at any point of a surface that is subjected to the free stream, it will vary at different positions. It is worth analyzing it in such cases because an object like an airfoil, an aerodynamics object, by definition has small pressure stresses which results in small pressure drag. So, it is not worth examining pressure stresses, on the contrary, the component of stresses that dominates in objects like airfoils, are skin friction stresses which lead to large skin friction drag. Engineers try to minimize skin friction drag to limit the energy losses. So all the methods that try to prevent the separation of boundary layer and consequently the energy loss, attempt to minimize the skin friction drag and more especially local skin friction coefficient which is provided by the relation:

$$C_{fx} = \frac{\tau_w}{\frac{1}{2}\rho_e u_e^2}, \tag{4.27}$$

where τ_w is the stresses at the wall, given by the experimental law of Newton, or else the skin friction drag.

The following results, presented in the paper of Kafoussias and Xenos [14], depict the dimensionless mean velocity profiles with dimensionless distance, at a distance $x = 2.0$m from the leading edge of the plate, in the cases of no suction/injection and the cases of continuous suction and injection. It is observed that in low Mach numbers such as 0.75 in Figure 4.5, the application of suction reduces the mean velocity and of injection has the same effect even more, the mean velocity. In the case of larger Mach numbers such as 3.0 in Figure 4.6 continuous suction increases the mean velocity and continuous injection decreases it. In conclusion, the velocity field is affected by the suction/injection velocity applied on the wall as by the free stream Mach number.

From Figure 4.7 it can be observed that for various Mach numbers, the application of continuous injection helps in the reduction of friction drag but it moves the separation point downstream, and this is more intense for large Mach numbers. An interesting observation that is to be made, is that when the local skin friction drag coefficient becomes zero then there are no skin friction stresses so the separation of the boundary layer has occurred. Another interesting observation from this figure is that with the use of suction, the value of the skin friction coefficient is larger at any point but in return, separation is delayed and this is desirable as we want the separation to be delayed as far as possible.

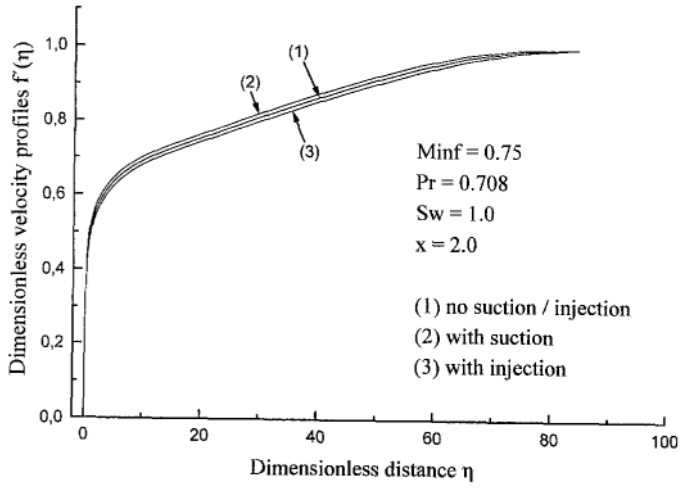

Figure 4.5: Variations of dimensionless velocity for $M_{inf} = 0.75$ [14].

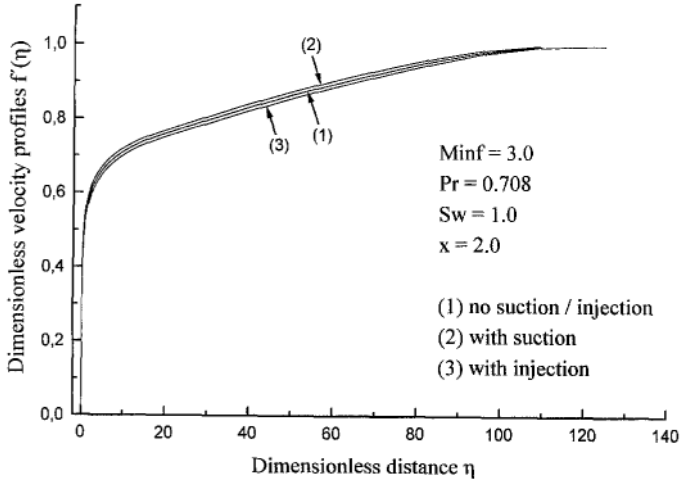

Figure 4.6: Variations of dimensionless velocity for $M_{inf} = 3.0$ [14].

In Figure 4.8 it can be observed that an increase in Mach numbers with no suction or injection results in a decrease in local skin friction coefficient at first, but the separation point moves closer which means that the separation occurs faster, a phenomenon undesirable.

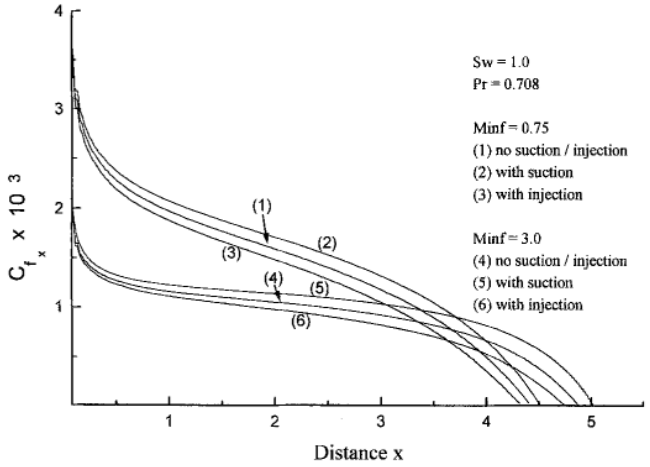

Figure 4.7: Variations of local skin friction coefficient C_{fx} [14].

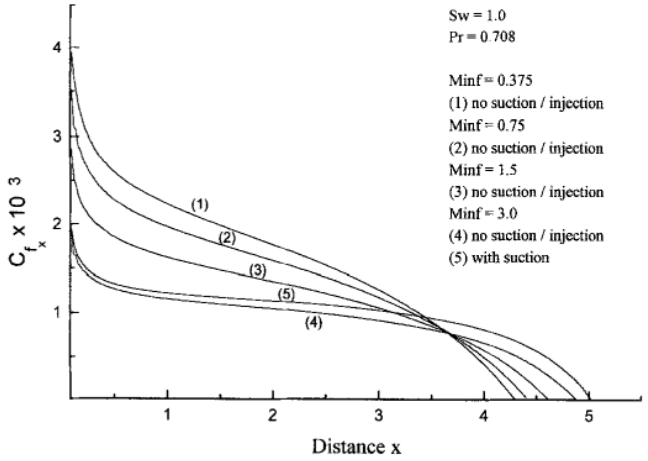

Figure 4.8: Variations of local skin friction coefficient C_{fx} [14].

Finally, the effect of continuous or localized suction/injection is presented in Figure 4.9 for $M_{inf} = 2.0$. By blowing air through the permeable wall the skin friction coefficient can be reduced at first stages, however the separation point moves downward in both cases of injection, localized or continuous, so the separation occurs faster. In the case of suction, the separation of turbulent boundary layer is delayed but the skin friction coefficient increases its value at the first stages.

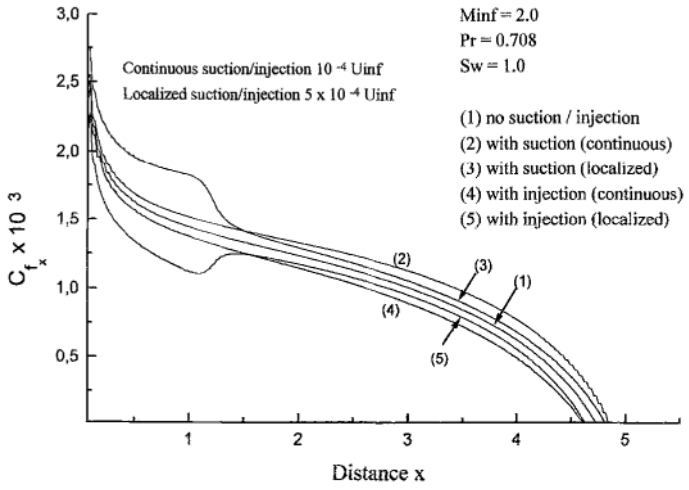

Figure 4.9: Variations of local skin friction coefficient C_{fx} [14].

4.2.2 Bubble Formation after B.L. separation

Another interesting work in the study of the after region of the thermal boundary layer is the bubble formation, in this thesis we will present the results of Xenos (2022) [46]. The BL before the separation point is depicted and these calculations are based on the classical formulation. The simulation below shows the velocity contours and the temperature distribution.

A notable quantity in mechanical applications, as mentioned, is the skin friction coefficient, so in many studies, this quantity is being examined and evaluated. Figure 4.10 presents the skin friction coefficient, C_{fx}, for the three studied cases, $M = 0.2$, 0.33, and 1.0, under adverse pressure gradient [46]. The skin friction coefficient begins from a large value and reduces as x increases, until it becomes zero, revealing the exact point of flow separation. The figure reveals the point of separation for each case. So, in detail and for Mach number $M = 0.2$ the flow separates at $x_s = 0.9594$ m, from the leading edge of the flat plate. For the other two cases, $M = 0.33$ and 1.0 the separation point is $x_s = 0.9544$ and 0.8994 m, respectively.

The numerical data that has been obtained from the mathematical description of the laminar bubble formulation (inverse problem) for three different Mach numbers is also presented [46]. The numerical results of bubble formation in low Reynolds numbers reveal that after separation creation of a

laminar bubble in all studied cases, Mach numbers, $M = 0.2, 0.33$ and 1.0. The flow after separation reverses close to the wall and finally reattaches in the x-direction. More precisely, for the case where $M = 0.2$, a small recirculation region is observed close to the wall. The velocity is substantially reduced. After reattachment, the BL is again established but at a much lower energy level, and the velocity field is substantially reduced, compared to the initial flow field. The BL, due to the adverse pressure gradient, moves upward as shown in Figure 4.12 below.

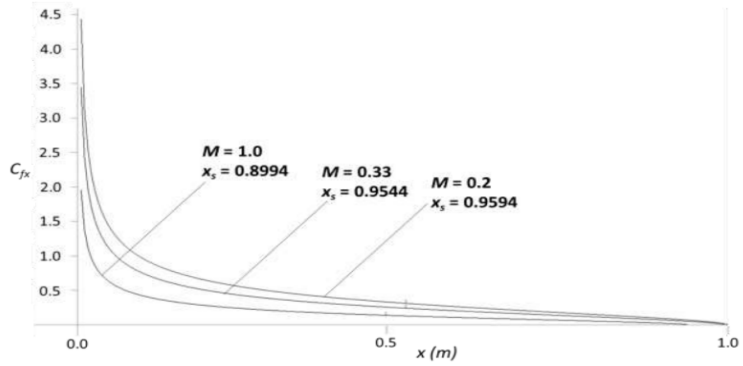

Figure 4.10: Skin friction coefficient, C_{fx}, of the laminar boundary layer for Mach numbers, $M = 0.2, 0.33$ and 1.0 and corresponding separation locations, x_s [46].

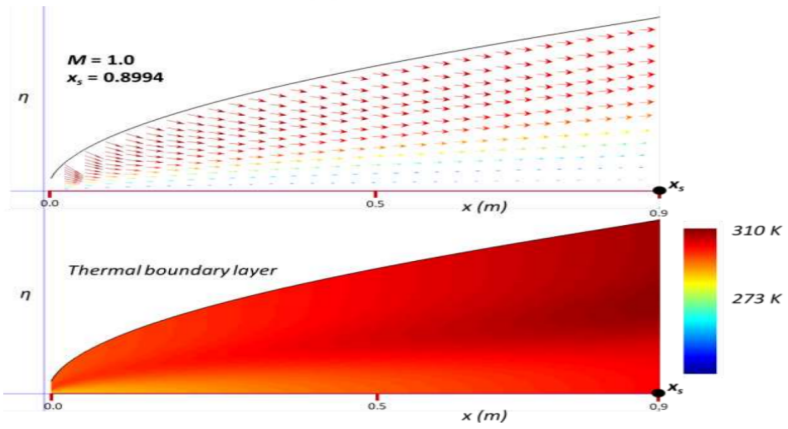

Figure 4.11: Velocity vectors and temperature distribution of the laminar BL for Mach number, M= 1.0, location of separation from the leading edge, $x_s = 0.8994m$ [46].

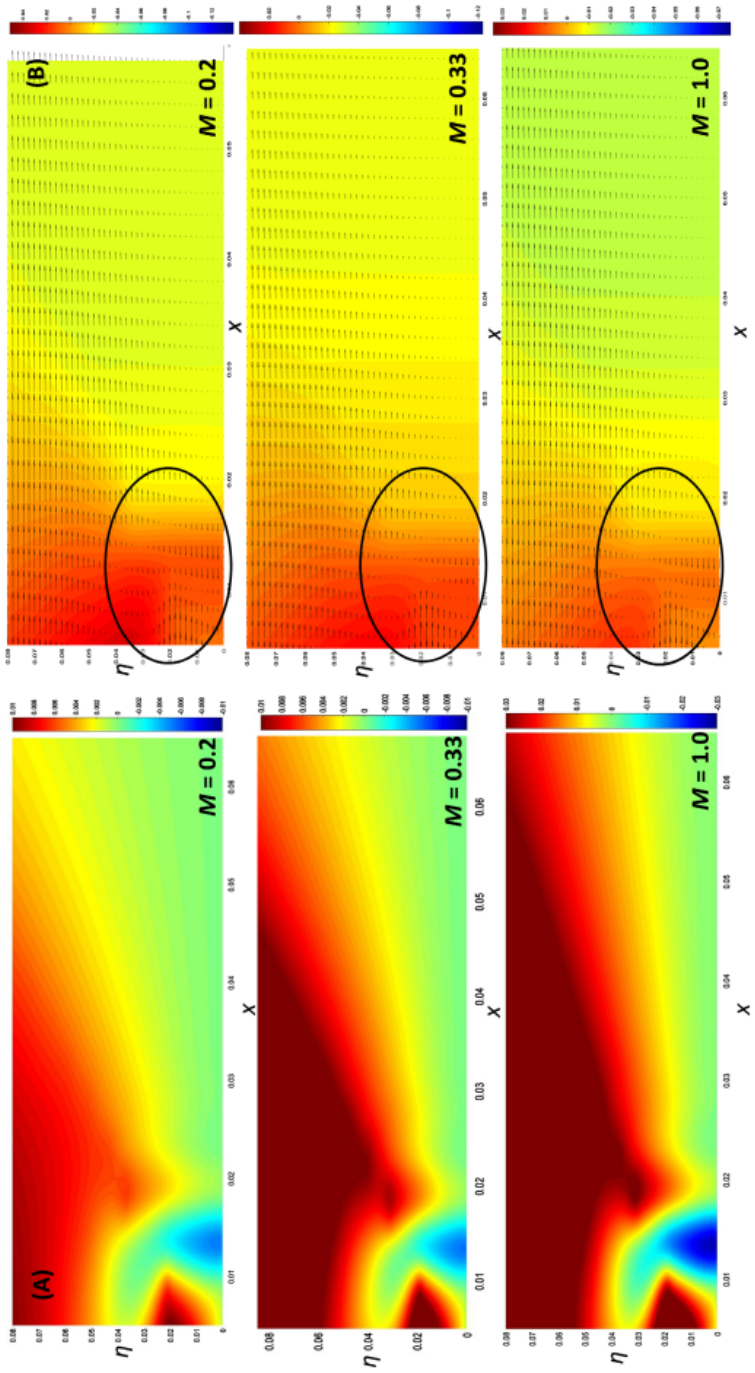

Figure 4.12: Velocity contours of bubble formation after separation for various Mach numbers, $M = 0.2, 0.33$ and 1.0 [46].

4.2.3 Turbulent Boundary Layer with Cebeci-Smith model

The turbulent B.L. differs significantly from the laminar B.L. and needs thorough study, its many real-life applications such as in aviation and ship-building push the scientific community to research more about this phenomenon. Many studies have been published about the turbulent B.L. Some of them have been the initial step for the creation of turbulent models, which used as a test study for the model accuracy, the turbulent B.L. some examples are the Cebeci-Smith [36] and the Baldwin-Lomax [1].

In this thesis, the turbulent B.L. numerical solution is simulated with the help of finite volume method discretization, the use of advanced mathematical computing programming language Matlab and the algebraic turbulent model of Cebeci and Smith as it is described in Chapter 3.1.1. It will be examined the case of a turbulent B.L. over a flat plate in which the no-slip condition exists in the plate and the geometry of interest is a rectangle with a height of H=0.2 and width of L=1 with a graded mesh, else called boundary layer mesh, since it is widely used in B.L. numerical solutions. This mesh is finer near the plate, the height of cells becomes bigger as it gets away from it as it can be observed in Figure 4.13. The mesh and geometry are generated through Matlab with the use of a technique that takes advantage of the geometric progression. The equations that are used are the RABL equations as described in the next section.

Reynolds Average Boundary Layer equations

Initially, the problem must be mathematically formulated, so the steady-state $\left(\dfrac{\partial q}{\partial t} = 0\right)$, two-dimensional, incompressible turbulent B.L. is described by the Reynolds Average Boundary Layer (RABL) equations. The problem under consideration can be described by the continuity and the momentum PDEs, Equations (4.28)-(4.30). The RABL equations, in closed form, are:

$$\overline{\nabla} \cdot \overline{q} = \frac{\partial u}{\partial x} + \frac{\partial v}{\partial y} = 0, \qquad \text{continuum equation} \qquad (4.28)$$

$$\frac{\partial u^2}{\partial x} + \frac{\partial (uv)}{\partial y} = -\frac{1}{\rho}\frac{\partial p}{\partial x} + \frac{\partial}{\partial y}\left[(\nu + \varepsilon_t)\frac{\partial u}{\partial y}\right], \qquad \text{x-momentum} \qquad (4.29)$$

$$\frac{\partial (uv)}{\partial x} + \frac{\partial v^2}{\partial y} = -\frac{1}{\rho}\frac{\partial p}{\partial y} + \frac{\partial}{\partial y}\left[(\nu + \varepsilon_t)\frac{\partial v}{\partial y}\right]. \qquad \text{y-momentum} \qquad (4.30)$$

To ensure that the problem is well-defined, to the above equations must be added the following boundary conditions:

$$y = 0 : u = 0, v = 0,$$
$$y = \delta : u = u_\infty,$$

where u_∞ is the free stream velocity out of the boundary layer, in the dynamic flow region.

Numerical Result of the Turbulent Boundary Layer

With the use of the F.V.M. method, details can be found in the Appendix, and by replacing each term in the system of Equations (4.28)-(4.30) that describe the turbulent B.L. we conclude in the following discrete form-equation of differences:
Conservation of Mass

$$\frac{(u_E - u_W)\Delta y}{2} + \frac{(v_N - v_S)\Delta x}{2} = 0, \tag{4.31}$$

x-momentum

$$\frac{(u_E^2 - u_W^2)\Delta\, y}{2} + \left(\frac{u_N v_N - u_S v_S}{2}\right)\Delta\, x = -\frac{1}{\rho}(P_E - P_P)\Delta y$$
$$+ \left[(\nu + (\varepsilon_t)_n)\,\frac{u_N - u_P}{\Delta y} - (\nu + (\varepsilon_t)_s)\,\frac{u_P - u_S}{\Delta y}\right]\Delta x, \tag{4.32}$$

y-momentum

$$\left(\frac{u_E v_E - u_W v_W}{2}\right)\Delta\, y + \frac{(v_N^2 - v_S^2)\Delta\, x}{2} = -\frac{1}{\rho}(P_N - P_P)\Delta x$$
$$+ \left[(\nu + (\varepsilon_t)_n)\,\frac{v_N - v_P}{\Delta y} - (\nu + (\varepsilon_t)_s)\,\frac{v_P - v_S}{\Delta y}\right]\Delta x. \tag{4.33}$$

Geometry and Mesh of Boundary Layer

The geometry of the problem under consideration is this of a turbulent flow over a flat plate with length L and height H. For the problem that is being studied in this thesis H=0.2 and L=1. The initial velocity that is being applied in the inlet of the geometry is constant and equal to $u_0 = 10$ m/s.

With a large velocity gradient close to the bottom wall, and consequently, large wall shear stresses that are created, we are obliged to impose a graded mesh, or else called boundary layer mesh since it is necessary for turbulent B.L. flow study. The ability of the mesh to resolve the smallest scales of turbulence can be verified by the value of y^+ as it is presented in Chapter 2. In most laminar cases a uniform mesh can cope well enough but in turbulent flow near solid boundaries, graded mesh is required. It is described by a graded mesh from the bottom to the upper wall in the y-direction, which implies that the height of the cells is smaller closer to the wall, finer mesh, and uniform in the x-direction, equal width for the cells. The height of the cells starts to increase at a certain rate (K) that we apply.

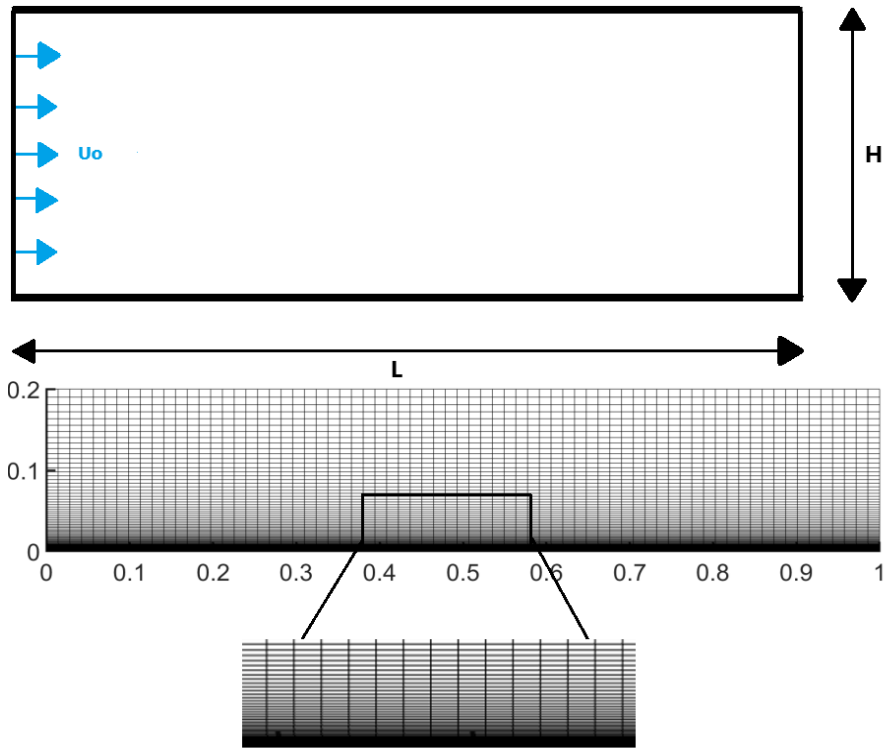

Figure 4.13: The 2D pipe channel geometry and grid.

The grid is constructed with the help of Matlab and according to the source [2], y-direction (height) graded mesh that is used in this thesis is described by the geometric progressions that have the property that the ratio of the lengths

of any two adjacent intervals is a constant, so $h_i = Kh_{i-1}$ where the distance to the $i-$th line is provided by:

$$y_i = h_1 \frac{K^i - 1}{K - 1}, \quad i = 1, 2, ..., J, \quad K > 1, \tag{4.34}$$
$$h_1 = M \left(\frac{K - 1}{K^J - 1} \right).$$

The second relation ensures that the grid stops at M, at the end of the geometry barriers, at the end of the geometry height. The two parameters that is being used are h_1 which is the length of the first Δy-step and the second is K, the ratio of two successive steps. In the existing problem $h_1 = 6.8057 \cdot 10^{-5}$ and $K = 1.08$ for the final solution that is obtained in a 70×70 grid. The visualization of this grid can be observed above in Figure 4.13.

Results in Turbulent Boundary Layer

The two-dimensional steady-state flow over a smooth plate with the geometry-grid-system of equations, as discussed above using the advanced mathematical computing programming language Matlab numerical solution is obtained, with the discretization using F.V.M. The inlet velocity was set as constant and equal to 10m/s and the fluid properties viscosity has to be adjusted, $\mu = 2 \cdot 10^{-5} \frac{kg}{ms}$, density $\rho = 1 \frac{kg}{m^3}$, these properties are approaching good enough the properties of air.

The RABL equations with the use of the F.V.M. are transformed to algebraic-discrete equations (4.31)-(4.33). The mesh is created in the rectangle domain, creating volumes via the F.V.M. applied to the RABL equations transforming them from a differential system into a system of coupled non-linear algebraic equations. The desired variables are the unknown values of u-v velocity components and pressure at each control volume at the mesh grid. For the solution of the non-linear coupled algebraic system a non-linear solver is required, the most common one is the Newton-Raphson method as described in subsection 4.1.3. The vector $\overline{x}^{(\nu)}$ represents unknown variables created by the mesh grid, while $\overline{f}\left(\overline{x}^{(\nu)}\right)$ represents the interconnected algebraic functions (system) assessed at $\overline{x}^{(\nu)}$. The numerical solution given for a complex problem like that of the turbulent boundary layer is of great interest and will therefore be thoroughly analyzed. The numerical solution is obtained in a direct way, using Newton's solver which adds robustness to the results as the equations remain unchanged.

The boundary conditions are applied and remain unchanged, in the domain, the geometry has been divided into rectangles as it is described, with a grid of 70×70 used, so there are 4900 of each variable equation or $4900 \times 3 = 14700$ Degrees of Freedom. The algebraic system is given by evaluating each of the discretized equations in each control volume of the partition so in the x-momentum equation in each control volume an algebraic equation is generated, in the grid 70×70 there are generated 70×70 algebraic equations. By doing the same in y-momentum and conservation of mass equations which have the same amount of equations, the final number of equations, that form the algebraic system and need to be solved, is $3 \times 70 \times 70 = 14700$. Finally, the whole domain's equations (three equations for each control volume) are solved simultaneously at each iteration of Newton's algorithm as described in 4.1.3.

The aforementioned procedure results in the numerical solution to the studied problem, as well as for the RANS equations of turbulent channel flow in the next subsection. The magnitude of velocity and pressure distribution are presented and commented on below, in-depth information related to u-velocity and v-velocity components is available in the dedicated Appendix. The turbulent B.L. is a phenomenon that occurs after the transition of a laminar boundary, all laminar B.L. will transition to turbulent if they have an infinite plate. The mixing motion in turbulence is important for the drag of turbulent flows, and for the friction drag. As presented in Chapter 2, the turbulent B.L. velocity distribution consists of three main regions where the turbulent and laminar stresses change their behavior, depending on the region. Similarly to the laminar B.L. the changes in the x-momentum can be taken to be small enough to be neglected in the main flow direction $\partial/\partial x \ll \partial/\partial y$. The shear stress consists of two components the molecular exchange (laminar) and the additional due to turbulent exchange.

Remark: In a B.L. the flow is laminar if $Re < 5 \cdot 10^5$ and turbulent if $Re > 5 \cdot 10^5$.

The analysis of the magnitude of the velocity $u_{mag} = \left(\sqrt{u^2 + v^2}\right)$ is crucial for the investigation of the turbulent B.L. The boundary layer thickness is decreased in comparison with the laminar boundary layer and this is because shear stresses near a solid boundary are more intense since turbulence transfers momentum closer to the walls and reduces the thickness of the B.L. In the viscous region (laminar sublayer) of the B.L. the viscous shear stress dominates, in contrast with the outer layer in which the turbulent shear stresses overcome the laminar ones, due to the eddy viscosity effects through macroscopic movement of eddies. So, in Figure 4.14 it can be observed the contours of the

magnitude of the turbulent B.L., this can be divided into two big regions, the outer region where dynamic flow is preserved and the inner layer of the B.L. which is the region that the viscous effects create the laminar sublayer, the boundary layer thickness (δ) is noticeably smaller than laminar B.L. as the enhanced mixing that due to turbulence (macroscopic mixing, as the eddies are a collection of molecules that moves as whole) brings more momentum close to the wall, because the more intense turbulence is mixing more effective the fluid near the surface, consequently the velocity gradient is reducing as well as the thickness of the boundary layer.

The pressure of the boundary layer is increased at the starting region and it instantaneously becomes zero as observed in Figure 4.15, this increase in pressure is due to viscosity in reaction to the velocity that is applied in the inlet. This is typical behavior of the pressure distribution, in contrast with the turbulent pipe, in which the difference of pressure is moving the fluid and the pressure is gradually descending.

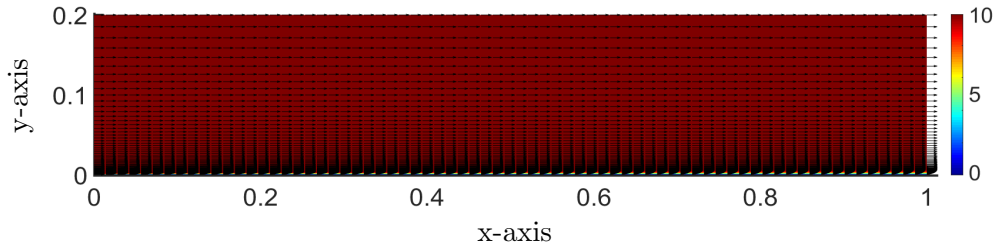

Figure 4.14: Magnitude of Turbulent Boundary layer

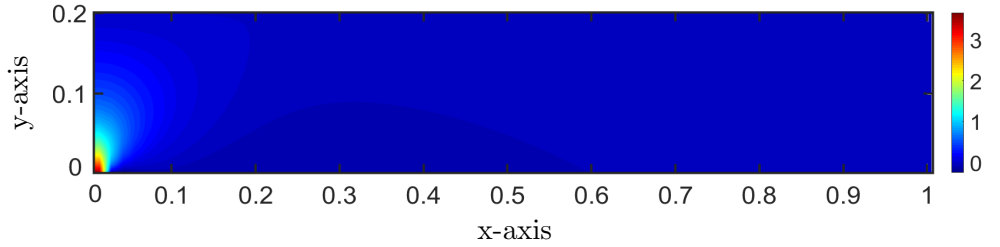

Figure 4.15: Pressure in Turbulent Boundary Layer

The profile of u-velocity in the B.L. is compared to that of outlet u-velocity in Figure 4.16, the inlet velocity is constant and equal to 10m/s, the outlet velocity is following the analysis that is done in the previous chapter in which the velocity goes through all the layers of inner layer (viscous sublayer), in

which the viscous stresses dominate, then from the overlap layer and finally from the outer layer in which the velocity is almost constant as it is anticipated, due to the increased momentum transfer which leads to a rapid raise of the velocity and consequently a homogenization of the velocity profile. The profile presents a maximum value as it enters the outer layer and this is a common behavior that is studied in the bibliography, as our inlet velocity is constant and not parabolic, in any of these two cases the profile in the outlet is steeper than the laminar one.

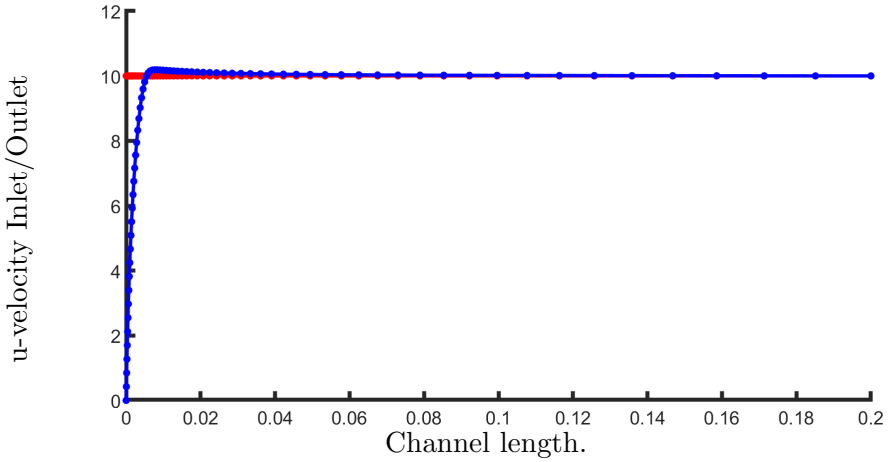

Figure 4.16: Comparison of Inlet (red) and Outlet (blue) u-velocity profile in Turbulent Boundary Layer.

In the following figures, some important properties of the flow can be observed. Initially in Figure 4.19 the y-plus (y^+) value is less than 5, so the first cell of the simulation is in the viscous sublayer, and all the scales are resolved properly. Another property of the turbulent flow is the mixing length which is increasing as we move away from the plate, this is expected as the mixing length is proportional to the height of the geometry. Finally, the stresses at the wall are presented in Figure 4.17, they follow Newton's experimental law as the effects of Reynolds stresses near the wall, in the laminar sublayer, are negligible. The stresses are slightly increased in comparison with the laminar B.L. as the gradient of velocity in the y-direction is larger, the behavior of the stresses is decreasing as the stresses are smaller because the gradient of the velocity is essentially reducing.

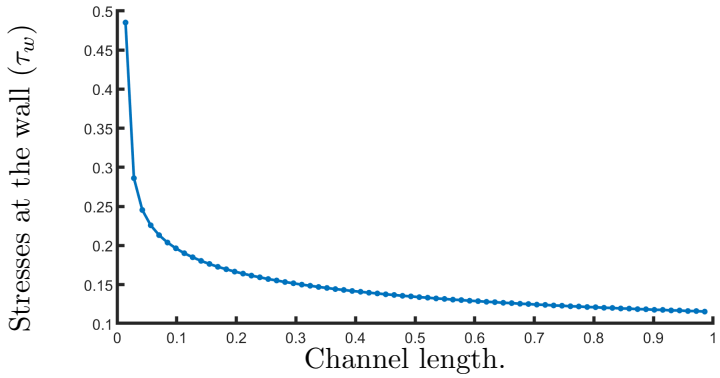

Figure 4.17: Stresses at the wall in Turbulent Boundary Layer.

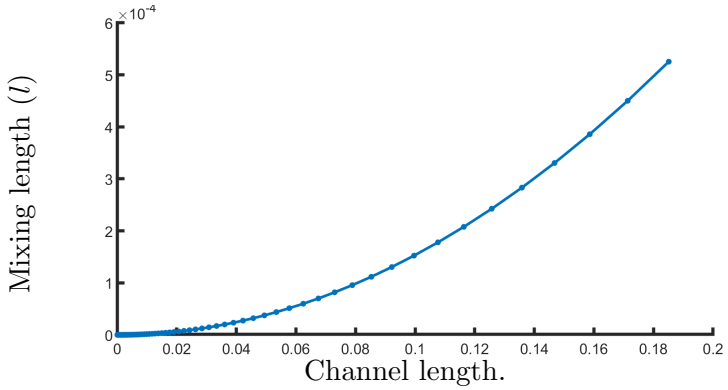

Figure 4.18: Mixing length in channel length.

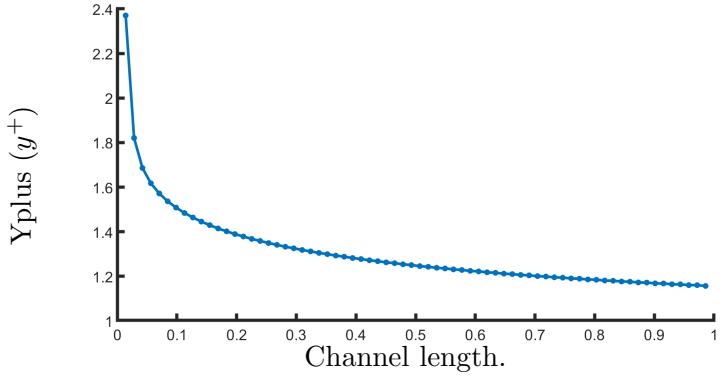

Figure 4.19: Yplus value across the channel length.

Turbulent Boundary Layer with $k-\omega$ model

In this section the turbulent boundary layer with $k-\omega$ model is implemented through the help of the advanced fluid mechanics program Ansys Fluent, the properties of the fluid remained unchanged as in the case of Cebeci-Smith so the inlet velocity was set as constant and equal to $10m/s$ and the fluid properties viscosity has to be adjusted, $\mu = 2 \cdot 10^{-5} \frac{kg}{ms}$, density $\rho = 1 \frac{kg}{m^3}$.

The geometry is a rectangle with a length of L=1 and height of H=0.2 and the mesh is a graded mesh with a finer grid at the bottom of the geometry, as can be seen in Figure 4.20 to fully resolve the smaller scales. The model $k-\omega$ is included in the family of two differential partial equations turbulence models, which is a vital difference in comparison with C-S which is an algebraic model as described in Chapter 2. The discretization of the RABL equations is implemented with the use of the Upwind scheme as described in 4.1.2 and the solver that is used is one of the most common ones in the fluid mechanics scientific community, the algorithm SIMPLE as described in 4.1.4.

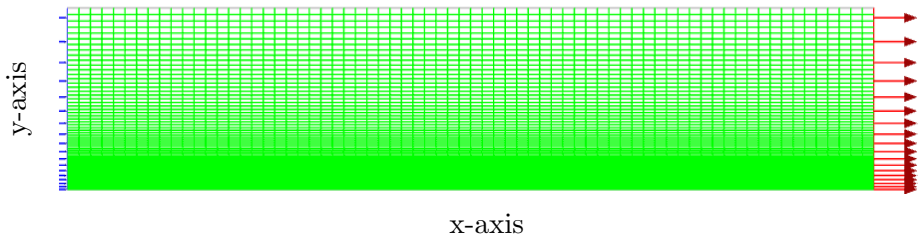

Figure 4.20: Graded grid for Turbulent Boundary Layer.

The variation of the $k-\omega$ model that is used is Wilcox's 2006 variation [43] which is considered the standard version of $k-\omega$ models due to his advanced accuracy and the wide range of flows that it covers. This model uses two extra quantities the turbulent kinetic energy (k) and the specific dissipation rate (ω) and with the use of these two the eddy viscosity variable is obtained as discussed in a previous chapter. In Figure 4.21 it is presented the magnitude of the flow in comparison with the C-S model in Figure 4.22. This result is identical to our flow in terms of the qualitative comparison as the flow is closer to the wall (thickness of B.L. is thinner compared to laminar one) due to the enhanced mixing and increased momentum transfer in macroscopic level (turbulent). Additionally the momentum transfer due to molecules move (laminar), in the wall the no-slip condition exists so the velocity is zero in the

flat plate.

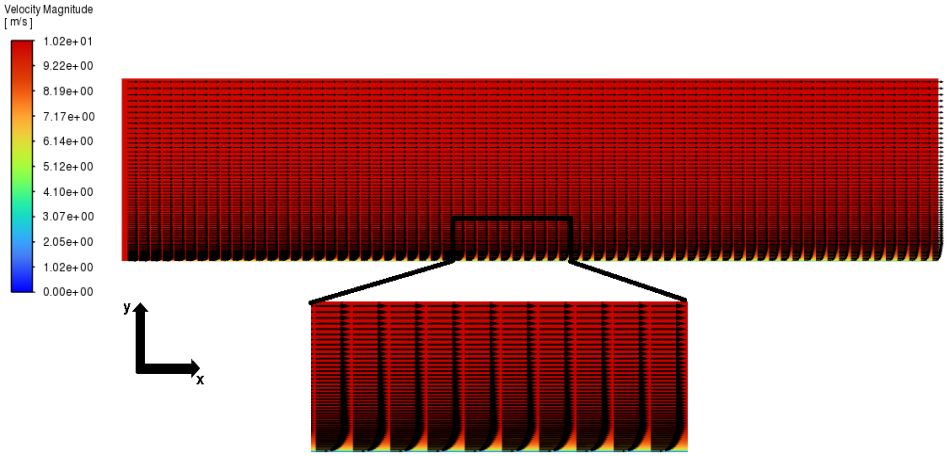

Figure 4.21: Magnitude of Turbulent Boundary Layer with $k-\omega$ model.

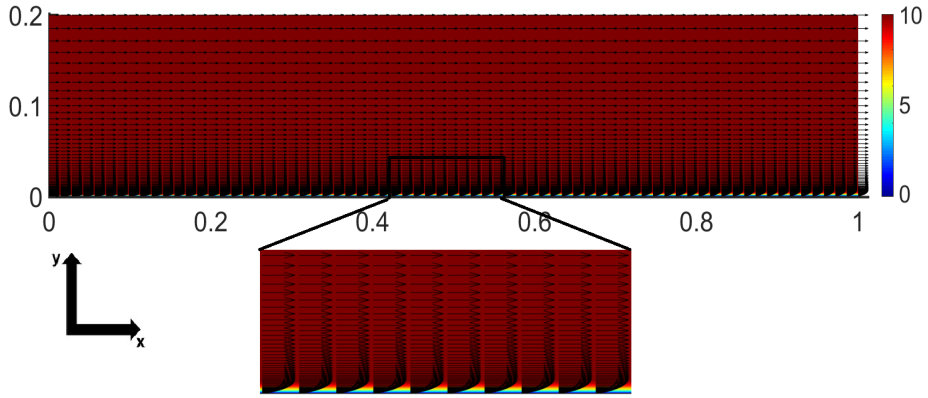

Figure 4.22: Magnitude of Turbulent Boundary Layer with Cebeci-Smith model.

The quantitative comparison is very difficult to achieve in turbulent flows due to a lack of analytical solutions and since the differences in discretization and the solver selection are creating reasonably quantitative differences. The only two ways to obtain a quantitative study are by collecting experimental data for the problem or by implementing DNS, neither of the two are of interest

in this thesis.

The differences that are expected in this comparison are negligible to the simplicity of the geometry and the low Reynolds number as we are at the threshold of the turbulent regime in turbulent B.L., $Re = 5 \times 10^5 - 5 \times 10^6$.

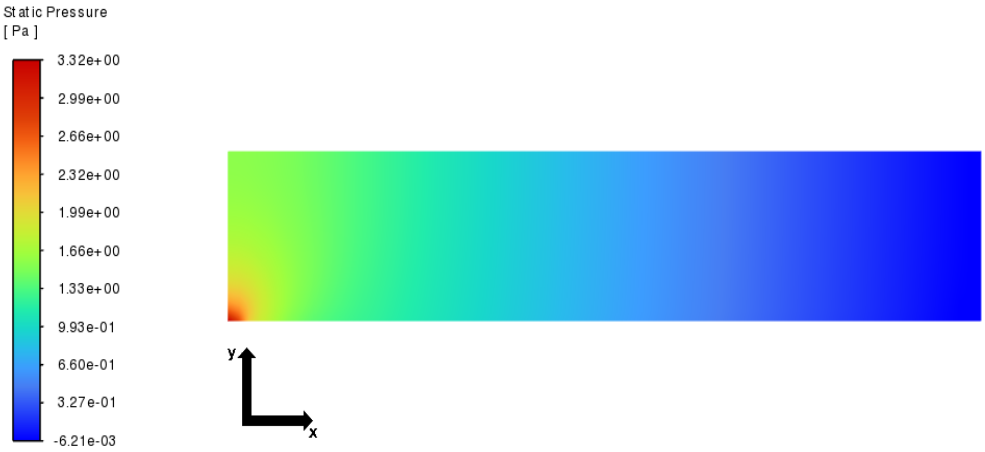

Figure 4.23: Pressure Distribution in Turbulent B.L. with $k - \omega$ model.

For the pressure distribution, the same conclusions can be drawn with the C-S model since the pressure shows a rapid increase at the beginning of the geometry. This is due to the balance of viscous forces, and momentum transfer and then gradually drops to zero. The increased pressure at the bottom left part of the geometry is due to the momentum transfer which overcomes the viscous forces and sets the fluid in motion.

4.3 Turbulent Internal Flows

Turbulence in internal flows is a common phenomenon in engineering and nature as pipes, and ducts are essential for the understanding of turbulence nature which have a lot of applications in the world of fluid mechanics like industrial pipelines, water distribution systems on aerospace engineering the jet engines flows or in biomedical engineering problems such as the blood flow in arteries or veins. The case of internal turbulent flows is special since near solid boundaries the gradient of velocity have large changes that need finer

grids and large computational power. Turbulence in pipes occurs when the Reynolds number is high enough to transition from laminar to turbulent flow which leads to an increase in momentum and kinetic energy.

This thesis focuses on examining the internal turbulent flow within a pipe of height H=2 and L=10 in a pipe that follows the no-slip condition in the upper and bottom wall with an initial stable velocity of $u_0 = 5\text{m/s}$ that is applied in the inlet of the pipe. The mesh of this pipe is a graded mesh in both walls, which is designed to be denser near the two walls and the cell height becomes more sparse while is reaching the center of the pipe, the mesh is symmetrical with an axis of symmetry the line y=1. The grid size that is being used after the independence grid study is defined to be 70×70.

4.3.1 Turbulent Pipe Flow with Cebeci-Smith model

The case that is being studied in this section is this of the incompressible, steady-state $\left(\frac{\partial q}{\partial t} = 0\right)$ two-dimensional turbulent pipe channel which is described by the Reynolds Average Boundary Layer (RANS) equations. The problem under consideration can be described by the continuity and the momentum PDEs, equations (4.35)-(4.37). The RANS equations, in closed form, are:

$$\overline{\nabla} \cdot \overline{q} = \frac{\partial u}{\partial x} + \frac{\partial v}{\partial y} = 0, \tag{4.35}$$

$$\frac{\partial u^2}{\partial x} + \frac{\partial (uv)}{\partial y} = -\frac{1}{\rho}\frac{\partial p}{\partial x} + \frac{\partial}{\partial x}\left[(\nu + \varepsilon_t)\frac{\partial u}{\partial x}\right] + \frac{\partial}{\partial y}\left[(\nu + \varepsilon_t)\frac{\partial u}{\partial y}\right], \tag{4.36}$$

$$\frac{\partial (uv)}{\partial x} + \frac{\partial v^2}{\partial y} = -\frac{1}{\rho}\frac{\partial p}{\partial y} + \frac{\partial}{\partial x}\left[(\nu + \varepsilon_t)\frac{\partial v}{\partial x}\right] + \frac{\partial}{\partial y}\left[(\nu + \varepsilon_t)\frac{\partial v}{\partial y}\right]. \tag{4.37}$$

To ensure that the problem is well-defined, to the above equations must be added the following boundary conditions:

$$y = 0 \quad \text{and} \quad y = h : u, v = 0, \tag{4.38}$$

$$x = L : p = c, \tag{4.39}$$

where u_{inf} is the free stream velocity out of the boundary layer, in the dynamic flow region.

Numerical Result of the Turbulent Pipe

With the use of F.V.M. method, Appendix provides a detailed examination of the method, and by replacing each term in the starting system of the equations in turbulent B.L. we conclude in the following discrete form-equation of differences:

Conservation of Mass

$$\frac{(u_E - u_W)\Delta y}{2} + \frac{(v_N - v_S)\Delta x}{2} = 0, \tag{4.40}$$

x-momentum

$$\begin{aligned} &\frac{(u_E^2 - u_W^2)\Delta\, y}{2} + \left(\frac{u_N v_N - u_S v_S}{2}\right)\Delta\, x = -\frac{1}{\rho}(P_E - P_P)\Delta y \\ &+ \left[(\nu + (\varepsilon_t)_n)\,\frac{u_N - u_P}{\Delta y} - (\nu + (\varepsilon_t)_s)\,\frac{u_P - u_S}{\Delta y}\right]\Delta x \\ &+ \left[(\nu + (\varepsilon_t)_e)\,\frac{u_E - u_P}{\Delta x} - (\nu + (\varepsilon_t)_w)\,\frac{u_P - u_W}{\Delta x}\right]\Delta y, \end{aligned} \tag{4.41}$$

y-momentum

$$\begin{aligned} &\left(\frac{u_E v_E - u_W v_W}{2}\right)\Delta\, y + \frac{(v_N^2 - v_S^2)\Delta\, x}{2} = -\frac{1}{\rho}(P_N - P_P)\Delta x \\ &+ \left[(\nu + (\varepsilon_t)_n)\,\frac{v_N - v_P}{\Delta y} - (\nu + (\varepsilon_t)_s)\,\frac{v_P - v_S}{\Delta y}\right]\Delta x \\ &+ \left[(\nu + (\varepsilon_t)_e)\,\frac{v_E - v_P}{\Delta x} - (\nu + (\varepsilon_t)_w)\,\frac{v_P - v_W}{\Delta x}\right]\Delta y. \end{aligned} \tag{4.42}$$

Geometry and Mesh of Turbulent Pipe

Turbulent pipe geometry is described by two parallel walls, with both upper and down to obey the no-slip condition and the inlet velocity to be a constant with the value of $u_0 = 5$m/s. The walls have a length of L=10 and a height of H=2. The mesh that is required in turbulent pipe flows, is graded at both walls, in y-direction, because of the large shear stresses that occur close to the solid boundaries. The mesh in the x-direction is uniform, and for this case, a 70x70 mesh is used. For the generation of a graded mesh in both directions in y-direction the hyperbolic tangent function is being used, this is a common technique for the generation of stretched structured grids. Many variations of hyperbolic tangent meshes have been published such as this of [39].

The variant exploited in this thesis is described below:

$$c = \frac{2i - J - 3}{J - 1}, \quad y_i = \left[\frac{1 + tanh(K \cdot c)}{K_1}\frac{M}{2}\right], i = 1, 2, ..., J \tag{4.43}$$
$$\text{where} \quad K = 1.2, \qquad K_1 = tanh(K).$$

In this variation J is the number of points in the y-direction, M is the height of the pipe, and K is the stretch rate at which the mesh becomes more or less graded in each wall with the same rate. The need for graded meshes is born from the fact that the gradient of velocity near solid boundaries in turbulent flows is large and so the velocity profiles are steep, in order to resolve correctly all the scales of the energy spectrum a graded mesh is required.

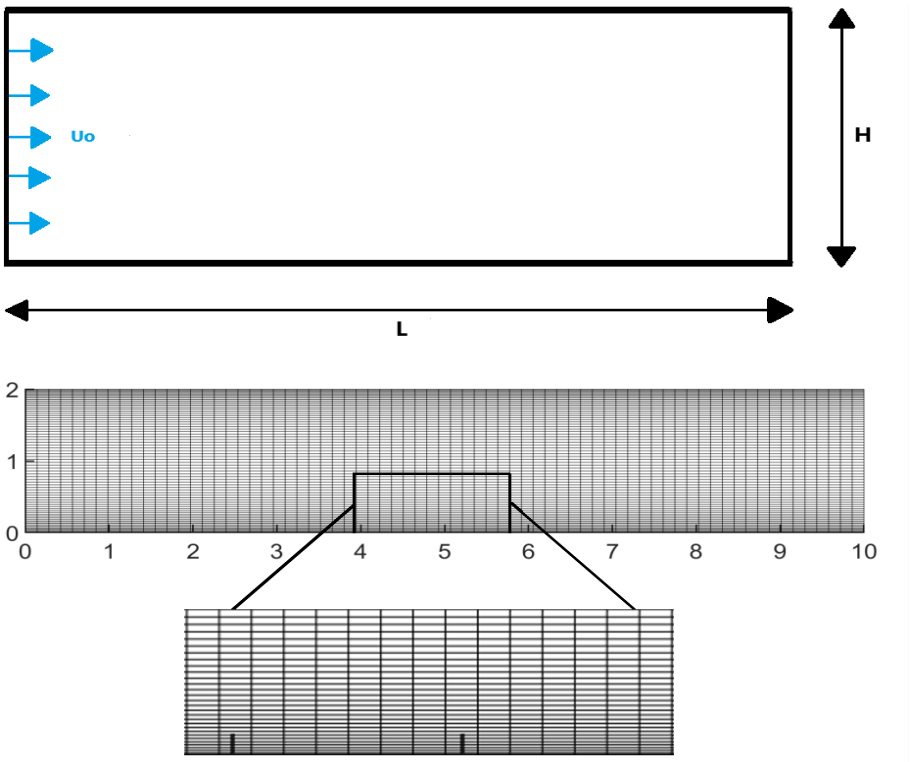

Figure 4.24: The 2D pipe channel geometry and grid.

Root Mean Square

The Root Mean Square (RMS) value of a matrix is the scalar quantity that corresponds to the type above:

$$x_{RMS} = \sqrt{\frac{1}{N}\sum_{n=1}^{N}|x_n|^2}, \tag{4.44}$$

where x_n is the elements of the matrix. The RMS gives a measure of the magnitude or else the average value of the matrix. This value is used for the grid independence study that is being conducted in the next chapter to decide about the percentage differences between different grids. Independence grid study is a crucial approach to decide what is the optimal grid, with the purpose of minimization of computational cost.

Grid Independence Study

To optimize the CFD code that is presented, a grid independence study is needed to obtain the smallest possible grid, with the purpose of saving computational cost, by calculating the percentage difference and demanding the error to be smaller than 2%, compared to the largest grid of 80×80. To compare the grids, Root Mean Square (RMS) is utilized.

Table 4.1 presents the results of percentage differences over all grid sizes and at the final line can be seen that the percentage difference is smaller than 2% in all three quantities, thus is can be concluded that the optimal grid size has achieved.

Turbulent Pipe-Percentage Changes			
Grid size	**U-Velocity**	**V-Velocity**	**Pressure**
30-80	1,88 %	16,73%	15,75%
40-80	1,11%	12,24%	13,40%
50-80	0,70%	8,57%	7,35%
60-80	0,41%	4,49%	3,38%
70-80	0,18%	1,63%	1,32%

Table 4.1: Percentage Changes in Turbulent Pipe

The percentage error is calculated through the following type:

$$\left(\frac{RMS_{ixi} - RMS_{80X80}}{RMS_{80X80}}\right) 100\%, \quad i = 30, 40, 50, 60, 70. \tag{4.45}$$

Results in Turbulent Pipe

The fully turbulent pipe flow numerical solution is obtained through the above procedure including the equations, geometry, grid and the solver. The procedure of numerical solution is described analytically in the subsection "Results in Turbulent Boundary Layer". The properties of the fluid are density $\rho = 1\frac{kg}{m^3}$ the viscosity $\mu = 0.001\frac{kg}{ms}$ and the velocity is constant in the inlet as $u_0 = 5$m/s, these properties lead to a smaller Reynolds number than in Turbulent B.L.

The fully developed flow of a turbulent pipe can be driven either by gravitational forces that create the hydrostatic pressure. In pipes in most cases is negligible, due to the small height of the pipe or by the difference in pressure at the inlet and outlet of the pipe. The viscous force is resistant to the flow whose magnitude, is the same as the force that is created due to the pressure difference, in a fully turbulent flow. So, the flow is moving with no acceleration and maintains its velocity. If the fluid has zero viscosity then it would be ideal and the pressure would be constant, except for its small fluctuations that are caused by hydrostatic pressure.

In the inlet region where the flow is not fully developed, the fluid is accelerating or decelerating, so there is a balance between pressure forces, viscosity, and inertia and this balance drives the pressure along the pipe. The magnitude of the gradient of the pressure $\frac{\partial p}{\partial x}$ is bigger at the inlet compared to the fully developed region where pressure is approaching a constant value, so the following remark can be made:

Remark: Due to the balance of forces, the force due to pressure is required to overcome the forces due to viscosity, to get the fluid flow.

The main difference in laminar and turbulent flows in pipes is the shear stresses, in laminar flow the shear stresses are a result of momentum transfer between randomly moving fluid molecules, so the phenomenon is due to the microscopic molecules motion. In turbulent pipes, the phenomenon can be described as macroscopic as the shear stresses are a result of momentum transfer between randomly moving fluid elements. So, the quantity τ_w is fundamentally different in these two cases.

Remark: In a pipe flow, the flow is laminar if $Re < 2300$ and turbulent if $Re > 4000$ [40].

Turbulent flow is characterized by a high mixing of the fluid, in laminar flow the mixing is orders of magnitude smaller, for this reason. It is easier to mix a cream in a coffee mug than two different paints, where the flow will be laminar due to the high viscosity. The effects of laminar flow are valuable because the pressure difference at the inlet-outlet is smaller, for example in a biomedical application, the heart provides blood to our body. This flow can be characterized as laminar and this is vital to retain our good health, as high Reynolds numbers could increase the shear stresses and rupture the arteries [43].

The stresses τ_w in turbulent flow don't follow the experimental law of Newton as the laminar flow does, by substituting the velocity u with the mean value of velocity, it is experimentally verified that it is not accurate and this is due to the nature of turbulence. As it is described in Theorem 2.4.1, the molecules that move create shear stresses, these shear stresses are much larger in the turbulent case since in laminar flows lumps of molecules are moving in small distances and travel in streamlines. In contrast in turbulent flows packages of molecules (eddies) are moving together so the shear stresses that created are much larger and can't be calculated by the Newton's experimental law. These additional stresses, as stated in Chapter 2, are called eddy viscosity and are treated as stresses.

So the chaotic behavior of the velocity components (velocity fluctuations) contributes to momentum transfer and consequently to the shear stresses. Close to the wall in the turbulent pipe the same velocity distribution as the turbulent B.L. applies. To connect this with the theory, in the velocity distribution of the turbulent layer, close to the wall at the viscous sublayer the laminar stresses dominate. Then, then turbulent stresses are negligible, in the overlap layer both turbulent and laminar stresses have an influence. At the outer layer turbulent stresses are orders of magnitude greater than the laminar ones.

The velocity profiles of turbulent flows have been observed to be more steep than those of laminar flows and are becoming steeper as the Reynolds number increases. This fact is a characteristic difference between the two cases and is explained as follows. The increased momentum transfer homogenizes the velocity profile and the large velocity values are mixed with the smaller ones driving the creation of a steeper profile as it can be observed in Figure 4.29. In this figure, we present respectively the results, of outlet velocity, in laminar

and turbulent pipe flow. In the pressure distribution, that is observable in Figures 4.27 and 4.28 for laminar and turbulent cases. respectively, it can be pinpointed that the intensity of the pressure is much larger, in turbulent case. As it has more intense behavior at the starting region and takes larger values overall. Something that is expected and tends to reach zero as the fluid flows. This is a vital observation as this is the reason for the fluid motion and the pressure difference in inlet-outlet in both laminar or turbulent cases.

In Figures 4.25 and 4.26 the magnitude of velocity ($u_{mag} = \sqrt{u^2 + v^2}$) for laminar and turbulent flow is presented, the values of magnitude are larger for the turbulent case due to the higher u_0 velocity that is applied in the inlet and consequently the higher Re number more specific in laminar case ($u_0 = 1, \quad \mu = 0.01, \quad Re = 200$) and in turbulent case ($u_0 = 5, \quad \mu = 0.001, \quad Re = 10000$). The B.L. thickness for each wall is thinner in the turbulent case as expected due to the increased mixing, and enhanced momentum transfer as it has higher mixing which makes the boundary layer thickness thinner.

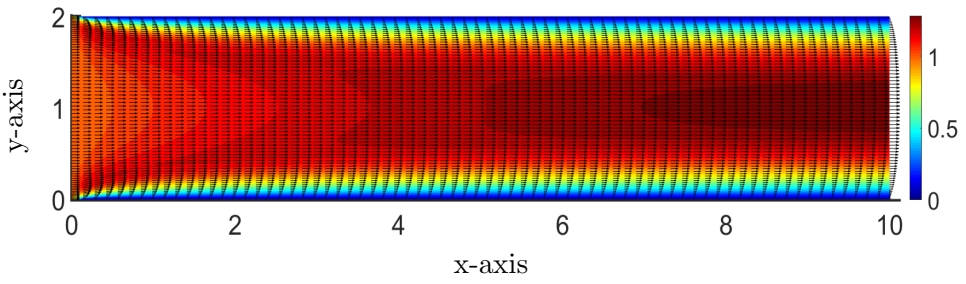

Figure 4.25: Magnitude of velocity in laminar case

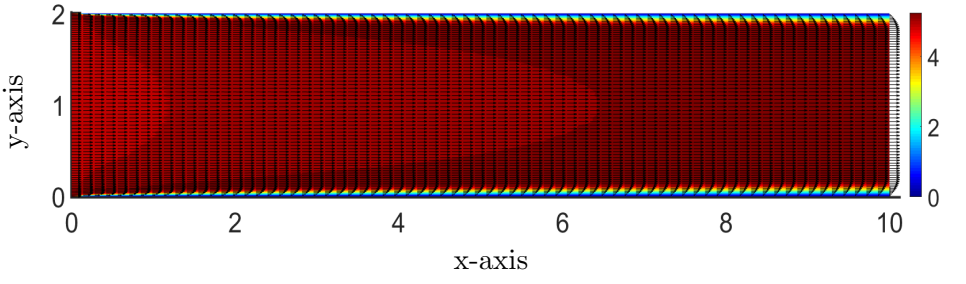

Figure 4.26: Magnitude of velocity in turbulent case

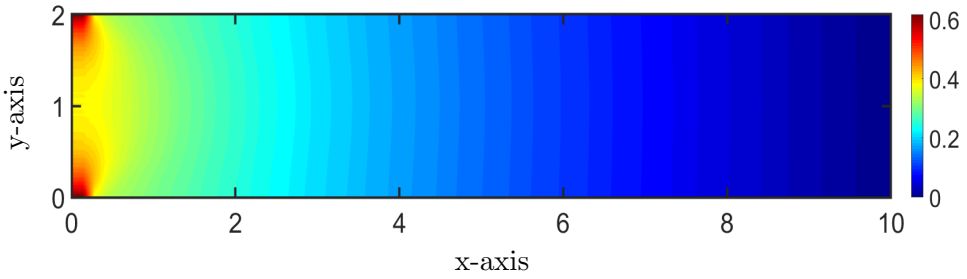

Figure 4.27: Pressure Distribution in laminar case

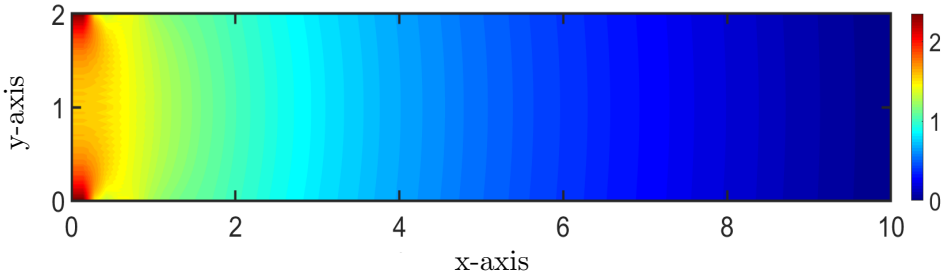

Figure 4.28: Pressure Distribution in turbulent case

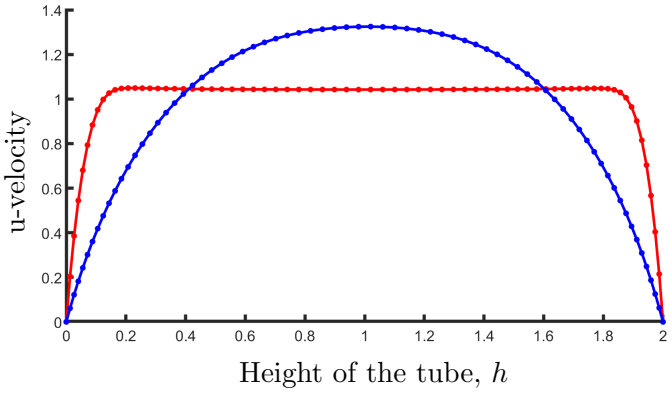

Figure 4.29: Comparison of outlet u-velocity profiles in Laminar (blue) and Turbulent (red) case.

Remark: The stresses near the wall are larger in turbulent flows since higher velocity exists close to the wall due to higher momentum transfer and enhanced mixing.

The following Figures 4.30 and 4.31, present the stresses at the wall for laminar and turbulent pipes. It is observed that the turbulent pipe has larger stresses at the wall because of the reasons mentioned before. Quantitatively it can be pointed out that in the turbulent case there is an increase by approximately 25%. The percentage of difference in stresses, as the center of the pipeline is reached, is increasing exponentially.

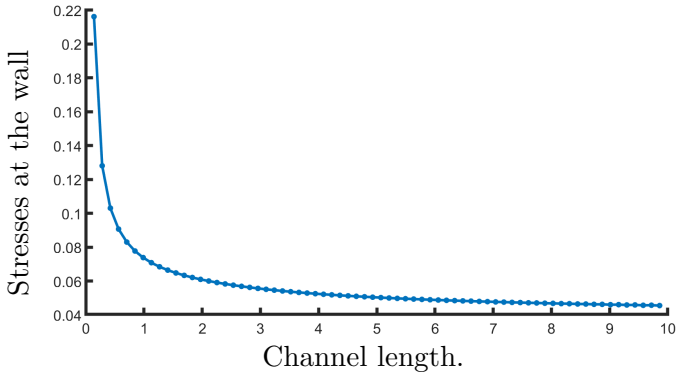

Figure 4.30: Stresses at the wall (τ_w) in laminar pipe.

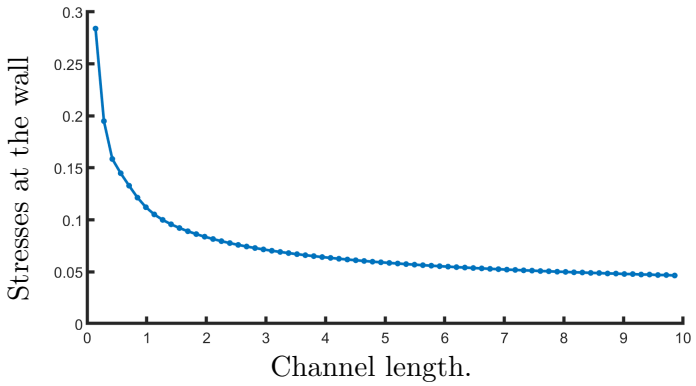

Figure 4.31: Stresses at the wall (τ_w) in turbulent pipe.

Finally, some other turbulence properties of turbulence can be shown, initially the mixing length, which is a property of the flow is presented for half of the pipe. The other half-pipe is the symmetrical of the Figure 4.32. As it is expected it is increasing as the center of the pipe is reached. Moving away from the wall and getting closer to the center of the tube the vortices start to

become bigger. Additionally, the yplus value (y^+) is presented in Figure 4.33, this value is an important indicator as it needs to be less than 5 to ensure that the laminar sublayer (viscous sublayer) is fully resolved due to the very small eddies that exist in this region. This is an important indicator for every turbulent flow simulation.

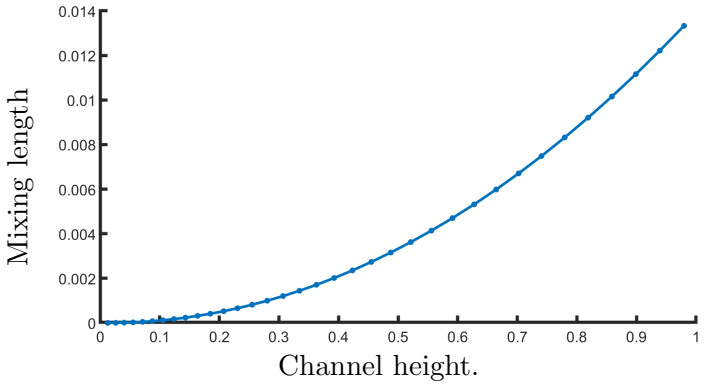

Figure 4.32: Mixing length in half channel length.

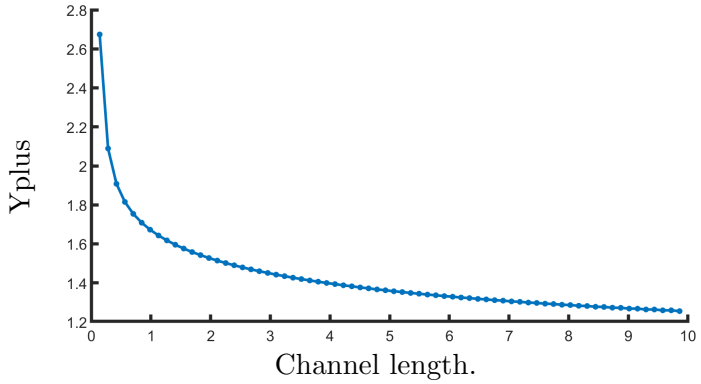

Figure 4.33: Yplus value across the channel length.

Turbulent Pipe with $k-\omega$ model

In this section, the two-dimensional, steady-state turbulent pipe flow numerical solution is studied. The solution is obtained through the computational fluid mechanics program Ansys Fluent. The properties of the fluid are density

$\rho = 1\frac{kg}{m^3}$ the viscosity $\mu = 0.001\frac{kg}{ms}$, and the velocity is constant in the inlet as $u_0 = 5$m/s, the geometry is a rectangle with height H=2 and width L=10. The grid of the geometry is 70×70, defined in Figure 4.34 as graded at the top and bottom walls with the intention to fully resolve from the smaller scales to the bigger ones.

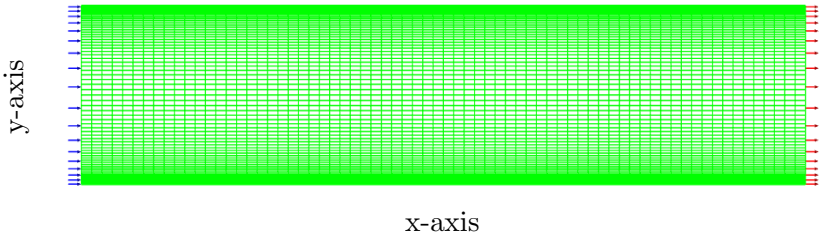

Figure 4.34: Graded grid for turbulent pipe with $k - \omega$ model.

The numerical solution is obtained with the use of the Upwind discretization scheme and the use of the advanced fluid mechanics iterative algorithm SIMPLE. The turbulence model that is used is Wilcox's (2006) $k - \omega$ model which utilizes the turbulent kinetic energy k and specific dissipation rate ω to calculate the eddy viscosity values in the scope of solving the closure problem.

The SIMPLE solver results to the solution presented in Figure 4.35, the behavior of the velocity magnitude is expected as the profile of outlet velocity is flatter than the laminar one due to the increased momentum transfer in a macroscopic level that overcomes the viscous forces and creates a thinner region of viscous sublayer near the wall. The Figures 4.35 and 4.37 below are a direct comparison of the C-S and $k-\omega$ velocity magnitude in which it can be pinpointed that the differences are negligible as the two models are accurate in simple geometry problems like this of the turbulent pipe. The pressure distribution in Figure 4.37 is characterized by a sudden increase in the starting region where the initial velocity is applied and the viscous stresses exert an opposite force to retard the flow. In the next region of pipe the pressure is decreasing gradually until the end of the pipe where the pressure reach the zero value.

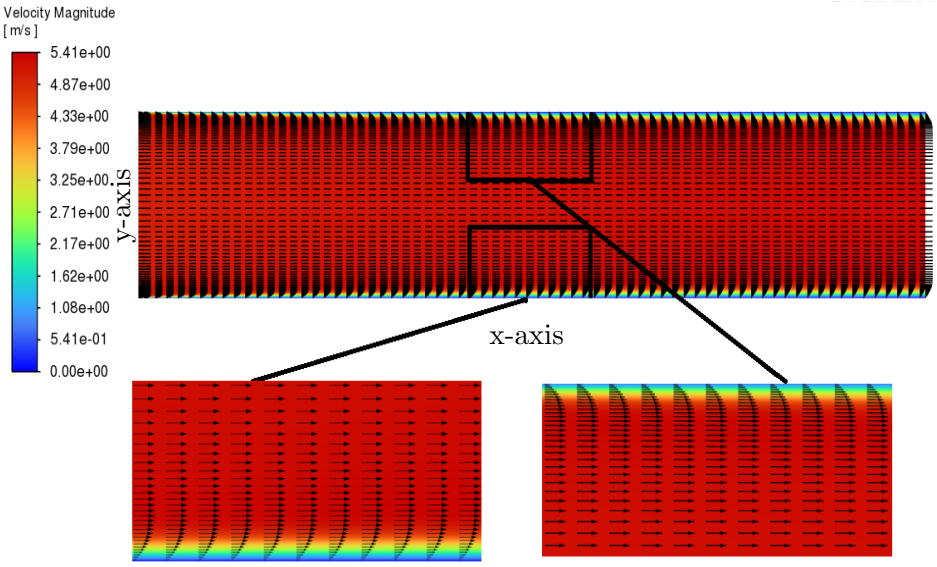

Figure 4.35: Magnitude velocity for turbulent pipe with $k-\omega$ model.

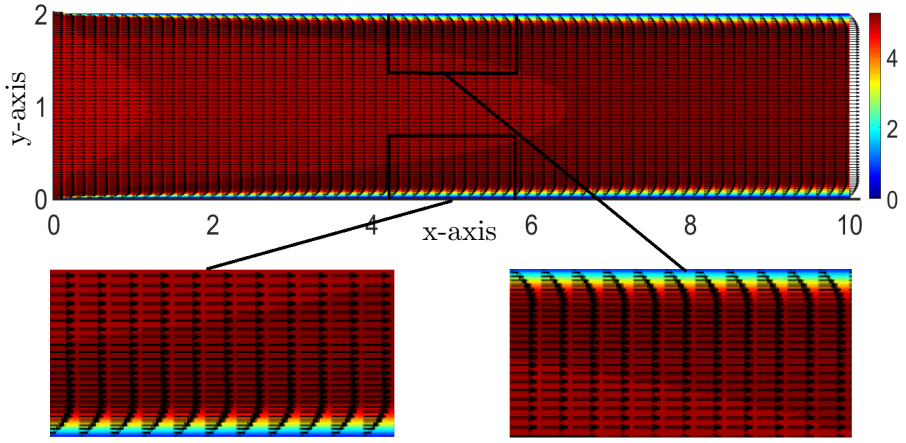

Figure 4.36: Magnitude velocity for turbulent pipe with Cebeci-Smith model.

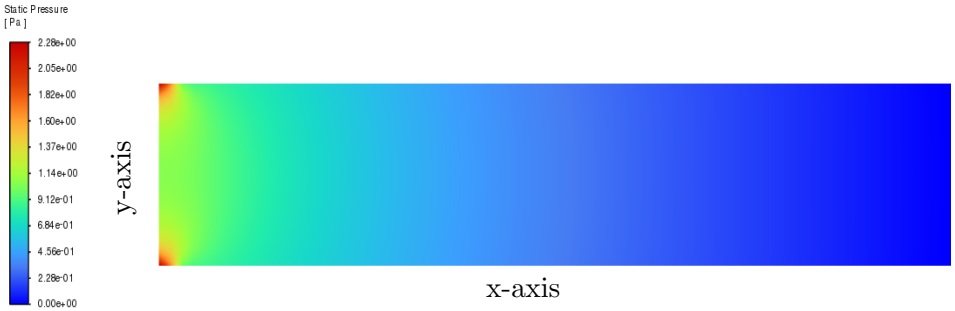

Figure 4.37: Pressure distribution for turbulent pipe with $k - \omega$ model.

CHAPTER 5

Advanced Concept in Fluid Dynamics - Backward Facing Step Flow

Most physical phenomena are described by complex geometries, a factor that adds computational complexity and requires special handling due to the large grids that require, especially in the three-dimensional world. Boundary layers for example can occur in the top and bottom of an airfoil that has an optimal shape such as tear droplets, and not a straight line as in the example of the previous chapter. Pipes or ducts can also be bent or even don't have solid boundaries and move as the arteries in hemodynamics, with severe consequences in the life of the patient, a rupture can occur.

An advanced concept in fluid mechanics will be studied, the two-dimensional, time-dependent, backward-facing step flow, a problem that is fundamental to testing new models of solving fluid mechanics problems with separation and calculating their performance. The main reason of interest in this problem is the complex geometry that is used, which creates eddies in the lower part of the geometry in both laminar and turbulent cases. The main interest of this thesis remains, as in previous chapters, the turbulence behavior of fluids at high Reynolds numbers.

Initially, in Figure 5.1, in which the geometry can be observed, the scheme consists of three parts, the A_1 which is a rectangle with a height of $2,5$m and width of 7m, for A_2 part the height is $2,5$m and the width is 23m and finally the part A_3 which presents the most interesting behavior in this simulation consists of a height of 5m and width of 23m. The grid that is being used is as in Chapter 4 numerical solutions collocated and structured and consists of the 3 sub-grids of A1-A2-A3. The grids are boundary layer grids (graded) to

achieve good results in the center of the geometry. So for A_1 and A_2 the mesh is finer near the bottom and starts to become coarser as it goes up. In contrast the A_3 is reversed, it is finer in the upper boundary and becomes coarser as it goes down. This is a common technique to achieve good enough results in the backward step [18].

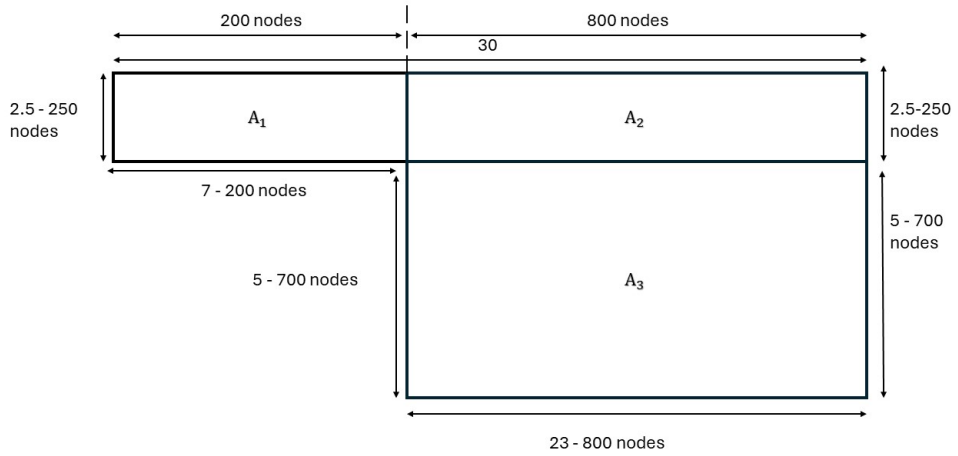

Figure 5.1: Geometry and Grid point nodes for the Backward Facing Flow.

A problem such this one, is difficult to solve with the use of RANS equations as the fluctuations play a crucial role in this problem due to the recyclings of flow in the part A_3 of the geometry. So, a Large Eddy Simulation model is needed to resolve properly this problem. This family of models (LES) is described in Chapter 3. The purpose of this study is to achieve preliminary results through the help of the advanced commercial program, ANSYS FLUENT.

The fluid that is used is the air with its properties, density $\rho = 1.225\text{kg}/m^3$ and dynamic viscosity $\mu = 1.7894 \cdot 10^{-5}$ kg/m s. The velocity in the inlet of the part A_1 is constant and equal to $u_0 = 1$ m/s. The solver that is used is the SIMPLE algorithm used in the Turbulent Boundary Layer and Turbulent Pipe problem as is described in Section 4.1.4.

The LES model which is used is the Smagorinsky-Lilly variation which is

described in [40] by the following:

$$\tau_{ij} - \frac{1}{3}\tau_{kk}\delta_{ij} = -2\left(C_s\Delta\right)^2 \left|\bar{S}\right| S_{ij}. \tag{5.1}$$

In the Smagorinsky-Lilly model, the eddy viscosity is modeled by,

$$\mu_{sgs} = \rho\left(C_s\Delta\right)^2 \left|\bar{S}\right|. \tag{5.2}$$

Where the filter width is usually taken to be,

$$\Delta = (\text{Volume})^{\frac{1}{3}} \tag{5.3}$$

and

$$\bar{S} = \sqrt{2S_{ij}S_{ij}}. \tag{5.4}$$

The effective viscosity is calculated from,

$$\mu_{eff} = \mu_{mol} + \mu_{sgs}. \tag{5.5}$$

The Smagorinsky constant has the value:

$$C_s = 0.1. \tag{5.6}$$

The Smagorinsky-Lilly model is used to solve the complex geometry of the backward-facing step, this model takes advantage of the large eddies that resolve properly and the computational equilibrium that offers, as it solves only the large scales since these scales have the full information of the flow as Kolmogorov's scale requires the direction of the scales to be from the larger to smaller eddies and not in the reverse direction. For spatial discretization, the finite volume method is used as described in previous chapters, and for time discretization (transient) a second-order implicit method is used, for the calculations a time step equal to 1 second per frame is used and the total time of the simulation is 200 seconds which corresponds in 200 different frames per second.

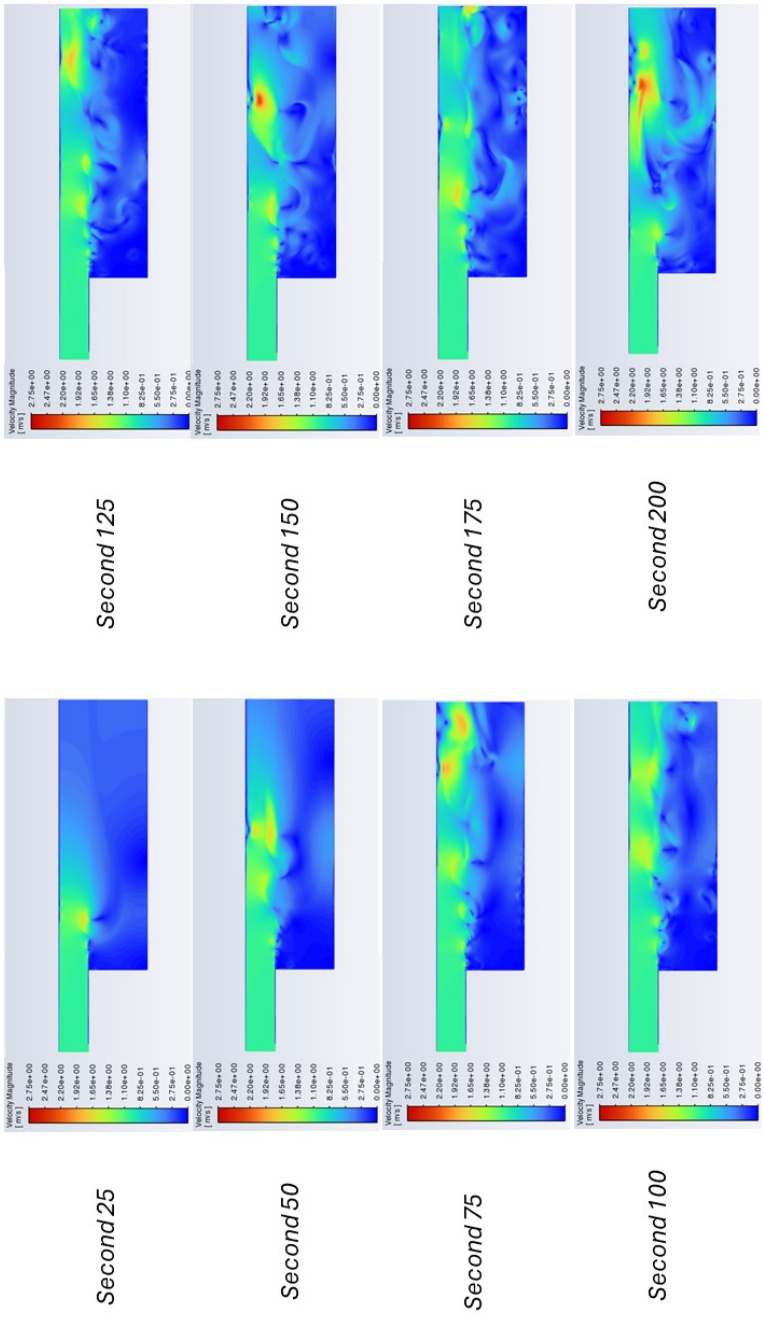

Figure 5.2: Different time frames for the Backward Facing Flow.

In figure 5.2, it can be observed the evolution of the magnitude of velocity at different moments. It can be concluded that as time passes the flow transitions to fully turbulent as large and medium-sized vortices are being formed, since the LES resolve fully only the large and medium size vortices, excluding the smaller ones as they are computationally expensive leading to a non-efficient simulation. In LES the fluctuations are resolved in constant with RANS models so the eddies that are included in the simulation are a result of both mean values and fluctuating components. In A_3 the shear layer rolls up forming a large-scale structure behind the step and as this structure grows, the reattachment location travels downstream. The location between the step and the reattachment locations is called the recirculation zone in which large vortices occur.

5.1 Conclusions and Future Steps

In this thesis, the fundamental principles governing turbulent flow were analyzed, as well as the mathematical modeling of turbulence which was thoroughly described. The case of the turbulent boundary layer is of great interest to scientists so the velocity distribution is presented. The cornerstone problem of turbulent flows is the closure problem, which needs turbulence modeling, so the turbulence models categories were introduced and some of the most popular of each category were analyzed and compared with each other. One such case was the $k-\epsilon$ family models which are two-equations models family and the three most popular variations were compared (Standard-RNG-Realizable).

Also, a wide range of internal and closed flows was studied, with different discretization methods such as upwind and finite volumes for steady and unsteady state (time-dependent) flows with iterative methods such as SIMPLE but also direct methods such as the direct solution approach coupled with Newton's method as it is described in Chapter 4, which give robustness to the obtained numerical results. Advanced mathematics programs were used, more specifically the programming language Matlab is utilized, in which internal and closed flows numerical solutions were studied, using code as well as commercial programs such as Ansys Fluent. For the modeling of eddy viscosity, the algebraic turbulence model of Cebeci-Smith is utilized, and the two differential equation model of $k-\omega$, to cover a wide range of turbulence models. Additionally, LES and more specifically the Smagorinsky-Lilly variation is used and some preliminary results were presented, all of the above are visualized in Figure 5.3.

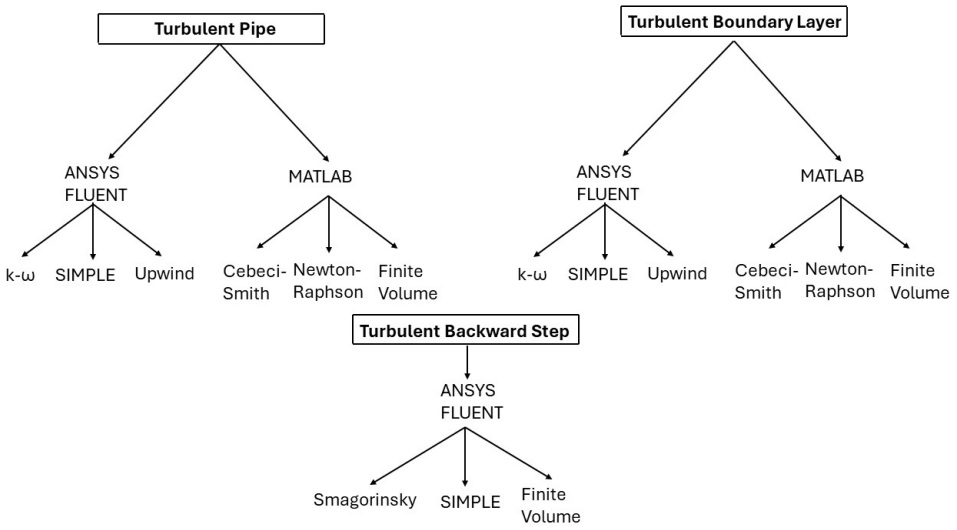

Figure 5.3: A summary of key simulations in this thesis.

Some of the future steps include:

- More advanced turbulence models simulation such as variations of the family of LES models or the simulation of Direct Numerical Simulation in the advanced programming language Matlab.
- The coupling of MHD and turbulence is of great interest as it is directly applicable to astronomical applications.
- Aerodynamics applications, such as the flow past airplanes or airfoils simulation, phenomena that are described by turbulent flows.
- The three-dimensional turbulent flow over an airfoil would be a challenge that would have enormous scientific value, as most scientists who interact with such problems, work on commercial codes and not on fully adjustable codes in programming languages.
- Finally, the energy equation can be utilized to study temperature changes in flows.

APPENDIX A

Appendix

A.1 F.V.M. Discretization for Turbulent Flows

A.1.1 RABL Discretization

Initially for the RABL equations, the discretization with the help of the Finite Volume Method.
Conservation of Mass

$$\bullet \iint_{CV} \frac{\partial u}{\partial x}\, dx\, dy = \int_w^e \frac{\partial u}{\partial x}\, dx \int_s^n 1\, dy = u\Big|_w^e \Delta y = (u_e - u_w)\Delta y$$
$$= (\frac{u_E + u_P}{2} - \frac{u_P + u_W}{2})\Delta y = \frac{(u_E - u_W)\Delta y}{2}$$
$$\bullet \iint_{CV} \frac{\partial v}{\partial y}\, dx\, dy = \int_s^n \frac{\partial v}{\partial y}\, dy \int_w^e 1\, dx = v\Big|_s^n \Delta y = (v_n - vs)\Delta x$$
$$= (\frac{v_N + v_P}{2} - \frac{v_P + v_S}{2})\Delta x = \frac{(v_N - v_S)\Delta x}{2}$$

x-momentum For the **Diffusion terms** and more specific for the **Pressure**:

$$\bullet \iint_{CV} \frac{\partial p}{\partial x}\, dx\, dy = (P_E - P_P)\Delta y$$

For the **Laplacian term**:

$$\bullet \iint_{CV} \frac{\partial}{\partial y}\left[(\nu + \varepsilon_t)\frac{\partial u}{\partial y}\right] dy\, dx = \int_s^n \frac{\partial}{\partial y}\left[(\nu + \varepsilon_t)\frac{\partial u}{\partial y}\right] dy \int_w^e 1\, dx$$
$$\left[(\nu + \varepsilon_t)\frac{\partial u}{\partial y}\right]_s^n = \left(\left[(\nu + \varepsilon_t)\frac{\partial u}{\partial y}\right]_n - \left[(\nu + \varepsilon_t)\frac{\partial u}{\partial y}\right]_s\right)\Delta x =$$
$$\left[(\nu + (\varepsilon_t)_n)\frac{u_N - u_P}{\Delta y} - (\nu + (\varepsilon_t)_s)\frac{u_P - u_S}{\Delta y}\right]\Delta x,$$

where the eddy viscosity calculated in north and south is provided by the following:

$$(\varepsilon_t)_n = \frac{(\varepsilon_t)_N + (\varepsilon_t)_P}{2}, \qquad (\varepsilon_t)_s = \frac{(\varepsilon_t)_P + (\varepsilon_t)_S}{2}.$$

Convective terms
In order to use the F.V.M. scheme we have to transform the convective terms in their closed form.

$$u\frac{\partial u}{\partial x} + v\frac{\partial u}{\partial y} \overset{\text{(closed-form)}}{=} \frac{\partial u^2}{\partial x} + \frac{\partial (uv)}{\partial y}$$

$$\bullet \iint_{CV} \frac{\partial u^2}{\partial x}\, dx\, dy = \int_w^e \frac{\partial u^2}{\partial x}\, dx \int_s^n 1\, dy = u^2\Big|_w^e \Delta y = (u_e^2 - u_w^2)\Delta\, y$$

$$= \left(\frac{u_E^2 + u_P^2}{2} - \frac{u_W^2 + u_P^2}{2}\right)\Delta y = \frac{(u_E^2 - u_W^2)\Delta\, y}{2}$$

$$\bullet \iint_{CV} \frac{\partial (uv)}{\partial y}\, dx\, dy = \int_s^n \frac{\partial (uv)}{\partial y}\, dy \int_w^e 1\, dx = [uv]_s^n \Delta\, x$$

$$= \left(\frac{u_P v_P + u_N v_N}{2} - \frac{u_P v_P + u_S v_S}{2}\right)\Delta\, x = \left(\frac{u_N v_N - u_S v_S}{2}\right)\Delta\, x$$

y-momentum For the **RHS terms** and more specific for the **Pressure**:

$$\bullet \iint_{CV} \frac{\partial p}{\partial y}\, dy\, dx = (P_N - P_P)\Delta x$$

For the **Laplacian term**:

$$\bullet \iint_{CV} \frac{\partial}{\partial y}\left[(\nu + \varepsilon_t)\frac{\partial v}{\partial y}\right] dy\, dx = \int_s^n \frac{\partial}{\partial y}\left[(\nu + \varepsilon_t)\frac{\partial v}{\partial y}\right] dy \int_w^e 1\, dx$$

$$\left[(\nu + \varepsilon_t)\frac{\partial v}{\partial y}\right]_s^n = \left(\left[(\nu + \varepsilon_t)\frac{\partial v}{\partial y}\right]_n - \left[(\nu + \varepsilon_t)\frac{\partial v}{\partial y}\right]_s\right)\Delta x =$$

$$\left[(\nu + (\varepsilon_t)_n)\frac{v_N - v_P}{\Delta y} - (\nu + (\varepsilon_t)_s)\frac{v_P - v_S}{\Delta y}\right]\Delta x,$$

where the eddy viscosity calculated in north and south is provided by the following:

$$(\varepsilon_t)_n = \frac{(\varepsilon_t)_N + (\varepsilon_t)_P}{2}, \qquad (\varepsilon_t)_s = \frac{(\varepsilon_t)_P + (\varepsilon_t)_S}{2}.$$

Convective terms
In order to use the F.V.M. scheme we have to transform the convective terms in their closed form.

$$u\frac{\partial v}{\partial x} + v\frac{\partial u}{\partial y} \overset{\text{(closed-form)}}{=} \frac{\partial (uv)}{\partial x} + \frac{\partial v^2}{\partial y}$$

$$\bullet \iint_{CV} \frac{\partial (uv)}{\partial x}\, dx\, dy = \int_w^e \frac{\partial (uv)}{\partial x}\, dx \int_s^n 1\, dy = [uv]_w^e \Delta\, y$$

$$= \left(\frac{u_E v_E + u_P v_P}{2} - \frac{u_P v_P + u_W v_W}{2} \right) \Delta\, y = \left(\frac{u_E v_E - u_W v_W}{2} \right) \Delta\, y$$

$$\bullet \iint_{CV} \frac{\partial v^2}{\partial y}\, dx\, dy = \int_s^n \frac{\partial v^2}{\partial y}\, dy \int_w^e 1\, dx = v^2 \Big|_s^n \Delta x = (v_n^2 - v_s^2) \Delta\, x$$

$$= \left(\frac{v_N^2 + v_P^2}{2} - \frac{v_P^2 + v_S^2}{2} \right) \Delta x = \frac{(v_N^2 - v_S^2) \Delta\, x}{2}$$

A.1.2 RANS Discretization

The RANS differential system of equations is being discretized with the F.V.M. method in the following discrete equations.
Conservation of Mass

$$\bullet \iint_{CV} \frac{\partial u}{\partial x}\, dx\, dy = \int_w^e \frac{\partial u}{\partial x}\, dx \int_s^n 1\, dy = u \Big|_w^e \Delta y = (u_e - u_w) \Delta y$$

$$= (\frac{u_E + u_P}{2} - \frac{u_P + u_W}{2}) \Delta y = \frac{(u_E - u_W) \Delta y}{2}$$

$$\bullet \iint_{CV} \frac{\partial v}{\partial y}\, dx\, dy = \int_s^n \frac{\partial v}{\partial y}\, dy \int_w^e 1\, dx = v \Big|_s^n \Delta x = (v_n - vs) \Delta x$$

$$= (\frac{v_N + v_P}{2} - \frac{v_P + v_S}{2}) \Delta x = \frac{(v_N - v_S) \Delta x}{2}$$

x-momentum For the **RHS terms** and more specific for the **Pressure**:

$$\bullet \iint_{CV} \frac{\partial p}{\partial x}\, dx\, dy = (P_E - P_P) \Delta y$$

For the **Laplacian term**:

$$\bullet \iint_{CV} \frac{\partial}{\partial y}\left[(\nu+\varepsilon_t)\frac{\partial u}{\partial y}\right] dy\,dx = \int_s^n \frac{\partial}{\partial y}\left[(\nu+\varepsilon_t)\frac{\partial u}{\partial y}\right] dy \int_w^e 1\,dx$$

$$\left[(\nu+\varepsilon_t)\frac{\partial u}{\partial y}\right]_s^n \Delta x = \left(\left[(\nu+\varepsilon_t)\frac{\partial u}{\partial y}\right]_n - \left[(\nu+\varepsilon_t)\frac{\partial u}{\partial y}\right]_s\right)\Delta x =$$

$$\left[(\nu+(\varepsilon_t)_n)\frac{u_N-u_P}{\Delta y} - (\nu+(\varepsilon_t)_s)\frac{u_P-u_S}{\Delta y}\right]\Delta x,$$

where the eddy viscosity calculated in north and south is provided by the following:

$$(\varepsilon_t)_n = \frac{(\varepsilon_t)_N + (\varepsilon_t)_P}{2}, \qquad (\varepsilon_t)_s = \frac{(\varepsilon_t)_P + (\varepsilon_t)_S}{2}.$$

$$\bullet \iint_{CV} \frac{\partial}{\partial x}\left[(\nu+\varepsilon_t)\frac{\partial u}{\partial x}\right] dy\,dx = \int_w^e \frac{\partial}{\partial x}\left[(\nu+\varepsilon_t)\frac{\partial u}{\partial x}\right] dx \int_s^n 1\,dy$$

$$\left[(\nu+\varepsilon_t)\frac{\partial u}{\partial x}\right]_w^e \Delta y = \left(\left[(\nu+\varepsilon_t)\frac{\partial u}{\partial x}\right]_e - \left[(\nu+\varepsilon_t)\frac{\partial u}{\partial x}\right]_w\right)\Delta y =$$

$$\left[(\nu+(\varepsilon_t)_e)\frac{u_E-u_P}{\Delta x} - (\nu+(\varepsilon_t)_w)\frac{u_P-u_W}{\Delta x}\right]\Delta y,$$

where the eddy viscosity calculated in north and south is provided by the following:

$$(\varepsilon_t)_e = \frac{(\varepsilon_t)_E + (\varepsilon_t)_P}{2}, \qquad (\varepsilon_t)_w = \frac{(\varepsilon_t)_P + (\varepsilon_t)_W}{2}.$$

Convective terms

In order to use the F.V.M. scheme we have to transform the convective terms in their closed form.

$$u\frac{\partial u}{\partial x} + v\frac{\partial u}{\partial y} \overset{\text{(closed-form)}}{=} \frac{\partial u^2}{\partial x} + \frac{\partial (uv)}{\partial y}$$

$$\bullet \iint_{CV} \frac{\partial u^2}{\partial x}\,dx\,dy = \int_w^e \frac{\partial u^2}{\partial x}\,dx \int_s^n 1\,dy = u^2\Big|_w^e \Delta y = (u_e^2 - u_w^2)\Delta\, y$$

$$= \left(\frac{u_E^2+u_P^2}{2} - \frac{u_W^2+u_P^2}{2}\right)\Delta y = \frac{(u_E^2-u_W^2)\Delta\, y}{2}$$

$$\bullet \iint_{CV} \frac{\partial (uv)}{\partial y}\,dx\,dy = \int_s^n \frac{\partial (uv)}{\partial y}\,dy \int_w^e 1\,dx = [uv]_s^n \Delta\, x$$

$$= \left(\frac{u_P v_P + u_N v_N}{2} - \frac{u_P v_P + u_S v_S}{2}\right)\Delta\, x = \left(\frac{u_N v_N - u_S v_S}{2}\right)\Delta\, x$$

y-momentum For the **RHS terms** and more specific for the **Pressure**:

$$\bullet \iint_{CV} \frac{\partial p}{\partial y}\, dy\, dx = (P_N - P_P)\Delta x$$

For the **Laplacian term**:

$$\bullet \iint_{CV} \frac{\partial}{\partial y}\left[(\nu+\varepsilon_t)\,\frac{\partial v}{\partial y}\right] dy\, dx = \int_s^n \frac{\partial}{\partial y}\left[(\nu+\varepsilon_t)\,\frac{\partial v}{\partial y}\right] dy \int_w^e 1\, dx$$
$$\left[(\nu+\varepsilon_t)\,\frac{\partial v}{\partial y}\right]_s^n \Delta x = \left(\left[(\nu+\varepsilon_t)\,\frac{\partial v}{\partial y}\right]_n - \left[(\nu+\varepsilon_t)\,\frac{\partial v}{\partial y}\right]_s\right)\Delta x =$$
$$\left[(\nu+(\varepsilon_t)_n)\,\frac{v_N - v_P}{\Delta y} - (\nu+(\varepsilon_t)_s)\,\frac{v_P - v_S}{\Delta y}\right]\Delta x,$$

where the eddy viscosity calculated in north and south is provided by the following:

$$(\varepsilon_t)_n = \frac{(\varepsilon_t)_N + (\varepsilon_t)_P}{2}, \qquad (\varepsilon_t)_s = \frac{(\varepsilon_t)_P + (\varepsilon_t)_S}{2}.$$

$$\bullet \iint_{CV} \frac{\partial}{\partial x}\left[(\nu+\varepsilon_t)\,\frac{\partial v}{\partial x}\right] dy\, dx = \int_w^e \frac{\partial}{\partial x}\left[(\nu+\varepsilon_t)\,\frac{\partial v}{\partial x}\right] dx \int_s^n 1\, dy$$
$$\left[(\nu+\varepsilon_t)\,\frac{\partial v}{\partial x}\right]_w^e \Delta y = \left(\left[(\nu+\varepsilon_t)\,\frac{\partial v}{\partial x}\right]_e - \left[(\nu+\varepsilon_t)\,\frac{\partial v}{\partial x}\right]_w\right)\Delta y =$$
$$\left[(\nu+(\varepsilon_t)_e)\,\frac{v_E - v_P}{\Delta x} - (\nu+(\varepsilon_t)_w)\,\frac{v_P - v_W}{\Delta x}\right]\Delta y,$$

where the eddy viscosity calculated in north and south is provided by the following:

$$(\varepsilon_t)_e = \frac{(\varepsilon_t)_E + (\varepsilon_t)_P}{2}, \qquad (\varepsilon_t)_w = \frac{(\varepsilon_t)_P + (\varepsilon_t)_W}{2}.$$

Convective terms
In order to use the F.V.M. scheme we have to transform the convective terms

in their closed form.

$$u\frac{\partial v}{\partial x} + v\frac{\partial u}{\partial y} \overset{\text{(closed-form)}}{=} \frac{\partial (uv)}{\partial x} + \frac{\partial v^2}{\partial y}$$

$$\bullet \iint_{CV} \frac{\partial (uv)}{\partial x}\, dx\, dy = \int_w^e \frac{\partial (uv)}{\partial x}\, dx \int_s^n 1\, dy = [uv]_w^e \Delta\, y$$

$$= \left(\frac{u_E v_E + u_P v_P}{2} - \frac{u_P v_P + u_W v_W}{2} \right) \Delta\, y = \left(\frac{u_E v_E - u_W v_W}{2} \right) \Delta\, y$$

$$\bullet \iint_{CV} \frac{\partial v^2}{\partial y}\, dx\, dy = \int_s^n \frac{\partial v^2}{\partial y}\, dy \int_w^e 1\, dx = v^2 \Big|_s^n \Delta x = (v_n^2 - v_s^2) \Delta\, x$$

$$= \left(\frac{v_N^2 + v_P^2}{2} - \frac{v_P^2 + v_S^2}{2} \right) \Delta x = \frac{(v_N^2 - v_S^2) \Delta\, x}{2}$$

A.2 Additional Results in Turbulent Flows

A.2.1 Turbulent Boundary Layer with Cebeci-Smith model

The following remarks are some additional insights about the turbulent flow in B.L., providing more specific details on the v velocity component with the Cebeci-Smith turbulence model. The u component exhibits similar behavior with the magnitude of velocity as this component is larger since the main information of the flow is presented in the x-direction, additionally, the v component is highly affected by the conservation of mass equation. The graph of the u component of velocity is identical to the magnitude of velocity as it is described in Chapter 4.

Remarks:

• The no-slip condition applies in the wall, in consequence, the velocity in the wall is zero.

• The v velocity component is much smaller than the u component because the motion of fluid in the y-direction is negligible in comparison with the x-direction.

• The v component of velocity is described by an increase in the leading edge of the plate in order to verify the conservation of mass equation. This creates a rapid increase in motion upwards.

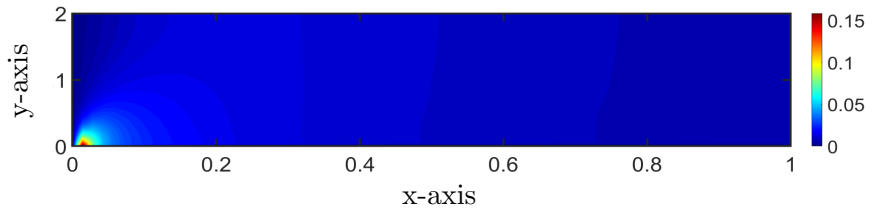

Figure A.1: v Velocity component in Turbulent Boundary Layer.

A.2.2 Turbulent Boundary Layer with $k-\omega$ model

The following remarks supply additional insights into turbulent flow within the boundary layer, offering specific details on the v velocity component using the Cebeci-Smith turbulence model. The behavior of the u component in velocity magnitude resembles that of the main flow direction in the x-axis, while the v component is greatly influenced by the conservation of mass equation. The graph of the u component of velocity is similar to the magnitude of velocity as it is described in Chapter 4.

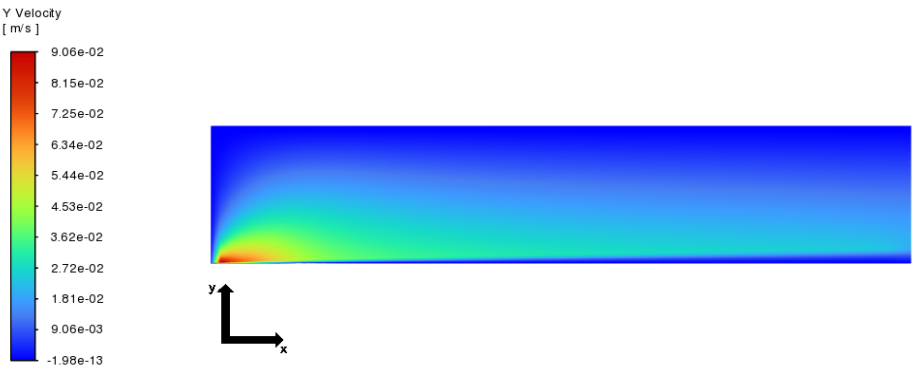

Figure A.2: v Velocity component in Turbulent Boundary Layer.

• The no-slip condition is verified in the wall, consequently, the velocity in the wall is zero.

• The contours of u-velocity present similar behavior with the velocity magnitude figure in Chapter 4 as u component of velocity dominates the velocity magnitude.

• The v velocity component is significantly smaller than the u component because the motion of fluid in the y-direction is negligible in comparison with the x-direction.

• The vertical velocity component,v velocity, presents an increase in the leading edge of the plate, as it confirms the conservation of mass equation, leading to a rapid upward acceleration in motion.

A.2.3 Turbulent Pipe with Cebeci-Smith model

Some additional information about the turbulent pipe flow with the Cebeci-Smith model are analyzed in the following remarks. The two components of the two-dimensional steady-state turbulent pipe compose the magnitude of velocity. In the following figures present the comparison of the u and v components of velocity in laminar and turbulent cases.

• The no-slip condition is applied in both walls, consequently, the velocity in the wall is zero.

• The u velocity contours graph is divided in two regions the dynamic flow where the velocity is constant and equal to the free stream velocity and the inner region of the B.L. close to both walls where the B.L. is created and the viscous forces dominate (laminar sublayer).

• The u velocity takes significantly higher values in the turbulent case in comparison with the laminar case and the flow is moving closer to the walls as the momentum transfer is increased due to the strong mixing of the fluid,

• The v velocity component is significantly smaller than the u component because the motion of fluid in the y-direction is negligible in comparison with the x-direction.

• The vertical velocity component,v velocity, presents an increase in the leading edge of the plate, as it confirms the conservation of mass equation, leading to a rapid upward acceleration in the lower region of the plate and a declaration in the upper region. This fact follows from the fact that at the upper region, the flow tends to go lower and at the lower region the flow tends to go upwards.

• The values of v velocity are increased in the turbulent case since the turbulence increases the horizontal and vertical motion of the fluid.

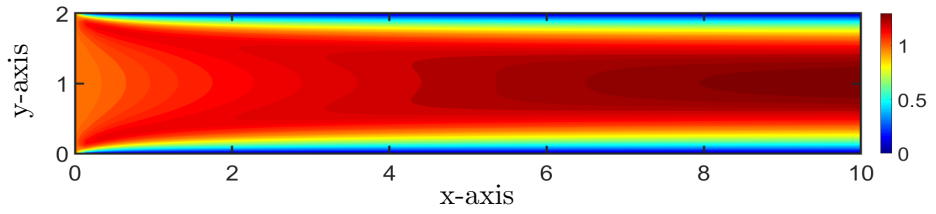

Figure A.3: u Velocity component in laminar case.

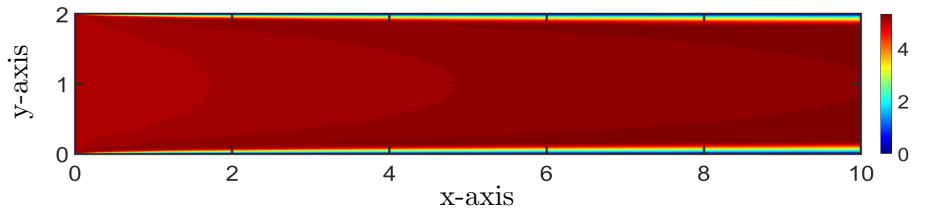

Figure A.4: u Velocity component in turbulent case.

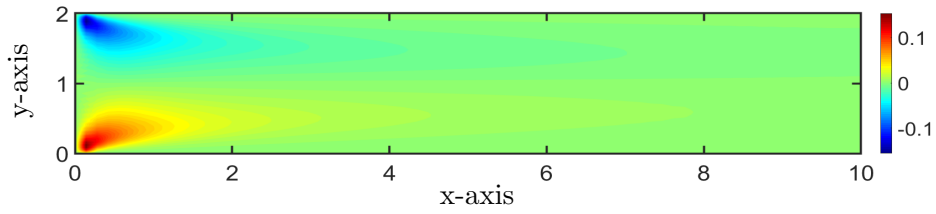

Figure A.5: v Velocity component in laminar case.

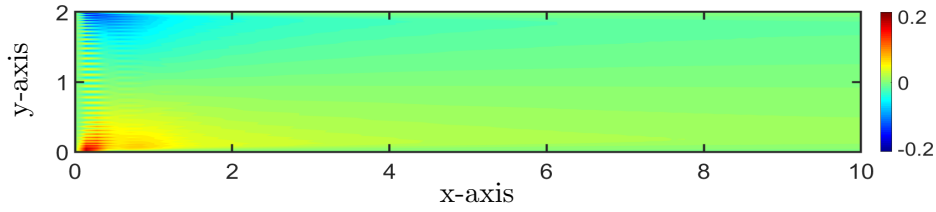

Figure A.6: v Velocity component in turbulent case.

A.2.4 Turbulent Pipe with $k-\omega$ model

Some additional observations follow from the study of the turbulent pipe with the use of the $k-\omega$ turbulence model. Specifically the two components of velocity in the two-dimensional steady-state case.

The following presented remarks are important to note:

• The velocity at the walls is equal to zero as the no-slip condition is applied in both walls.

• In the graph of u velocity the flow follows the velocity distribution of the B.L. velocity near the walls, the region near the wall is dominated by the viscous forces(laminar sublayer) and in the outer region the velocity is constant and equal to the free stream velocity.

• The u velocity takes significantly higher values in the turbulent case in comparison with the laminar case and the flow is moving closer to the walls as the momentum transfer is increased due to the strong mixing of the fluid,

• The v velocity component is significantly smaller than the u component because the motion of fluid in the y-direction is negligible in comparison with the x-direction.

• The vertical velocity component, v velocity, presents an increase in the leading edge of the plate, as it confirms the conservation of mass equation, leading to a rapid upward acceleration in the lower region of the plate and a declaration in the upper region. This fact follows from the fact that at the upper region, the flow tends to go lower and at the lower region the flow tends to go upwards.

• The values of v velocity are increased in the turbulent case since the turbulence increases the horizontal and vertical motion of the fluid.

Figure A.7: u Velocity for turbulent pipe with $k-\omega$ model.

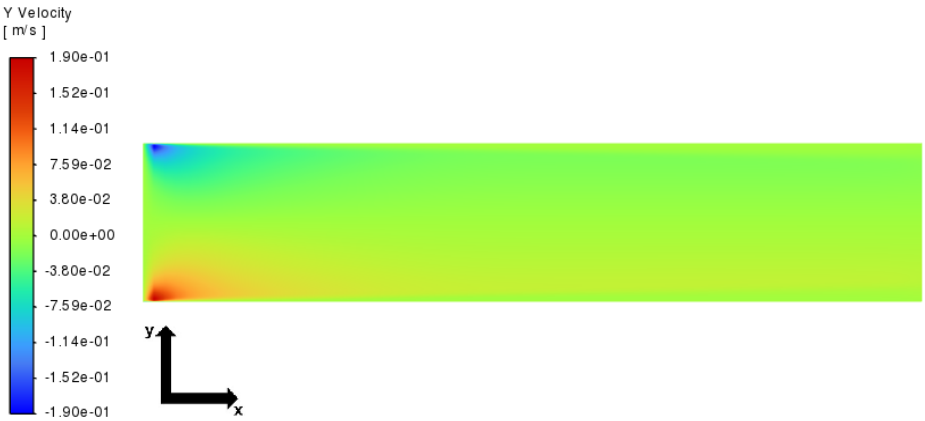

Figure A.8: v Velocity for turbulent pipe with $k-\omega$ model.

Bibliography

[1] Baldwin, B., and Lomax, H. Thin-layer approximation and algebraic model for separated turbulent flows. In *16th Aerospace Sciences Meeting* (1978).

[2] Cebeci, T. *Turbulence Models and Their Application.* Springer Science & Business Media, 12 2003.

[3] Cebeci, T., and Bradshaw, P. *Physical and computational aspects of convective heat transfer.*, 1st edition ed. New York Springer, 1984.

[4] Cebeci, T., and Smith, A. A finite-difference method for calculating compressible laminar and turbulent boundary layers. *Journal of Basic Engineering 92* (1970).

[5] Chrimatopoulos, G., Tzirtzilakis, E. E., and Xenos, M. A. Magnetohydrodynamic and ferrohydrodynamic fluid flow using the finite volume method. *Fluids 9*, 1 (2024).

[6] Coakley, T. J. Turbulence modeling methods for the compressible navier-stokes equations. *American Institute of Aeronautics and Astronautics, Fluid and Plasma Dynamics Conference, 16th, Danvers* (07 1983).

[7] Conejo, A. J., and Baringo, L. *Power System Operations.* Springer, 2017.

[8] Davidson, P. A. *Turbulence : An introduction for scientists and engineers*, 2. aufl. ed. Oxford University Press, 2015.

[9] Einstein, A. Investigations on the theory of the brownian movement. *American Mathematical Monthly 35* (jun 1928).

[10] Gad-el-Hak, M., and Bushnell, D. M. Status and outlook of flow separation control. *29th Aerospace Sciences Meeting* (01 1991).

[11] Govindarajan, R. Boundary layer stability and transition to turbulence. *Resonance 26* (10 2021), 1403–1415.

[12] Hou, Q., and Zou, Z. Comparison between standard and renormalization group k-εmodels in numerical simulation of swirling flow tundish. *ISIJ International 45* (01 2005), 325–330.

[13] Johnson, D., and King, L. A new turbulence closure model for boundary layer flows with strong adverse pressure gradients and separation. In *22nd Aerospace Sciences Meeting* (1984).

[14] Kafoussias, N., and Xenos, M. Numerical investigation of two-dimensional turbulent boundary-layer compressible flow with adverse pressure gradient and heat and mass transfer. *Acta Mechanica 141* (09 2000), 201–223.

[15] Kolmogorov, A. N. Turbulence and stochastic process: Kolmogorov's ideas 50 years on the local structure of turbulence in incompressible viscous fluid for very large reynolds numbers. *Proceedings Mathematical Physical & Engineering Sciences 434* (jul 1991).

[16] Kyriakoudi, K. C.and Xenos, M. A. Magnetohydrodynamic effects on a pathological vessel: An euler–lagrange approach. *Physics of Fluids 35*, 12 (2023).

[17] Launder, B. E., and Spalding, D. B. *Lectures in mathematical models of turbulence*. Academic Press, 1972.

[18] Le, H., Moin, P., and Kim, J. Direct numerical simulation of turbulent flow over a backward-facing step. *Journal of Fluid Mechanics 330* (01 1997).

[19] Li, X. Fundamentals of fluid mechanics. *Journal of Non-newtonian Fluid Mechanics - J NON-NEWTONIAN FLUID MECH 91* (07 2000).

[20] Menter, F. Zonal two equation $k-\omega$ turbulence models for aerodynamic flows. In *23rd Fluid Dynamics, Plasmadynamics, and Lasers Conference* (07 1993).

[21] Menter, F. R. Two-equation eddy-viscosity turbulence models for engineering applications. *AIAA Journal 32*, 8 (1994), 1598–1605.

[22] Moukalled, F., Mangani, L., and Darwish, M. *The Finite Volume Method in Computational Fluid Dynamics: An Advanced Introduction with OpenFOAM® and Matlab®*, vol. 113. Springer, 10 2015.

[23] Nocedal, J., and Wright, S. J. *Numerical optimization*, springer series in operations research and financial engineering ed. New York, Springer, 2006.

[24] Orszag, S., and Patterson, G. Numerical simulation of three-dimensional homogeneous isotropic turbulence. *Physical Review Letters 28* (01 1972).

[25] Pandya, S. *Experimental Study of Proppant Transport in Horizontal and Directional Wells*. PhD thesis, University of Oklahoma, 05 2013.

[26] Patankar, S. V. *Numerical heat transfer and fluid flow*. Hemisphere Pub, 1980.

[27] Pope, S. B. *Turbulent flows*. CUP, 2000.

[28] Quarteroni, A., Sacco, R., and Saleri, F. *Numerical Mathematics*. Springer Science & Business Media, 11 2010.

[29] Reynold, O. On the dynamical theory of incompressible viscous fluids and the determination of the criterion. *Philosophical Transactions of the Royal Society of London 186* (01 1895), 123–164.

[30] Robinson, D. F., Harris, J. E., and Hassan, H. A. Unified turbulence closure model for axisymmetric and planar free shear flows. *AIAA Journal 33* (12 1995), 2325–2331.

[31] Sayed, M. A., Kandil, H. A., and Shaltot, A. Aerodynamic analysis of different wind-turbine-blade profiles using finite-volume method. *Energy Conversion and Management 64* (2012), 541–550. IREC 2011, The International Renewable Energy Congress.

[32] Schlichting, H., and Gersten, K. *Boundary-Layer Theory*. Springer Berlin Heidelberg, 2017.

[33] Shaheed, R., Mohammadian, A., and Kheirkhah Gildeh, H. A comparison of standard $k-\epsilon$ and realizable $k-\epsilon$ turbulence models in

curved and confluent channels. *Environmental Fluid Mechanics 19* (04 2019).

[34] Shih, T. H., Liou, W. W., Shabbir, A., Yang, Z., and Zhu, J. A new k-ε eddy viscosity model for high reynolds number turbulent flows. *Computers & Fluids 24*, 3 (1995), 227–238.

[35] Sinha, N. *Towards RANS Parameterization of Vertical Mixing by Langmuir Turbulence in Shallow Coastal Shelves.* PhD thesis, University of South Florida, 11 2013.

[36] Smith, A. M. O., and Cebeci, T. *Analysis of Turbulent Boundary Layers.* ACADEMIC PRESS, INC., 1974.

[37] Taylor, G. I. Statistical theory of turbulence. *Proceedings Mathematical Physical & Engineering Sciences 151* (sep 1935).

[38] Tennekes, H., and Lumley, J. L. *A First Course in Turbulence.* The MIT Press, 1972.

[39] Thompson, J. F., Warsi, Z. U., and Mastin, C. W. *Numerical grid generation: foundations and applications.* Elsevier North-Holland, Inc., USA, 1985.

[40] Versteeg, H., and Malalasekera, W. *An Introduction to Computational Fluid Dynamics: The Finite Volume Method.* Pearson Education Limited, 2007.

[41] White, F. M., and Majdalani, J. *Viscous fluid flow.* Mcgraw-Hill, 2021.

[42] Wilcox, D. C. Reassessment of the scale-determining equation for advanced turbulence models. *AIAA Journal 26*, 11 (1988), 1299–1310.

[43] Wilcox, D. C. *Turbulence Modeling for CFD (Third Edition)*, 3rd ed. Dcw Industries, Incorporated, 2006.

[44] Xenos, M., and Tzirtzilakis, E. *Fluid mechanics with applications.* Gotsis, 2018.

[45] Xenos, M. A. *Study of Two-Dimensional Magnetohydrodynamics Compressible Flow in the Boundary Layer over a Plane Surface with Adverse Pressure and Heat and Mass Transfer.* PhD thesis, University of Patras, 2002.

[46] Xenos, M. A. Mathematical formulation of bubble formation after compressible boundary layer separation: Preliminary numerical results. *Open Journal of Fluid Dynamics 12*, 4 (2022), 304–320.